From Neural Oscillations to Clinical Decisions: Machine Learning for Predicting Optimal Deep Brain Stimulation Parameters in Parkinson's Disease

Inaugural dissertation

presented to the Faculty of Mathematics and Natural Sciences
of Heinrich Heine University Düsseldorf
for the degree of
Doctor of Philosophy in Natural Sciences

Submitted by

Fayed Rassoulou
from Mayotte, France

Düsseldorf, March 2026

From the Institute of Clinical Neuroscience and Medical Psychology of
Heinrich Heine University Düsseldorf

Printed by permission of the
Faculty of Mathematics and Natural Sciences of
Heinrich Heine University Düsseldorf

Supervisor: Prof. Dr. Alfons Schnitzler
Mentor: Prof. Dr. Eckart Zimmermann

Date of the oral examination: 07 May 2026

"*I have striven not to laugh at human actions, not to weep at them, nor to hate them, but to understand them.*"

– Baruch Spinoza

Summary

Deep brain stimulation (DBS) of the subthalamic nucleus (STN) provides effective symptom relief for patients with advanced Parkinson's disease (PD). However, DBS programming remains challenging: identifying optimal electrode contacts currently relies on time-intensive monopolar reviews where neurologists systematically test all contacts through trial-and-error. This process lacks objective biomarkers and depends heavily on clinical expertise. Decades of research have characterized pathological oscillatory signatures in PD, yet these neural biomarkers have remained largely confined to basic research without informing clinical decision-making.

This thesis investigated whether electrophysiological recordings can predict therapeutic outcomes and guide contact selection. I pursued three aims: first, curating a unique dataset of simultaneous magnetoencephalography and local field potential recordings from twenty PD patients, organized according to Brain Imaging Data Structure (BIDS) standards; second, applying machine learning to this dataset to identify which neural signatures predict the therapeutic window of individual electrode contacts; third, validating predictions in an independent cohort of eight newly recruited patients.

Machine learning successfully predicted therapeutic windows based on neurophysiological markers, achieving significant correlations in both the training cohort ($r = 0.45$, $p < 0.001$) and independent validation cohort ($r = 0.30$, $p < 0.001$). Predictions relied mainly on high-frequency subthalamic activity (>35 Hz) and STN-cortex coherence patterns across multiple brain regions, rather than the widely studied beta oscillations. This dissociation likely reflects different functional roles: beta power indicates disease severity, while high-frequency signals and connectivity patterns better mark optimal electrode for stimulation.

This work establishes proof-of-concept that electrophysiological signatures contain information about clinically relevant parameters, such as the optimal DBS contact. However, important limitations must be acknowledged: magnetoencephalography (MEG) is not widely available; the therapeutic window does not capture long-term quality of life; and sample sizes were relatively small, though successful validation in an independent cohort mitigates overfitting concerns. Critically, this thesis demonstrates feasibility rather than clinical implementation. Whether electrophysiology-guided programming improves outcomes compared to standard approaches would require prospective randomized trials. Nonetheless, by demonstrating that prediction is possible, this work provides a foundation for future translational efforts and contributes to evolving DBS therapy toward data-driven precision medicine.

List of abbreviations

BIDS	Brain Imaging Data Structure
DBS	Deep brain stimulation
EEG	Electroencephalogram
LFP	Local field potential
MEG	Magnetoencephalography
PD	Parkinson’s disease
SNc	substantia nigra pars compacta
SNr	substantia nigra pars reticulata
STN	subthalamic nucleus

Table of Contents

1. Introduction

Parkinson's disease (PD) is the second most common neurodegenerative disorder worldwide, affecting approximately 10 million people and representing one of the fastest-growing neurological conditions (Dorsey et al., 2018; Bloem et al., 2021). PD affects quality of life through motor and non-motor symptoms. (Postuma et al., 2015; Poewe et al., 2017; Kalia & Lang, 2015; Moustafa et al., 2016). With the aging of the global population, the burden of PD is expected to double by 2040, creating an urgent need for more effective therapeutic strategies (Dorsey et al., 2018). While pharmacological treatments remain the mainstay of PD management, their long-term efficacy is limited by motor fluctuations, dyskinesias, and decreasing therapeutic windows as the disease worsens (Olanow et al., 2004; Poewe et al., 2017). For patients whose symptoms can no longer be relieved by medication alone, deep brain stimulation (DBS) has become the best therapeutic option, allowing a significant reduction in motor symptoms and medication dose (Deuschl et al., 2006; Schuepbach et al., 2013; Krack et al., 2019; Fasano & Lozano, 2015). DBS involves the surgical implantation of electrodes into specific brain targets, such as the subthalamic nucleus (STN). The electrodes deliver continuous high-frequency electrical stimulation to modulate abnormal neural activity (Benabid et al., 2009; Lozano & Lipsman, 2013). Despite its efficacy, optimization of DBS programming remains a challenging and time-consuming process that relies heavily upon subjective clinical judgment (Volkmann et al., 2002; Moro et al., 2006). The selection of optimal electrode contacts for therapeutic stimulation currently lacks objective and data-driven approaches, representing a significant limitation in personalized medicine for movement disorders. (Picillo et al., 2016; Dembek et al., 2017).

This thesis presents a comprehensive investigation of electrophysiological signatures in PD and evaluates their potential for predicting therapeutic outcomes in DBS. These signatures are of significant interest from both a basic research and a clinical perspective. From a research standpoint, they provide unique insights into the dynamics of subcortico-cortical networks (Hirschmann et al., 2011; Litvak et al., 2011). Clinically, these markers hold the potential to inform objective electrode contact selection and guide the development of future adaptive DBS paradigms. In my thesis, I followed a two-part approach: first, I curated a large-scale dataset combining magnetoencephalography (MEG) with local field potential (LFP) recordings from deep brain electrodes; and second, I applied machine learning methods to this dataset to explore how these neural signals can be leveraged for the automated identification of optimal stimulation contacts.

The following introduction establishes the scientific and clinical foundation for this thesis. I begin by examining the pathophysiology of PD and current treatment challenges, which provides the clinical context and unmet medical needs that motivate this research. I then discuss DBS therapy as an established intervention while highlighting the specific optimization challenges relevant to this work. Next, I explore electrophysiological recording methods, focusing particularly on the unique advantages of combined MEG-LFP recordings

for characterizing disease-related network dysfunction. I also review machine learning applications in clinical neuroscience, showing how computational approaches can leverage electrophysiological biomarkers for data-driven therapeutic decision-making. Finally, I outline the specific aim and objectives that this thesis addresses, demonstrating how this work contributes to advancing personalized medicine in movement disorders through the integration of neurophysiological insights and predictive modelling.

1.1 Parkinson's Disease: Pathophysiology and Treatment

PD primarily manifests through characteristic motor symptoms: bradykinesia (slowness of movement), resting tremor, rigidity, and postural instability which progressively worsen over years as neurodegeneration advances (Moustafa et al., 2016, Postuma et al., 2015). However, the clinical picture extends far beyond motor dysfunction. Patients experience a wide spectrum of non-motor symptoms, including cognitive impairment, mood disorders, sleep disturbances, autonomic dysfunction, and sensory abnormalities, which collectively have profound impacts on quality of life (Chaudhuri et al., 2006). Many of these non-motor features can emerge years or even decades before motor symptoms become apparent, reflecting the widespread nature of pathological changes throughout the nervous system (Berg et al., 2015).

The burden of PD is substantial and growing. Age represents the greatest risk factor, with incidence rising steeply after 60 years and prevalence reaching approximately 1–2% among individuals over 65 (Lau & Breteler, 2006; Poewe et al., 2017). Beyond demographic factors, genetic predisposition also plays a role in the disease. Mutations in certain genes can directly cause some forms of parkinsonism, while variations in many other genes make a person more likely to develop the condition (Kalia & Lang, 2015; Bandres-Ciga et al., 2020). Environmental factors, including pesticide exposure, head trauma, and lifestyle factors, further modify disease risk through mechanisms that remain incompletely understood (Ascherio & Schwarzschild, 2016).

The main motor symptoms of PD arise from the progressive degeneration of dopaminergic neurons in the substantia nigra pars compacta (SNc), a midbrain structure that forms part of the basal ganglia circuitry (DeLong & Wichmann, 2009; Xia & Mao, 2012). These neurons project to the striatum (caudate nucleus and putamen), where they release dopamine: a neurotransmitter essential for modulating motor function, motivation, and reward processing (Bustos et al., 2004; Schultz, 2007). By the time motor symptoms emerge in PD, typically 60–80% of these dopaminergic neurons have already been lost, and striatal dopamine content is reduced by roughly 70–80% (Kish et al., 1988; Fearnley & Lees, 1991). This severe depletion prior to symptom onset reflects a significant compensatory capacity within the basal ganglia. However, it also means that by the time of clinical diagnosis, extensive and irreversible damage has already occurred. Crucially, current pharmacological and surgical interventions remain symptomatic rather than disease-modifying; while they effectively

manage motor symptoms, they do not reverse existing neuronal loss or halt the ongoing neurodegenerative process.

The hallmark neuropathological feature of PD, beyond dopaminergic cell loss, is the presence of Lewy bodies and Lewy neurites (intracellular protein inclusions found in surviving neurons) (Spillantini et al., 1997; Goedert et al., 2013). These inclusions are composed of aggregated α-synuclein, a presynaptic protein involved in the transport of synaptic vesicles and the release of neurotransmitter (Burré et al., 2010). In pathological conditions, α-synuclein misfolds and aggregates, forming insoluble fibrils that accumulate within neurons.

The mechanisms driving dopaminergic neurodegeneration in PD are multifactorial and not fully understood. Understanding these mechanisms remains a central goal of PD research, as they represent potential targets for disease-modifying therapies that could slow or halt neurodegeneration rather than merely treating symptoms.

1.1.1 Basal Ganglia Dysfunction

The loss of dopaminergic neurons disrupts the finely tuned communication within the basal ganglia: a network of interconnected subcortical nuclei critical for motor control, action selection, procedural learning, and motivated behaviour (Carvey et al., 2006; Lanciego et al., 2012; Obeso et al., 2008). The basal ganglia comprise several major structures: the striatum, which serves as the primary input structure receiving cortical projections; the globus pallidus, divided into external (GPe) and internal (GPi) segments; the subthalamic nucleus (STN); and the substantia nigra, divided into pars compacta (SNc, the dopaminergic neurons) and pars reticulata (SNr, a major output structure). These nuclei are interconnected through complex circuits that process cortical inputs and send modulated outputs back to cortex via the thalamus, forming cortico-basal ganglia-thalamo-cortical loops (Alexander et al., 1986; Middleton & Strick, 2000).

Under normal physiological conditions, the basal ganglia coordinate movements through the dynamic interaction of three major pathways: the *direct*, *indirect*, and *hyperdirect* pathways (**Figure 1**). These pathways operate in parallel to ensure the activation of intended actions while inhibiting competing actions, enabling smooth and efficient motor control (Middleton & Strick, 2000; Lanciego et al., 2012; Ikemoto et al., 2015). In the direct pathway, cortical excitation of the striatum reduces the inhibition exerted by the GPi and the SNr on the thalamus, allowing increased thalamic stimulation of the motor cortex and facilitating movement (Alexander & Crutcher, 1990; DeLong & Wichmann, 2009). The indirect pathway, on the other hand, inforces thalamic inhibition via striatal suppression of the GPe, which disinhibits the STN, thereby increasing excitation of the GPi/SNr and consequently reducing cortical motor activity (Smith et al., 1998; Obeso et al., 2008; Purves et al., 2001). The hyperdirect pathway provides an even faster inhibitory route: cortical projections

directly activate the STN, leading to a rapid increase in GPi/SNr activity, and inhibiting motor activity (Parent & Hazrati, 1995; Nambu et al., 2002; Rocha et al., 2023).

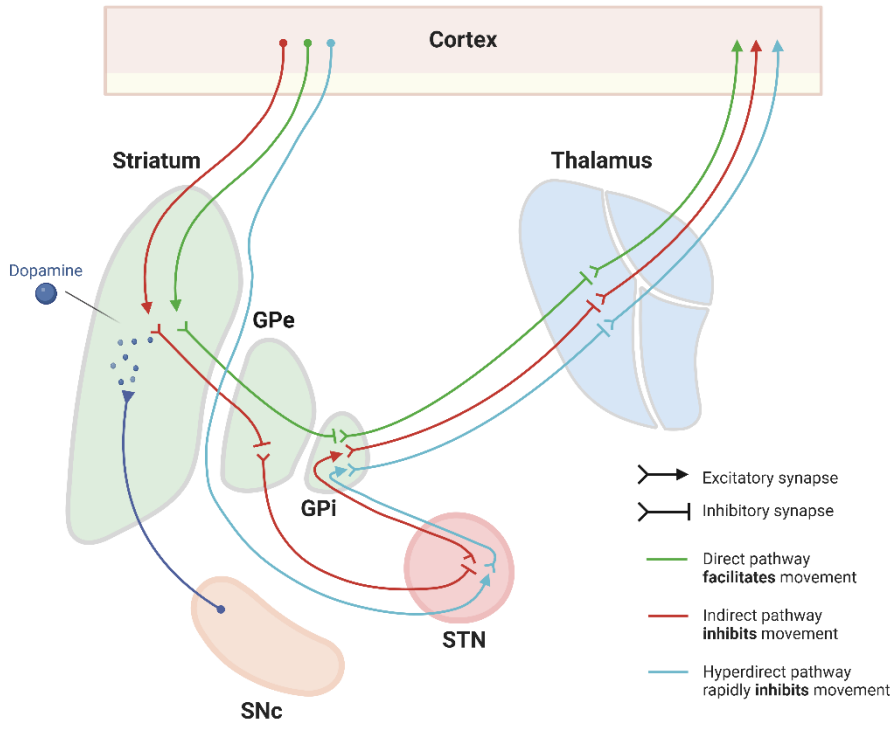

Figure 1. Schematic representation of the direct, indirect, and hyperdirect pathway. In the healthy state, dopamine from the substantia nigra pars compacta modulates the direct (green arrows), indirect (red arrows) and hyperdirect pathway (light blue arrows), resulting in a balanced thalamic output to the motor cortex. In Parkinson's disease, the loss of dopaminergic neurons leads to overactivity in the indirect and the hyperdirect pathway. This results in an excessive inhibition of the thalamus and subsequent motor symptoms like bradykinesia and rigidity. Abbreviations: GPe (external globus pallidus), GPi (internal globus pallidus), SNc (substantia nigra pars compacta), STN (subthalamic nucleus). I created this figure myself in https://BioRender.com.

Dopamine, released from SNc terminals throughout the striatum, plays a crucial modulatory role in balancing these pathways. Dopamine acts on two classes of receptors with opposing effects: D1-like receptors, expressed primarily by direct pathway neurons, strengthen excitation; D2-like receptors, expressed primarily by indirect pathway neurons, strengthen inhibition (Gerfen & Surmeier, 2011). Thus, dopamine simultaneously strengthens the direct pathway (promoting movement) and weakens the indirect pathway (reducing movement suppression), creating a coordinated effect that enables smooth initiation and execution of voluntary actions. This mechanism allows dopamine to act as a gain control signal, modulating the relative strength of competing motor programs and enabling selection of contextually appropriate actions while suppressing alternatives (Frank, 2005; Hikosaka et al., 2000).

In PD, the degeneration of dopaminergic neurons in the SNc reduces the activation of the direct pathway and over-activates the indirect and hyperdirect circuits, resulting in excessive inhibition of thalamo-cortical projections, causing bradykinesia (Obeso et al., 2002; Wichmann & DeLong, 1996).

1.1.2 Pharmacological Treatment

The main therapeutic approach to PD relies on dopamine replacement therapy, most often through the administration of levodopa, a dopamine precursor (Poewe et al., 2017). Levodopa remains the gold standard treatment for PD due to its high efficacy in improving motor symptoms (Cotzias et al., 1969). Its mechanism of action is based on restoring dopaminergic signalling in the depleted striatum, thus partially rebalancing the activity of the direct and indirect pathways.

However, the long-term efficacy of levodopa is progressively compromised by the ongoing degeneration of dopaminergic neurons and the decreased capacity of the brain to store and release dopamine. This results in a reduced duration of benefit, higher motor fluctuations and a “wearing-off” phenomena which corresponds to periods of worsening parkinsonian symptoms as the effect of the drug fades (Rascol et al., 2000; Colosimo & Michele 1999). Furthermore, the stimulation of dopamine receptors induced by intermittent levodopa administration contributes to the development of levodopa-induced dyskinesia, characterized by involuntary choreiform movements that can be as debilitating as the initial parkinsonian symptoms (Obeso et al., 2000). Studies indicate that a decrease in treatment efficacy occurs in approximately 50% of patients within 2 to 5 years of starting levodopa therapy, with dyskinesia affecting up to 40% of patients within 4 to 6 years after treatment start (Ahlskog & Muenter, 2001).

These drug-related complications, combined with the progressive nature of neurodegeneration, pose a therapeutic challenge, where pharmacological interventions are becoming increasingly insufficient to maintain adequate symptom control (Schuepbach et al., 2013). The narrowing therapeutic window between effective symptom management and intolerable side effects necessitates the use of alternative therapeutic approaches for patients with advanced PD, for whom medication alone is no longer optimal.

1.1.3 Deep Brain Stimulation

DBS has emerged as one of the most effective surgical interventions for motor symptom control (Benabid et al., 2009, Fasano & Lozano, 2015). Although PD affects nearly 10 million people worldwide (Jankovic, 2025), only about 300 000 patients have undergone DBS to date (Martinez-Nunez et al., 2025). This disparity reflects both the highly selective eligibility criteria for DBS and persistent barriers to access this treatment, including the limited number of specialized neurosurgical centers, the variability in health insurance

coverage, and patient reluctance toward invasive brain procedures (Bronstein et al., 2011; Okun, 2012; Fenoy & Simpson, 2014).

DBS involves the surgical implantation of electrodes in specific nuclei of the basal ganglia (**Figure 2**). These electrodes deliver high-frequency electrical stimulation (generally 130 Hz) via an implantable pulse generator (Volkmann et al., 2002). In Europe, the STN is the preferred target for DBS in PD due to its central role in basal ganglia circuitry (**Figure 1**).

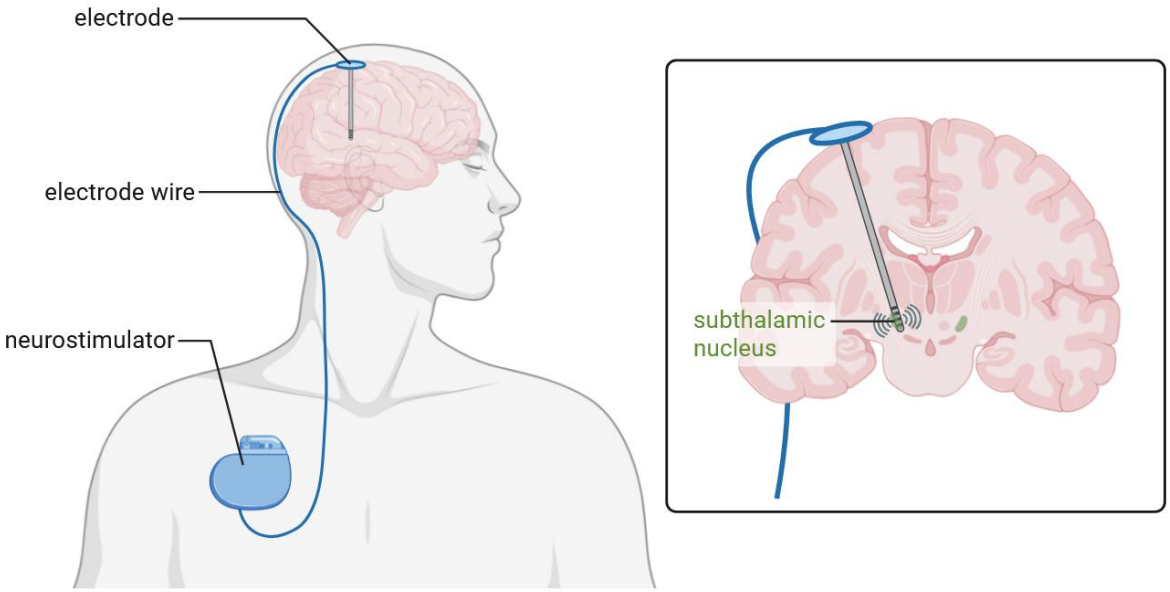

Figure 2. Subthalamic nucleus deep brain stimulation. Schematic representation of STN-targeted DBS in Parkinson's disease. The left panel illustrates the implanted DBS system, comprising an electrode positioned in the STN, connected by a subcutaneous extension to a neurostimulator implanted in the chest or abdomen. This neurostimulator delivers high-frequency electrical pulses to modulate pathological neural activity within the basal ganglia circuits. The right panel depicts a coronal section of the brain highlighting the anatomical location of the subthalamic nucleus (green). I created this figure myself in https://BioRender.com.

STN-DBS yields robust and sustained therapeutic benefits. Meta-analyses reveal an approximately 50% improvement in motor symptoms, as measured by the Unified Parkinson's Disease Rating Scale (UPDRS-III) in the medication-off state, accompanied by a reduction in medication requirements of up to 50% (Limousin et al., 1998; Deuschl et al., 2006). Long-term follow-up studies, spanning more than 15 years, confirm long-lasting efficacy, with maintained improvement in motor function and a sustained ability to reduce dopaminergic medications (Castrioto et al., 2011; Krack et al., 2019). Furthermore, DBS provides continuous symptom control throughout the day, ameliorating the motor fluctuations associated with intermittent medication administration and significantly improving the quality of life for appropriately selected patients (Schuepbach et al., 2013).

Despite its clinical success, the precise mechanisms by which DBS exerts its therapeutic effects remain incompletely understood and likely involve multiple interacting processes.

High-frequency stimulation of the STN is thought to disrupt pathological activity patterns, replacing them with more desynchronized activity that facilitates motor control (McIntyre et al., 2004; Herrington et al., 2016; Neumann et al., 2023). Mechanistically, DBS may act by: (i) suppressing hyperactive neuronal firing through sustained depolarization, (ii) activating cortico-subthalamic axons upstream of the stimulation site, (iii) modulating corticobasal and thalamocortical circuits downstream, and (iv) disrupting or entraining of aberrant oscillatory activity (Chiken & Nambu, 2016; Lozano & Lipsman, 2013).

This multifaceted network-level modulation explains why DBS is not simply an inhibitory lesion mimicry, but rather a dynamic neuromodulatory therapy capable of remodelling the pathological activity of circuits.

1.1.4 DBS Programming

DBS represents a highly effective treatment modality but achieving optimal therapy requires sophisticated programming, i.e., the systematic selection and adjustment of stimulation parameters that maximize therapeutic benefit while minimizing adverse effects (Volkmann et al., 2002). This programming process, also known as monopolar review, involves determining the optimal combination of active electrode contacts, stimulation amplitude (voltage or current), pulse width, and frequency for each individual patient. Modern DBS systems, particularly those with directional leads, offer an exponentially expanding parameter space with millions of possible stimulation configurations (Dembek et al., 2017).

Monopolar review is further complicated by the highly individualized nature of optimal parameters, which depend on factors including electrode placement, patient anatomy and disease progression (Moro et al., 2006). Together, these factors shape the patient-specific therapeutic windows (**Figure 3**).

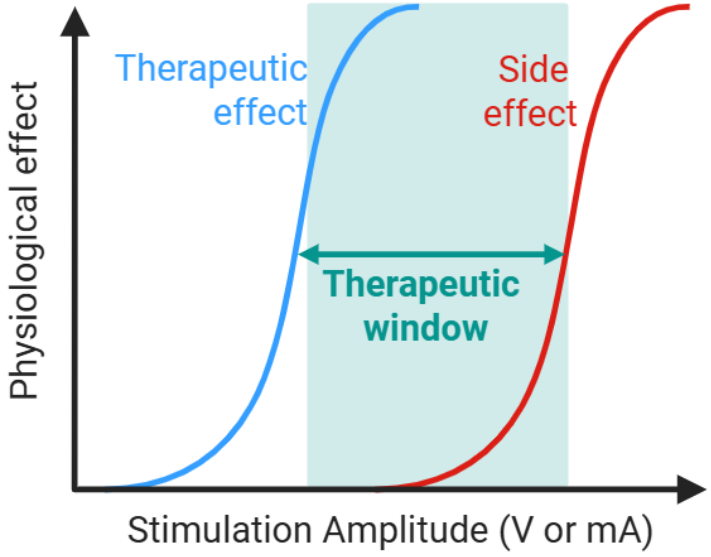

Figure 3. Schematic representation of the clinical response to increasing stimulation amplitudes during a monopolar review. The blue curve illustrates the therapeutic effect (e.g., tremor or rigidity suppression),

which increases with amplitude until saturation. The red curve indicates the emergence of side effects (e.g., dysarthria or dyskinesia) as the electrical field spreads to non-target structures. The therapeutic window (shaded green area) is defined as the range of amplitudes between the inflection point of clinical benefit and the inflection point for adverse events. A wider window allows for safer and more robust chronic stimulation.

Current clinical practice relies heavily on trial-and-error approaches guided by immediate clinical assessment, making the process lengthy and highly dependent on the neurologist's expertise. Studies indicate that DBS programming requires multiple sessions spread over several months, each lasting 1 to 2 hours, representing a significant burden on patients and healthcare systems (Picillo et al., 2016). The complexity of achieving optimal programming is underscored by the fact that 37% of DBS failures are due to an inappropriate choice of parameters rather than surgical or hardware issues (Okun et al., 2005). This highlights the critical importance of developing more efficient and objective approaches to optimize DBS programming, particularly as technology evolves toward increasingly sophisticated stimulation paradigms, such as directional stimulation and closed-loop adaptive systems (Cole & Miocinovic, 2025).

Optimizing DBS therapy is therefore a major obstacle to accessing this highly effective treatment for the millions of PD patients who could potentially benefit from neurosurgical intervention. Addressing this optimization challenge through objective, data-driven approaches represent a crucial step forward in the development of personalized medicine for movement disorders.

1.2 Neural Signals to Guide DBS

The challenges of DBS programming described above motivate the search for more objective, data-driven approaches that can guide contact selection and parameter optimization. One promising avenue involves leveraging electrophysiological recordings to identify neural signatures that predict therapeutic outcomes. At the cellular level, these signals originate from neurons. They are highly specialized cells that generate electrical activity through variations in membrane potential. They communicate via action potentials that propagate along axons and transmit information across synapses to the dendrites of target cells (Kandel et al., 2013). When recorded, these individual cellular events aggregate into population-scale oscillatory patterns, reflecting the coordinated activity of the network across different frequency bands (**Figure 4**), from slow delta waves (1-4 Hz) to fast gamma oscillations (30-100 Hz) (Buzsáki, 2006). The strength and distribution of these oscillations across different frequencies provide crucial insights into information processing, brain function and dysfunction (Ward, 2003; Siegel et al., 2012; Schmidt et al., 2018). Based on this physiological framework, the fundamental premise is straightforward: if pathological neural activity patterns correlate with symptoms, and if DBS efficacy depends on modulating these patterns, then measuring neural oscillations directly might reveal which electrode contacts are optimally positioned to provide therapeutic benefit.

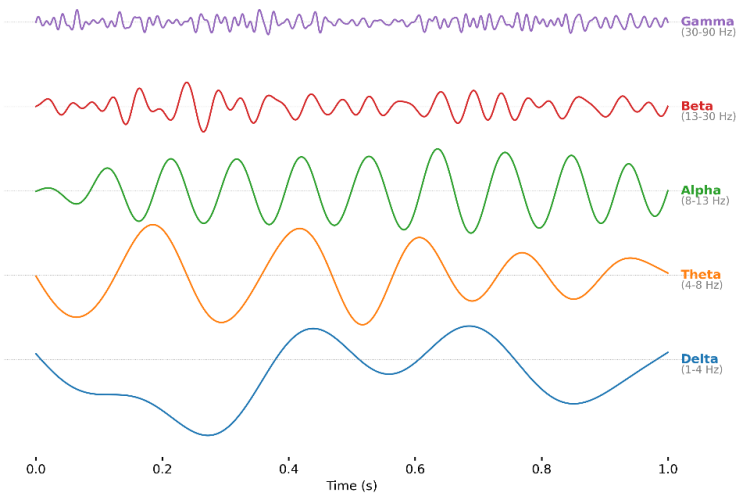

Figure 4. Neural oscillations across frequency bands. Electrophysiological oscillations in the human brain at different frequencies: delta (1-4 Hz), theta (4-8 Hz), alpha (8-12 Hz), beta (13-30 Hz), and gamma (>30 Hz). I created this figure myself in Python.

This electrophysiology-guided approach to DBS programming has gained popularity over the past decade, driven by several converging lines of evidence. First, extensive research has established robust relationships between specific oscillatory patterns and motor symptoms in PD, with beta band activity in the STN being particularly well characterized as a marker of bradykinesia and rigidity (Brown et al., 2001; Kühn et al., 2009). Second, studies have demonstrated that the strength of these pathological oscillations varies spatially within and around the STN, suggesting that electrode contacts positioned in regions with more pronounced oscillatory abnormalities might be better stimulation targets (Zaidel et al., 2010**;** Telkes et al., 2018). Third, pioneering work has shown that electrophysiological features recorded during surgery or in the immediate postoperative period can indeed predict which contacts will ultimately be selected for chronic stimulation (Telkes et al., 2016; Shah et al., 2023; Binder et al., 2023).

Early attempts to use electrophysiology for contact selection focused primarily on beta power as a single predictor. Strelow et al. (2022) showed that STN beta activity could successfully predict clinical efficacy, defined as the absolute improvement in motor symptoms at a fixed stimulation amplitude of 2 mA. While this provided important evidence for the functional relevance of beta oscillations, it focused on a single point of high efficacy rather than the therapeutic window. In contrast, the methodology employed in this thesis evaluates symptoms in 0.5 mA increments to capture the full therapeutic range, moving beyond binary success to a more nuanced prediction of clinical utility. Building on this foundation, more recent studies have validated beta power as a marker for contact selection in the context of directional leads. Fernández-García et al. (2022) compared beta power-guided programming to traditional monopolar review in a clinical trial, demonstrating that LFP-based selection could identify clinically effective contacts with comparable accuracy to extensive clinical testing, while substantially reducing programming time. Similarly, Binder et al. (2023) showed in a randomized controlled pilot study that LFP-guided

programming achieved non-inferior clinical outcomes compared to standard approaches. Finally, D'Onofrio et al. (2025) compared multiple beta-based contact selection strategies with standard clinical programming and found that focusing on signals recorded between two adjacent electrode contacts showed the strongest correlation with the results of a monopolar review. Collectively, these studies establish that single-feature biomarkers like beta power can effectively streamline DBS programming.

However, relying on beta power alone has important limitations. Beta oscillations are not present in all patients, particularly in those with prominent tremor or in the immediate postoperative period when a "stun effect" can temporarily suppress oscillatory activity (Chen et al., 2006). Furthermore, beta power does not capture the full complexity of network dysfunction in PD, which involves alterations across multiple frequency bands and disrupted connectivity between cortical and subcortical structures (Little & Brown, 2014). These observations have motivated the development of multivariate approaches that integrate information from multiple electrophysiological features simultaneously.

Machine learning provides a natural framework for such multivariate prediction, as these algorithms can identify nonlinear relationships between high-dimensional feature sets and clinical outcomes. Recent studies have begun to exploit this potential. Shah et al. (2023) combined multiple features (alpha, beta, gamma and high frequency oscillations) to predict therapeutic windows from intraoperative recordings, achieving a better performance with the features combined rather than beta activity alone. Averna et al. (2023) employed a multivariate kernel density estimation of STN spectral features to identify distinct neurophysiological phenotypes, demonstrating that contacts within certain clusters were more likely to be selected for chronic stimulation. These studies suggest that integrating diverse oscillatory features can provide more robust predictions than any single biomarker in isolation.

Beyond local oscillatory power, network connectivity measures offer additional predictive information. Functional connectivity patterns, particularly between the STN and cortex, reflect the broader network dysfunction underlying PD and may indicate how effectively stimulation at a given location can modulate pathological circuits (Litvak et al., 2011; van Wijk et al., 2022). For instance, contacts positioned in regions with strong connectivity to motor cortex in specific frequency bands might be better suited to normalize aberrant cortico-subcortical communication patterns. Preliminary evidence supports this hypothesis: Hirschmann et al. (2022) demonstrated that STN-cortex coherence patterns recorded in resting state could predict clinical outcomes following DBS, with coherence in multiple frequency bands contributing to prediction accuracy when combined through machine learning models.

The concept of using electrophysiology to guide DBS extends beyond static contact selection to continuous, adaptive parameter adjustment. Adaptive DBS systems monitor neural activity in real time and adjust stimulation intensity based on fluctuations in pathological

biomarkers, most commonly beta power (Little et al., 2013; Tinkhauser et al., 2017). Clinical trials have demonstrated that adaptive DBS can provide symptom control comparable to or better than conventional continuous stimulation while reducing overall stimulation exposure and potentially extending battery life (Oehrn et al., 2024; Bronte-Stewart et al., 2025). Recent work has expanded the set of control signals beyond beta to include gamma oscillations and other frequency-specific markers that may better track different symptom domains or medication states (Colombo et al., 2025; Olaru et al., 2025). While adaptive DBS focuses on temporal optimization of stimulation parameters, the underlying principle that neural oscillations provide actionable information about disease state and therapeutic need is conceptually aligned with using electrophysiology for contact selection.

Despite this progress, a fundamental challenge has limited the development and validation of electrophysiology-guided programming approaches: the scarcity of suitable data. Simultaneous recordings of cortical and subcortical activity in humans are technically demanding, requiring specialized equipment and expertise available in only a handful of research centers worldwide. In this work, I used simultaneous MEG and subthalamic recordings from externalized DBS electrodes. This setup is expensive, requires a magnetically shielded room, and necessitates close collaboration between neurology, neurosurgery, and neuroimaging departments.

The opportunity for combined MEG-LFP recordings exists only within a narrow perioperative window, typically occurring in centers that employ a two-stage surgical approach. In this workflow, the DBS electrodes are implanted during an initial surgery, but the subcutaneous pulse generator is not placed until few days later. During this interval, the electrodes are temporarily externalized using non-ferromagnetic extension cables. These cables allow the leads to be connected to external amplifiers while remaining compatible with the sensitive magnetic environment of the MEG. This configuration provides a unique, though brief (typically one day), opportunity to record direct subcortical activity simultaneously with whole-brain cortical dynamics. Once the second surgery is completed and the pulse generator is implanted, this window closes.

Due to the logistical complexity and the restrictive timeframe of this perioperative period, datasets containing such recordings remain very rare. This scarcity often results in relatively small study cohorts (Litvak et al., 2011; Hirschmann et al., 2011; Oswal et al., 2016), which can limit the generalizability of findings. Consequently, the need for robust, data-efficient computational models becomes crucial for making the most of these limited datasets.

Open science initiatives offer a potential solution to this data scarcity problem. By making well-curated electrophysiological datasets publicly available, research groups with access to these rare recording setups can enable researchers worldwide to develop and test analytical methods, train machine learning models, and validate hypotheses without requiring their own MEG-LFP infrastructure. This democratization of access to specialized data accelerates scientific progress by allowing computational neuroscientists, data scientists, and clinicians

to contribute to the field regardless of whether they work in centers equipped for such recordings (Poldrack & Gorgolewski, 2014; Wilkinson et al., 2016). Public data sharing also enhances reproducibility and transparency, as independent researchers can verify published findings and explore alternative analytical approaches using the same datasets (Nichols et al., 2017).

However, for data sharing to fulfil its potential, datasets must be more than simply available; they must be well-organized, comprehensively documented, and structured according to community standards that facilitate reuse. Raw data files without metadata, preprocessing scripts, or clear documentation of experimental protocols are of limited utility to researchers unfamiliar with the specific recording setup or analysis pipeline. This creates a critical gap: although the need for shareable electrophysiological data is clear, and that some research groups possess such data, the effort required to curate, standardize, and document datasets for public dissemination is substantial and often undervalued in traditional academic metrics. Further, there is a critical need to respect data privacy and the regulations for personal health data.

Against this background, the present thesis addresses both the scientific question of whether electrophysiological signatures can predict DBS outcomes and the practical challenge of making such investigations accessible to the broader research community. A core component of this work was the development of a searchable database that integrates patient metadata with recording parameters, providing a streamlined interface for identifying and extracting specific data subsets. This database is already actively utilized by researchers to facilitate cross-study comparisons and longitudinal analyses. By systematically curating this unique dataset of simultaneous MEG and LFP recordings, applying machine learning methods to predict therapeutic windows from multivariate electrophysiological features, and validating these predictions in an independent cohort, this work contributes both to the methodological infrastructure of the field and to our understanding of how neural oscillations can inform clinical decision-making in DBS programming.

1.2.1 Neural Signal Acquisition: from Cortical to Subcortical Recordings

Measuring neural oscillations in humans requires sophisticated recording techniques capable of capturing electrical activity at various spatial scales, from individual neurons to entire brain networks. Different recording modalities offer distinct advantages for interrogating neural dynamics, each with characteristic strengths that make them suited to specific research questions. For studying movement disorders like PD, understanding both cortical and subcortical network activity is essential, as the pathophysiology involves dysfunction across distributed cortico-basal ganglia circuits. This section describes the two complementary electrophysiological approaches that, when combined, enable comprehensive characterization of these networks: MEG for cortical recordings and LFP for subcortical measurements.

Magnetoencephalography

MEG detects the magnetic fields generated by synchronized postsynaptic currents in cortical neurons (Singh, 2014; Baillet, 2017). When large populations of pyramidal neurons are activated synchronously, their intracellular currents sum to produce magnetic fields measurable outside the skull. Modern MEG systems employ arrays of highly sensitive superconducting quantum interference devices (SQUIDs) to detect these magnetic fields, which are typically on the order of tens to hundreds of femtoteslas. To achieve this sensitivity, MEG recordings are conducted in magnetically shielded rooms that attenuate environmental noise from power lines, vehicles, and other sources of magnetic interference (**Figure 5**).

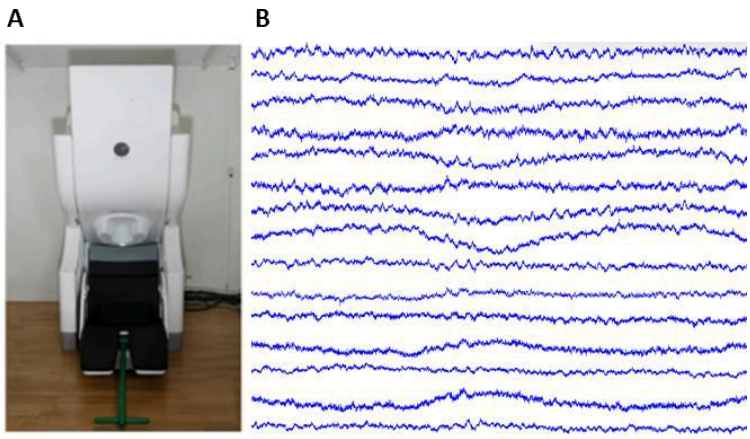

Figure 5. **Magnetoencephalography.** A) 306-channel MEG system (MEGIN) used for the non-invasive recording of cortical magnetic fields. The patient is seated in an upright position within a magnetically shielded room suppressing environmental noise. B) Representative raw MEG traces from a subset of sensors.

The primary strength of MEG lies in its combination of excellent temporal resolution and good spatial resolution for cortical sources. With sampling rates typically ranging from 1000 to 2000 Hz, MEG can capture neural dynamics at millisecond precision, enabling the study of rapid oscillatory fluctuations and transient network interactions that characterize motor control and cognition (Gross, 2019; Schoffelen & Gross, 2009). Spatial resolution typically ranges from several millimeters to a few centimeters depending on source depth, signal-to-noise ratio, and the sophistication of source reconstruction algorithms employed (Hillebrand & Barnes, 2002; Baillet et al., 2001). MEG's sensitivity to tangentially oriented dipoles, such as those produced by neurons in the cortical sulci, makes it particularly well-suited for detecting activity from motor cortex, which lies primarily within the central sulcus (Hämäläinen et al., 1993, Hillebrand & Barnes, 2002).

While MEG is often described as a cortical imaging technique, its sensitivity extends beyond purely cortical structures. Indeed, MEG can detect activity from cerebellar cortex and certain thalamic nuclei (Dalal et al., 2009). These subcortical structures can generate measurable magnetic fields when large populations of neurons are synchronously active, though the

signal-to-noise ratio is generally lower than for cortical sources. The feasibility of detecting such deeper sources depends critically on source strength, orientation, and the ability to average across a sufficient number of repetitions to reduce noise.

Understanding MEG's capabilities and limitations requires consideration of both the forward and inverse problems of electromagnetic source imaging. The forward problem involves calculating the electromagnetic fields at sensor locations given a known configuration of neural sources. It essentially models how activity at specific brain locations would manifest in the sensor array. This forward modelling can be solved accurately using physics-based models that account for sensor geometry, head anatomy, tissues conductivities and the laws of electromagnetic propagation (Sarvas, 1987; Hämäläinen et al., 1993). Common approaches include boundary element methods and finite element methods, which differ in their treatment of tissue boundaries and conductivity variations.

The inverse problem involves determining source configurations from measured sensor data and is considerably more challenging. This problem is mathematically ill-posed: an infinite number of source configurations could theoretically produce the same sensor measurements (Kirsch, 1988). To obtain unique solutions, inverse methods must incorporate additional constraints or assumptions about source properties, such as smoothness, sparsity, or spatial extent. Various algorithms have been developed to address this inverse problem, including minimum norm estimation, which finds the source distribution with minimal overall energy; beamforming, which constructs spatial filters to isolate activity from specific locations; and Bayesian approaches, which incorporate prior knowledge about likely source configurations (Van Veen et al., 1997; Baillet et al., 2001; Wipf & Nagarajan, 2009).

For deep brain structures like the subthalamic nucleus, the inverse problem becomes particularly challenging. Magnetic fields attenuate rapidly with distance from their source, meaning that deep structures produce progressively weaker signals at the sensors (Cohen, 2014; Nunez & Srinivasan, 2006). Additionally, volume conduction effects cause electrical currents to spread through the conductive brain tissue, blurring the spatial signature of deep sources and reducing the specificity with which source reconstruction algorithms can localize them (Schoffelen & Gross, 2009; Bastos & Schoffelen, 2016). While advanced source reconstruction methods can partially mitigate these limitations, the spatial resolution of MEG source localization degrades substantially with depth, making direct detection of STN activity challenging even with sophisticated algorithms (Hillebrand & Barnes, 2002; Brookes et al., 2008).

Local Field Potentials from Deep Brain Stimulation Electrodes

LFP recordings from DBS electrodes provide direct access to subcortical structures that are difficult to measure non-invasively. When electrodes are implanted for therapeutic DBS, they pass through brain tissue and terminate within the target nucleus. During the perioperative period between electrode implantation and pulse generator placement, these

electrodes can be temporarily externalized, meaning they are connected via extension cables to amplifiers. This configuration enables direct measurement of electrical activity within and around the target structure.

LFPs capture the summed synaptic activity of neural populations within a limited spatial extent around each electrode contact. The spatial reach of LFP recordings is determined by the biophysics of extracellular current flow: synaptic potentials generate local current sources that decrease in amplitude with distance from the generating neurons. Empirical and modelling studies suggest that LFPs primarily reflect activity within approximately 250 to 400 micrometers of the recording contact, though the exact spatial extent depends on the size and synchrony of the active neural population (Buzsáki et al., 2012; Einevoll et al., 2013; Pesaran et al., 2018). This highly localized recording provides a window into the intrinsic oscillatory dynamics of subcortical nuclei, revealing pathological activity patterns that would be difficult or impossible to detect with non-invasive methods (Miller et al., 2007).

However, this spatial specificity comes with an inherent limitation: LFPs provide only a restricted view of brain activity, limited to the immediate vicinity of the implanted electrodes (**Figure 6**). Standard DBS electrodes have four to eight contacts spaced 0.5 to 1.5 millimeters apart, providing sampling of a narrow cylinder of tissue. This configuration cannot assess activity across the broader cortical networks that interact with subcortical structures, nor can it characterize how these interactions are organized across the cortical surface (Kramer et al., 2008; Friston et al., 2015; Herreras, 2016). Additionally, LFP signals can be contaminated by reference electrode artifacts, volume conduction from distant sources, and stimulation artifacts when stimulation and recording occur simultaneously.

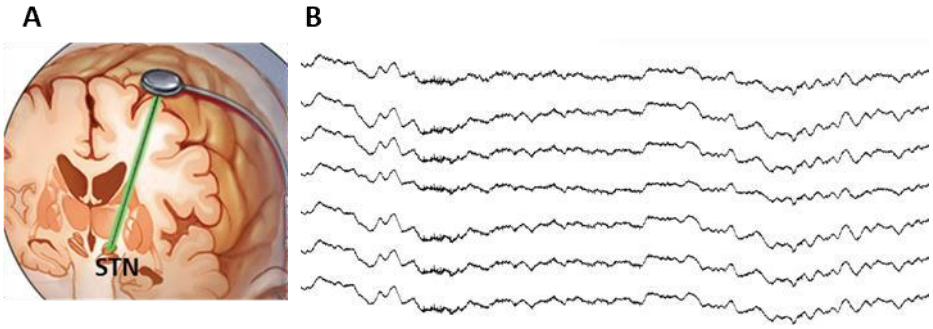

Figure 6. **Local field potential (LFP) recordings**. A) Schematic representation of a deep brain stimulation electrode implanted in the subthalamic nucleus (STN). During the perioperative interval, externalized electrodes allow for the direct recording of intracranial activity before the pulse generator is implanted. B) Representative LFP traces obtained from the STN.

Complementary Strengths of Combined MEG-LFP Recordings

The complementary nature of MEG and LFP recordings motivates their combined use: MEG provides whole-head cortical coverage but limited access to deep structures, while LFPs offer direct subcortical measurements but restricted spatial sampling. By recording both

modalities simultaneously, researchers can overcome the limitations inherent in each technique. MEG-LFP recordings capture cortical dynamics with good spatial and temporal resolution while simultaneously providing measurements of subcortical activity at the electrode locations. This dual-recording paradigm enables investigation of cortico-subcortical communication patterns that neither method could characterize in isolation (Hirschmann et al., 2011; Litvak et al., 2011; van Wijk et al., 2016).

Practically, combining MEG and LFP enables several specific analyses that leverage the strengths of both modalities. First, the direct STN measurements can serve as a reference point for validating MEG source reconstruction attempts to localize deep brain activity, helping to assess the accuracy and limitations of such reconstructions (Litvak & Friston, 2008; Oswal et al., 2016). Second, connectivity analysis between LFP and source-reconstructed MEG signals quantifies functional connectivity between specific subcortical locations and distributed cortical networks, revealing frequency-specific coupling patterns across cortico-basal ganglia circuits (Hirschmann et al., 2011; Litvak et al., 2011). Third, simultaneous recordings allow investigation of how therapeutic interventions, such as dopaminergic medication or DBS, modulate both local subcortical oscillations and their coupling to cortical activity, providing insights into network-level mechanisms of therapeutic action (Oswal et al., 2016; Abbasi et al., 2018).

Despite the scientific value of combined MEG-LFP recordings, such datasets remain scarce. The technical requirements mean that only a handful of research centers worldwide can routinely acquire these data (Hirschmann et al., 2011; Litvak et al., 2011; van Wijk et al., 2016; Oswal et al., 2016). The resulting dataset published in Study 1 (Rassoulou et al., 2024), contains cortical and subcortical signals and constitute the foundation for study 2 to develop predictive model for therapeutic windows.

1.2.2 Electrophysiological Biomarkers in Parkinson's Disease

The electrophysiological signatures captured by combined cortico-subcortical recordings have revealed a complex landscape of oscillatory biomarkers correlated with specific motor symptoms and therapeutic responses (Hirschmann et al., 2011; Hirschmann et al., 2013; Neumann et al., 2016). Understanding these neural signatures first requires grasping how oscillatory activity is quantified and interpreted within the context of brain function and dysfunction.

Neural oscillations represent rhythmic fluctuations in the electrical activity of neural populations, arising from the synchronized firing patterns of thousands, or even millions, of interconnected neurons. These oscillations constitute a fundamental mechanism for coordinating the flow of information across brain networks, with different frequencies underlying distinct computational functions (Mathalon & Sohal, 2015; Bonnefond et al., 2017; Wang, 2010). Power spectral analysis quantifies these oscillatory patterns by

decomposing complex neural signals into their constituent frequency components (Welch, 1967). Power spectral density measures the distribution of signal power across frequencies, revealing the amount of energy contained in the neural signal at each frequency. This transformation from the time domain to the frequency domain provides a quantitative assessment of oscillatory intensity that can be compared across different conditions, patients, and time points. In movement disorders, this frequency-domain representation is particularly valuable because specific oscillatory patterns correlate with distinct symptoms and therapeutic responses, offering objective biomarkers of disease severity and treatment efficacy.

Beta Oscillations: The Primary Biomarker

Beta oscillations (13–30 Hz) are the most well-established electrophysiological biomarker in PD. In a healthy brain, beta activity plays a crucial role in maintaining the current motor state and preventing unwanted movements. However, in PD, excessive beta power in the STN creates a pathologically stable state that impairs the initiation and execution of movements (Oswal et al., 2021). This abnormal beta synchronization is strongly correlated with motor symptoms such as bradykinesia and rigidity (Brown et al., 2001; Kühn et al., 2009; Neumann et al., 2016).

Recent advances have revealed that beta activity does not occur as continuous oscillations, but rather as transient bursts: brief episodes of high-amplitude activity typically lasting 100 to 300 milliseconds (Tinkhauser et al., 2017). In a healthy motor system, these beta bursts are short and infrequent, allowing for a smooth transition between motor states. In PD, beta bursts lengthen and become more frequent, leading to a pathological stabilization of the motor network (Pauls et al., 2022). The duration and amplitude of these bursts are more specific markers of motor impairment than average beta power, with longer bursts being particularly associated with more severe bradykinesia (Torrecillos et al., 2018; Feingold et al., 2015).

The therapeutic value of beta oscillations is highlighted by their response to treatment. Dopaminergic drugs and DBS effectively suppress excessive beta synchronization, with the degree of reduction in beta oscillations being closely correlated with symptom improvement (Kühn et al., 2004; Ray et al., 2008; Weinberger et al., 2006). Adaptive DBS systems that selectively target prolonged beta bursts can fragment them into shorter bursts that resemble more physiological patterns. This demonstrates that restoring normal beta dynamics rather than simply suppressing all beta activity is the basis of therapeutic efficacy (Tinkhauser et al., 2017).

Network Connectivity and Coherence

PD is fundamentally a network disorder affecting distributed corticobasal circuits rather than isolated brain regions. Therefore, quantifying connectivity between brain areas provides crucial information beyond local oscillatory power. Coherence, which measures the

consistency of phase relationships between oscillations in different brain areas, is a key indicator of functional connectivity (Bastos & Schoffelen, 2016). High coherence indicates that two regions maintain a stable phase relationship over time, suggesting functional coupling and information exchange.

In PD, pathological beta coherence appears both within basal ganglia structures and between the STN and the motor cortex (Hirschmann et al., 2013; Litvak et al., 2011; Oswal et al. 2013; Rassoulou et al., 2025). One widely discussed hypothesis is that these signals index a hyper-synchronized network state that restricts the flexible motor control necessary for smooth movement execution (Brown, 2003). According to this model, exaggerated cortico-subcortical beta coherence may lock the motor system into rigid patterns, potentially hindering the dynamic reorganization required for movement initiation and adaptation. However, the interpretation of these oscillatory peaks remains a subject of ongoing investigation. Recent evidence has identified similar beta coherence peaks in patients with obsessive-compulsive disorder who do not exhibit motor impairments (Winkler et al., 2026). This suggests that such connectivity might represent a physiological feature of subcortico-cortical communication that becomes pathologically amplified or altered in PD, rather than being a purely pathological marker.

Furthermore, while both levodopa and DBS have been shown to modulate these network synchronization patterns, the direct relationship between these changes and clinical outcomes is complex. Although these treatments often reduce excessive beta coherence, a consistent correlation between the magnitude of coherence reduction and the degree of motor symptom improvement has not been firmly established (Van Wijk et al., 2017). This suggests that while restoring flexible network dynamics may be an important component of therapy, the therapeutic efficacy of DBS likely involves a more nuanced modulation of aberrant communication patterns between brain regions (Neumann et al., 2023).

Beyond Beta: Multi-Frequency Biomarkers

Although beta oscillations are one of the most prominent markers in the pathophysiology of PD, the disease affects neural dynamics across the entire frequency spectrum. Each frequency band provides distinct biomarkers for different symptomatic domains, thus allowing for a comprehensive picture of the heterogeneous manifestations of PD.

Alpha oscillations (8–12 Hz) have emerged as promising electrophysiological biomarkers for PD. Recent studies using electroencephalography (EEG) or MEG have demonstrated that individuals with PD often exhibit altered alpha oscillatory activity compared to healthy controls, including changes in alpha power, peak frequency, and power asymmetry across brain regions (Rocha et al. 2025; Zhao et al. 2025; Ambrosanio et al. 2025; Norouzi et al. 2025). For example, reduced parietal alpha asymmetry and region-specific decreases in alpha power have been linked to motor symptoms such as tremor, gait disturbances, and freezing, as well as to cognitive deficits in attention and orientation (Rocha et al. 2025; Zhao et al. 2025). Meta-analytic evidence further supports that PD patients tend to show higher

alpha power and slower alpha peak frequency, with these alterations correlating with non-motor symptoms, particularly cognitive decline (Norouzi et al. 2025; Ye et al., 2022). Additionally, novel measures such as alpha band nonlinearity have shown potential for distinguishing PD patients from healthy individuals, even in early disease stages (Özkurt, 2024). Collectively, these findings highlight the utility of alpha oscillations as an accessible biomarker for the diagnosis and monitoring of PD progression.

Gamma oscillations (> 35 Hz) are key markers of hyperkinetic symptoms, including levodopa-induced dyskinesias. In the dopamine-depleted state, gamma activity is often suppressed (Guerra et al., 2020). However, under dopaminergic treatment, gamma power can become excessive, particularly in the 60–90 Hz range (Cassidy et al., 2002; Cheyne et al., 2008; Lofredi et al., 2018). This increase in gamma activity is directly correlated with the severity of involuntary movements and results primarily from dopaminergic overstimulation (Litvak et al., 2012; Swann et al., 2016; Wiest et al., 2021). Recent work has improved the distinction between narrowband gamma oscillations associated to voluntary movement and broader gamma activity, the latter providing a potential feedback signal for closed-loop modulation to facilitate movement (Colombo et al., 2025; Olaru et al., 2025; Oehrn et al., 2024).

Theta oscillations and tremor frequency oscillations (4–8 Hz) are direct electrophysiological correlates of resting tremor in PD (Hirschmann et al., 2013). These oscillations create coherent activity linking the STN, motor cortex, cerebellum, and peripheral muscles within a pathological oscillatory loop (Steina et al., 2025). The frequency of these oscillations corresponds to the clinical tremor frequency, generally around 4–6 Hz, and their amplitude is correlated with tremor severity (Hirschmann et al., 2013; Muthuraman et al., 2012). Recent studies have shown that tremor-related oscillations can be distinguished from voluntary movements (Todorov et al., 2024) and selectively targeted for suppression while preserving physiological motor control signals (Schreglmann et al., 2021).

High-frequency oscillations (200–400 Hz) are a recently discovered biomarker with emerging clinical relevance. These very fast oscillations show promise for differentiating movement phases and predicting therapeutic responses. Although their precise relationship to specific symptoms remains under investigation, converging evidence suggest that they may reflect the activity of small neural populations and serve as markers for identifying symptom severity (Özkurt et al., 2011; Wang et al., 2014; Hirschmann et al., 2016) and even guide optimal placement of stimulation electrodes in epilepsy (Cimbalnik et al., 2016; Kanai et al., 2025).

This multi-frequency perspective underscores that the pathophysiology of PD involves complex alterations across the entire oscillatory spectrum. Different frequency bands reflect distinct symptomatic domains and provide complementary information for a comprehensive characterization of the disease. Understanding these specific frequency signatures is crucial for developing personalized therapeutic approaches capable of targeting the heterogeneous

manifestations of PD in each patient. The integration of biomarkers across multiple frequencies provides a more complete picture of disease state and response to treatment than single oscillatory marker taken in isolation, paving the way for multi-dimensional approaches to the optimization of DBS programming and adaptive therapy.

1.3 Machine Learning

The integration of multimodal electrophysiological signals with advanced analytical approaches represents a fundamental shift, moving from descriptive neuroscience to data-driven predictive medicine. This transformation relies on machine learning, a branch of artificial intelligence that enables computers to discover patterns in data and make predictions without explicit programming (Bishop, 2006; Mitchell, 2013; Russell & Norvig, 2016). Essentially, machine learning addresses the challenge of extracting relevant information from complex multidimensional datasets. It is thus particularly well-suited to analyzing the rich electrophysiological signatures captured by combined MEG-LFP recordings.

Machine learning has revolutionized modern medicine by enabling computers to learn from medical data and improve clinical decision-making (Deo, 2015; Rajkomar et al., 2019). The exponential growth of health data from electronic health records, high-resolution medical imaging and continuous physiological monitoring, has created unprecedented opportunities for computational approaches capable of identifying subtle patterns imperceptible to human observation. In clinical neuroscience, machine learning algorithms have demonstrated remarkable effectiveness in predicting disease progression, optimizing treatment strategies, and discovering new biomarkers (Vieira et al., 2017; Glaser et al., 2019; Esteva et al., 2017). These applications demonstrate how computational approaches can enhance clinical expertise by providing objective, data-driven recommendations

A key advantage of machine learning is that it does not require explicit mathematical modelling of the underlying biological processes. Instead, algorithms learn statistical relationships directly from data, making them applicable even when mechanisms are incompletely understood. This learning process does not involve deriving first-principles equations or mechanistic models; instead, it relies on statistical pattern recognition. This data-driven approach is particularly valuable in medicine which has a lot of biological complexity.

Machine learning encompasses various paradigms, each suited to different types of problems. Supervised learning, the approach most relevant to this thesis, learns mappings between input features and target variables of interest by analysing labelled training datasets (Bishop, 2006; Hastie et al., 2009). For example, given electrophysiological recordings paired with therapeutic windows from past patients, supervised algorithms can learn to predict outcomes for new patients based on their neural signatures.

Unsupervised learning, in contrast, discovers hidden structure in unlabelled data, such as identifying patient subgroups with distinct disease phenotypes (Hastie et al., 2009). Reinforcement learning optimizes sequential decisions by learning from action consequences, with emerging applications in adaptive therapy and personalized treatment planning (Obermeyer & Emanuel, 2016; Sutton & Barto, 2018). In the context of DBS programming, supervised learning is particularly valuable because clinical outcomes from monopolar reviews provide the labelled training data needed to learn relationships between electrophysiological features and therapeutic windows.

1.3.1 Neural Encoding and Decoding

Neural encoding and decoding provide a conceptual framework for understanding how machine learning can be applied to electrophysiological data. Encoding describes how external stimuli, behavioural states, or clinical conditions are systematically represented by patterns of neural activity within distributed brain circuits (Dayan & Abbott, 2001; Paninski et al., 2007). This representation emerges from the intrinsic properties and connectivity of neural circuits and occurs automatically because of brain function. Importantly, encoding happens whether we understand the underlying principles: a visual stimulus evokes specific patterns of activity in visual cortex regardless of whether neuroscientists have characterized those patterns. Understanding encoding principles can provide insights into brain function, but such understanding is not required for encoding to occur (Quian Quiroga & Panzeri, 2009).

Neural decoding, conversely, refers to the process of inferring information from neural activity patterns (Kriegeskorte & Douglas, 2019; Naselaris et al., 2011). Given recorded neural signals, decoding attempts to determine what stimulus was presented, what movement was intended, or what cognitive state the subject is experiencing. Critically, successful decoding does not require knowing how information is encoded, it only requires finding statistical relationships between neural patterns and the variables of interest (Holdgraf et al., 2017). For example, one can decode intended arm movements from motor cortical activity to control a prosthetic limb without understanding precisely how the brain encodes movement parameters. This separation between encoding (how the brain represents information) and decoding (how we extract information from brain signals) is crucial: machine learning excels at decoding even when encoding mechanisms remain poorly understood.

As mentioned in the previous chapter about electrophysiological biomarkers in PD, there are characteristic neural signatures that are correlated with symptom severity and therapeutic response. From these neural patterns, we can decode pathological states. For instance, the severity of bradykinesia, the presence of tremor, or whether a patient is ON or OFF medication. These are states that are reflected in neural activity. What we cannot directly decode are optimal treatment parameters themselves, because parameters like stimulation amplitude or contact selection are not encoded in brain activity, they are external

interventions we apply. Instead, we focus on decoding neural markers that correlate with therapeutic efficacy. If specific neural signatures can predict which contacts will provide the widest therapeutic windows, they become primary tools for guiding electrode selection. The underlying logic follows a precise chain: pathological states are reflected in localized neural activity; electrodes positioned to best modulate these specific patterns are more effective; and therefore, these neural signatures can be utilized to predict optimal contact configurations and clinical outcomes (Hirschmann et al., 2022; Merk et al., 2022; Shah et al., 2023; Oliveira et al., 2023).

Practically implementing neural decoding for clinical applications involves two distinct steps: feature extraction and statistical decoding. Feature extraction transforms raw neural signals to create a balance between exhaustiveness (e.g., capturing all potentially relevant neural signatures) and parsimony (e.g., avoiding overfitting to noise in small training datasets) (Guyon & Elisseeff, 2003). Decoding, the subsequent step, uses these features to predict outcomes of interest using machine learning algorithms. The quality of features constrains what can be learned because poor features will yield poor predictions regardless of algorithm sophistication. Feature extraction and decoding serve fundamentally different purposes and should be recognized as separate stages of the analytical pipeline (Glaser et al., 2020).

Modern decoding approaches developed for DBS have leveraged the full richness of simultaneously recorded cortical and subcortical signals, moving beyond single-channel analysis to characterize network-wide activity profiles (Merk et al., 2025). This multi-regional decoding allows us to grasp the distributed nature of PD pathophysiology, recognizing that therapeutic benefit depends not only on local STN activity, but also on how stimulation modulates the broader corticobasal network (Hirschmann et al., 2011; Litvak et al., 2011; Neumann et al., 2023). Recent advances in population-scale decoding have also demonstrated that profiles distributed across multiple recording sites and frequency bands can provide more robust predictions than any single characteristic taken in isolation (Pandarinath et al., 2018; Glaser et al., 2020).

Machine learning algorithms can identify complex, nonlinear relationships between these distributed features and clinical outcomes, potentially capturing predictive patterns that would be difficult to specify through expert knowledge alone (Pandarinath et al., 2018). However, the value of these approaches depends critically on generalization: models must perform well on new patients not included in training data, requiring careful validation and attention to overfitting risks, particularly given the limited sample sizes typical of invasive electrophysiology studies.

1.3.2 Supervised Machine Learning in Clinical Neuroscience

The supervised learning workflow involves several key stages. It begins with feature engineering, a critical process that transforms raw, high-dimensional electrophysiological recordings into compact, informative representations (Domingos, 2012). By extracting specific biomarkers, feature engineering defines what features the model will use to interpret brain states. Consequently, the quality of these features fundamentally constrains the patterns the algorithm can learn, making this stage a primary determinant of model success.

Second, model selection involves choosing an algorithmic approach suited to the problem. Different families of models rely on different assumptions about the structure of this association, each with distinct advantages and limitations. Linear models (e.g., logistic regression) assume that outcomes depend on weighted combinations of features, thus offering robustness and clear interpretability but potentially failing to capture complex, non-linear biological interactions (Bishop, 2006). Conversely, tree-based methods (e.g., random forests) recursively partition the space of explanatory variables to identify localized decision rules. These non-linear approaches can naturally model complex interactions between neural signatures, though often at the cost of reduced transparency (Breiman, 2001; Friedman, 2001).

Once a model is selected, training the model optimizes its internal parameters to minimize prediction errors. A fundamental challenge in this phase is overfitting, where an algorithm memorizes the specific characteristics of the training data instead of learning generalizable biological patterns (Hastie et al., 2009). This problem is particularly relevant in clinical neuroscience, where patient cohorts are often small. To detect overfitting, validation strategies are essential: the model's performance on held-out data (examples not used during training) provides an estimate of how well it will generalize to new patients (Stone, 1974). Cross-validation, where data are repeatedly partitioned into training and test sets, offers a systematic approach to assessing generalization and selecting hyperparameters (Willmott & Matsuura, 2005).

This supervised framework has already demonstrated remarkable success in clinical neuroscience. In brain-computer interfaces, decoding algorithms translate cortical activity into control signals, enabling paralyzed patients to control prostheses with thought alone (Lebedev & Nicolelis, 2006; Hochberg et al., 2006). Similarly, seizure prediction systems use these methods to identify pre-seizure states from EEG, thus facilitating preventive interventions (Mormann et al., 2007; Kuhlmann et al., 2018). Voice prostheses decode intentional speech from intracranial recordings, offering the prospect of restoring communication in patients with severe speech disorders (Anumanchipalli et al., 2019; Chartier et al., 2018). Applying these same principles to DBS contact selection represents a promising avenue for improving standard care. By learning the multivariate relationships between MEG-LFP characteristics and therapeutic outcomes, supervised algorithms can

potentially identify optimal electrode contacts and stimulation parameters more effectively than traditional trial-and-error monopolar reviews (Shah et al., 2023; Merk et al., 2022; Picillo et al., 2016).

1.4 Aims of Thesis

The primary aim of this thesis was to demonstrate the feasibility of predicting the therapeutic window of DBS electrode contacts using electrophysiological signatures; specifically, STN-power and STN-cortex coherence across multiple frequency bands. While decades of research have characterized the oscillatory signatures of PD pathophysiology, these signatures have been remained largely confined to scientific research, without guiding clinical decision-making. Demonstrating such predictive capability could improve DBS programming by enabling data-driven contact selection based on neural oscillation patterns, potentially reducing the time-intensive monopolar review process required for each patient.

To achieve this primary aim, three specific interdependent objectives were pursued:

1) Dataset curation and open science contribution

When I began this work, simultaneous MEG and LFP recordings from PD patients existed but had not been organized in a format suitable for systematic machine learning analysis. Therefore, the first objective was to curate these unique data into a structured, searchable database following the Brain Imaging Data Structure (BIDS) standard, along with comprehensive metadata, preprocessing pipelines, and documentation. These recordings cover resting state and motor tasks across medication states. By making this dataset publicly available on OpenNeuro, Study 1 (Rassoulou et al., 2024) addresses the scarcity of such recordings and enables broader scientific community to explore subcortico-cortical network dynamics in PD.

2) Identifying predictive electrophysiological signatures

Using the curated dataset, I continued by investigating whether and which electrophysiological features can predict the therapeutic window of individual electrode contacts. I applied extreme gradient boosting combined with feature selection to identify oscillatory signatures most informative about therapeutic windows. The goal was not only to demonstrate the feasibility of such predictions but also to characterize which specific neural patterns (frequency bands and brain regions) contribute most to predicting therapeutic windows. This feature identification provides insights into the biomarkers of PD that could be related to the identification of contact selection.

3) Validation in an independent cohort

The last objective was to validate the predictive model on an independent cohort of patients to assess its generalizability. I collected new MEG-LFP data from eight additional PD patients in resting state. By applying the model trained on the original dataset to these

previously unseen patients, this validation tested whether the relationship between electrophysiological signatures and therapeutic windows is robust across different individuals. Such generalization is a critical requirement for any potential clinical application, as a model that only works on its training data would have no practical utility.

Together, these three objectives form a cohesive research program that progresses from data infrastructure (curation) to discovery (feature identification) to validation (independent cohort testing). The thesis establishes proof-of-concept that resting-state neural oscillations recorded from the subthalamic nucleus and cortex can inform DBS contact selection.

2. Study 1: Exploring the electrophysiology of Parkinson's disease with magnetoencephalography and deep brain recordings

scientific data

Check for updates

OPEN

DATA DESCRIPTOR

Exploring the electrophysiology of Parkinson's disease with magnetoencephalography and deep brain recordings

Fayed Rassoulou[1], Alexandra Steina[1], Christian J. Hartmann[1,2], Jan Vesper[3], Markus Butz[1], Alfons Schnitzler[1,2,4] & Jan Hirschmann[1,4] ✉

Aberrant information processing in the basal ganglia and connected cortical areas are key to many neurological movement disorders such as Parkinson's disease. Investigating the electrophysiology of this system is difficult in humans because non-invasive methods, such as electroencephalography or magnetoencephalography, have limited sensitivity to deep brain areas. Recordings from electrodes implanted for therapeutic deep brain stimulation, in contrast, provide clear deep brain signals but are not suited for studying cortical activity. Therefore, we combine magnetoencephalography and local field potential recordings from deep brain stimulation electrodes in individuals with Parkinson's disease. Here, we make these data available, inviting a broader scientific community to explore the dynamics of neural activity in the subthalamic nucleus and its functional connectivity to cortex. The dataset encompasses resting-state recordings, plus two motor tasks: static forearm extension and self-paced repetitive fist clenching. Most patients were recorded both in the medicated and the unmedicated state. Along with the raw data, we provide metadata on channels, events and scripts for pre-processing to help interested researchers get started.

Background & Summary

Parkinson's disease (PD) is a neurological movement disorder characterised by degeneration of dopaminergic neurons in the midbrain, leading to impaired information processing in the basal ganglia and associated cortical areas[1]. As both subcortical and cortical signalling is affected, it is important to study the electrophysiology of extended subcortico-cortical networks[2]. While this is feasible in animal models, it is challenging in patients. Non-invasive techniques, such as electroencephalography (EEG) and magnetoencephalography (MEG), struggle to obtain signals from deep brain locations that are critical for understanding the disease. Deep brain stimulation (DBS) electrodes, in contrast, provide direct access to these areas when used for recording rather than stimulation. Yet, they are not suited for studying cortical activity.

Here, we provide a dataset allowing for a range of analyses in patients, and the study of subcortico-cortical networks in particular. This dataset contains simultaneous MEG and deep brain recordings of 20 PD patients who were implanted with electrodes for therapeutic deep brain stimulation of the subthalamic nucleus (STN) the day before measurement. We acquired data from most subjects in both the medicated and unmedicated state and quantified motor symptom severity using the Unified Parkinson's Disease Rating Scale (UPDRS) part III[3]. Figure 1 depicts an overview of the study design.

The combination of MEG and deep brain recordings is rare and available in only a few centers worldwide[4–6]. Being a highly limited resource, such data remain unavailable to most researchers in the field unless they are shared with open access. In doing so, we hope to excel the exploration of neural activity in human basal ganglia-cortex loops.

[1]Institute of Clinical Neuroscience and Medical Psychology, Medical Faculty, Heinrich Heine University, 40225, Düsseldorf, Germany. [2]Center for Movement Disorders and Neuromodulation, Department of Neurology, Medical Faculty, Heinrich Heine University, 40225, Düsseldorf, Germany. [3]Department of Functional Neurosurgery and Stereotaxy, Medical Faculty, Heinrich Heine University, 40225, Düsseldorf, Germany. [4]These authors contributed equally: Alfons Schnitzler, Jan Hirschmann. ✉e-mail: Jan.Hirschmann@med.uni-duesseldorf.de

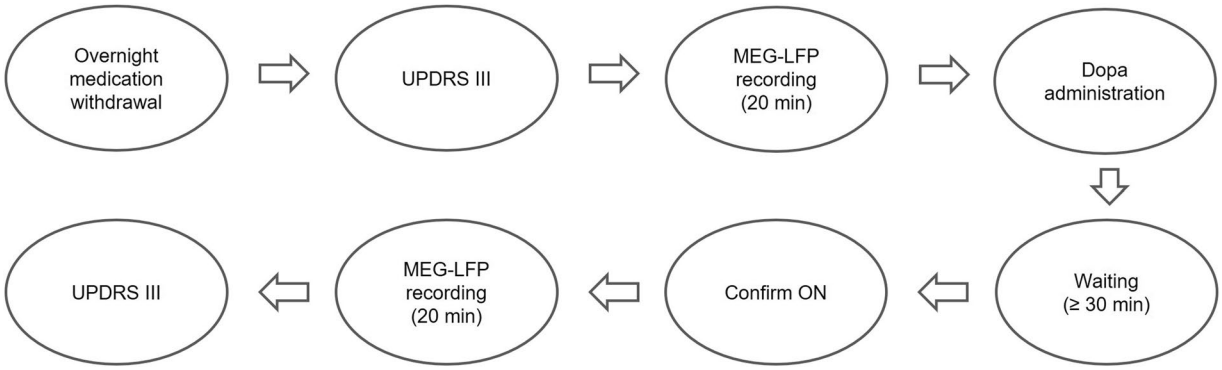

Fig. 1 Study design. The measurements were performed the day after electrode implantation using externalized leads. The pulse generator was implanted the day after the measurement.

The data offer several possibilities for sophisticated analyses, including verification and extension of previous analyses. The original aims of the study were to uncover resting-state STN-cortex networks[7] and to elucidate the modulations of brain activity associated with voluntary hand movement[8] and tremor[9,10]. The data have further been used in studies exploring the predictive potential of electrophysiological signals with respect to individual symptoms and therapeutic benefit, leveraging machine learning techniques[11–13]. Besides building on these previous analyses, there are countless possibilities to use the data in novel ways. This might include testing and informing computational models of basal ganglia-cortex loops, using the deep brain recordings as a ground truth for MEG source estimates of deep brain activity, or comparisons to similar datasets. To enable these and similar endeavors, we here present a structured and annotated dataset, a comprehensive description of the experimental protocol and of the dataset constituents, a technical validation addressing data quality, and Python code to get interested researchers started.

Methods

Participants. 20 PD patients eligible for STN DBS (six females), aged between 47 and 75 years (median age: 63 years), participated in the study with written informed consent in accordance to the Declaration of Helsinki (Table 1). Data collection was approved by the Ethics Committee of the Medical Faculty of Heinrich Heine University Düsseldorf (study no. 3209). Participants' consent to the open publication of the anonymized data was waived by the Data Protection Office of University Clinic Düsseldorf.

MEG System and recording setup. All recordings were conducted using a 306-channel whole-head MEG system (VectorView, MEGIN). Simultaneously, local field potentials (LFPs) from the subthalamic nucleus were recorded. The recording sessions took place the day following electrode implantation. In this phase, the stimulator had not been implanted yet. All patients were implanted with standard DBS electrodes (Table 1), having either 4 or 8 ring contacts. The electrodes were externalized, i.e. equipped with extension cables that allowed us to connect the electrodes to the built-in amplifiers of our MEG system. To ensure minimal magnetic interference, we used custom-made, non-ferromagnetic extensions (Medtronic Bakken Research Center, Maastricht, the Netherlands).

Acquisition. During the recording sessions, we simultaneously acquired various types of electrophysiological data, including MEG, LFPs, vertical and horizontal electro-oculograms, and the EMG of the extensor and flexor muscles of both forearms. The DBS electrode contacts were referenced against a surface electrode located at the left mastoid. EMG signals were recorded with reference to surface electrodes attached to the forearm tendons. A sampling rate of 2 kHz was used to capture the data. Online band-pass filtering was applied to MEG signals within the range of 0.03 to 660 Hz, while LFP and EMG signals were filtered between 0.1 and 660 Hz.

Medication withdrawal and OFF state verification. On the evening before the recordings, dopaminergic medication was discontinued until the end of the medication OFF measurement next morning. In case patients were equipped with an apomorphine pump, the pump was stopped at least 2 hours before the recordings started. The medication OFF state was verified by a UPDRS III rating before the recordings started.

Experimental design. The experiment consisted of four blocks: (i) rest followed by static forearm extension (HOLD) in medication OFF, (ii) rest followed by repetitive fist-clenching (MOVE) in medication OFF, (iii) rest followed by HOLD in medication ON and (iv) rest followed by MOVE medication ON. In patients 8RgPiG and 6m9kB5 we only acquired resting-state data.

In between the OFF and ON blocks, patients received 1.5 times their usual levodopa morning dose (mean = 205 mg, STD = 40 mg, min = 140 mg, max = 300 mg) and we waited for at least 30 minutes for the drug to take effect. Subsequently, we started to re-score selected UPDRS items such as diadochokinesia and finger tapping every ten minutes and continued with the MEG measurement as soon as we observed a clear motor improvement. After the medication ON measurement, we acquired another full UPDRS III score.

In the HOLD condition, patients elevated the forearm of their more affected body side (elbow joint about 60°) and kept this position until instructed via intercom to take a break. This process was repeated several times until we had collected about 300 seconds of forearm extension (M = 309.54, SD = 50.40).

Participant ID	Age [y]	Sex	Hand Moved	Disease Duration [y]	UPDRS OFF	UPDRS ON	Electrode Model
sub-0cGdk9	48	m	l	10	50	32	MDT
sub-2IU8mi	60	m	l	6	43	38	MDT
sub-2IhVOz	69	m	r	11	39	31	MDT
sub-6m9kB5	53	m	—	6	27	21	BSC
sub-8RgPiG	53	m	—	9	24	9	BSC
sub-AB2PeX	64	f	l	14	27	21	MDT
sub-AbzsOg	61	f	l	10	56	32	MDT
sub-BYJoWR	54	f	r	10	47	16	MDT
sub-FIyfdR	70	f	r	4	41	36	MDT
sub-FYbcap	66	m	l	8	40	29	MDT
sub-PuPVlx	71	m	l	6	51	17	MDT
sub-QZTsn6	72	m	l	17	36	—	MDT
sub-VopvKx	70	m	r	11	39	21	MDT
sub-dCsWjQ	68	m	l	6	39	20	MDT
sub-gNX5yb	62	f	l	15	31	20	MDT
sub-hnetKS	76	f	l	21	34	13	MDT
sub-i4oK0F	69	m	l	1	18	4	MDT
sub-iDpl28	53	m	r & l	11	55	33	MDT
sub-jyC0j3	62	m	r	16	26	13	MDT
sub-oLNpHd	54	m	l	12	27	—	SJM
Mean	**62.7**			**10.2**	**37.5**	**22.5**	
Median	**63**			**10**	**39**	**21**	
SD	**8**			**4.7**	**10.5**	**9.5**	

Table 1. Patient information. Age, disease duration and motor symptom severity (Unified Parkinson's Disease Rating Scale Part III) refer to the date of measurement. MDT: electrode with 4 ring contacts by Medtronic (model 3389); ø1.27 mm; contact length: 1.5 mm; contact spacing: 0.5 mm; BSC: electrode with 8 ring contacts by Boston Scientific (model Vercise Standard); ø1.3 mm; contact length: 1.5 mm; contact spacing: 0.5 mm; SJM: electrode with 4 ring contacts by St. Jude Medical (model 6148); ø1.4 mm; contact length: 1.5 mm; contact spacing: 0.5 mm. m = male, f = female, l = left, r = right. OFF: without medication. ON: with medication.

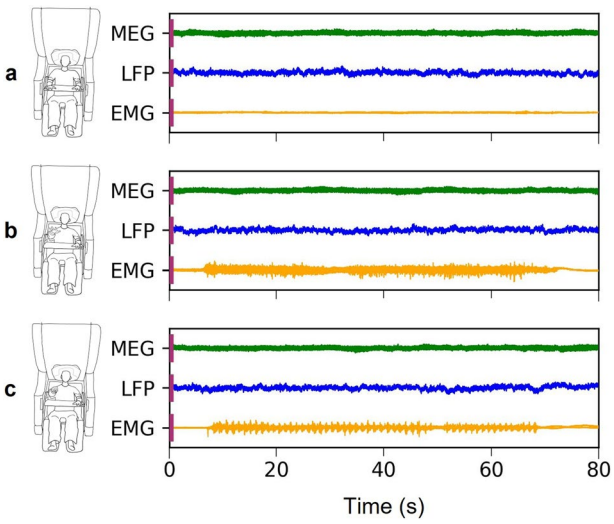

Fig. 2 Example data excerpt for each condition. The plots depict one MEG sensor (*green*), one LFP channel (*blue*), *and* one EMG channel (*yellow*): (**a**) Resting state; (**b**) Static forearm extension; (**c**) Repetitive fist-clenching. Movements are initiated at about 10 s and are terminated at about 70 s.

In the MOVE condition, patients performed repetitive fist-clenching with their more affected hand. Movement was self-paced, but patients were instructed to clench their fist about once per second for 300 seconds (M = 284.62, SD = 44.29). In line with the HOLD condition, we introduced pauses to avoid fatigue. Note that the change of hand position is captured by the EMG (Fig. 2).

Construction of head and source models. In this dataset, we provide head models and Montreal Neurological Institute (MNI)-aligned source models along with the raw data so that interested researchers can perform source analysis. Realistic, single-shell head model creation for MEG source analysis and the construction of source models were performed using the FieldTrip toolbox in MATLAB R2020a. The head models are based on individual T1-weighted MR images of the patients, which we segmented into different tissue types using SPM routines via the function *ft_volumesegment*. The triangulated brain-skull boundary served as the single shell, surface head model. Relating the head model to the MEG sensors in space (MEG-MRI co-registration) was achieved by identifying three anatomical landmarks, namely nasion, right and left periauricular point, in both the MRI and the MEG coordinate system. The former involved visual inspection of the MRI and marking the landmarks by hand. The latter was achieved by first determining the position of each landmark relative to four magnetic coils, attached to the subjects' head, using a Polhemus digitizer system. The coils, capable of producing a small current, were source-localized in the head position indicator (HPI) measurement preceding each MEG recording. Once the landmark coordinates are known in both coordinate systems, the MRI/head model and the sensors can be represented in the same coordinate system (defined by the landmarks). The forward solution was approximated using the theorem for the magnetic lead field in the quasi-static approximation[14].

The MNI-aligned source models, henceforth referred to as grids, define a set of locations spanning the entire brain. 3D coordinates in individual head space can be found in the grid.pos field ($N \times 3$ matrix, with N being the number of locations). During source reconstruction, brain activity is estimated for each of these locations. The grids were constructed by first normalizing the individual MRI, using SPM routines via *ft_volumenormalise*. The inverse of the resulting nonlinear transformation was then applied to a regular MNI template grid with a spacing of 4 mm. After the transformation, the template grid fits the individual MRI, but the regular spacing is lost. Importantly, each position in the MNI-aligned grid has a corresponding position in the template grid (X_{ind},Y_{ind},Z_{ind} in row *i* of individual_grid.pos corresponds to X_{MNI},Y_{MNI},Z_{MNI} in row *i* of template_grid.pos). When using these grids, one effectively estimates brain activity in homologous locations in each subject. The MNI coordinates of these locations are known and can be used to look up anatomical labels in an atlas, for example, or to plot source activity in a standard brain. The latter is particularly useful for group analyses of source images. These steps are exemplified in the Matlab script *source_analysis_example* available on GitHub (https://github.com/Fayed-Rsl/RHM_preprocessing).

Technical validation methods. The recordings were visually inspected and segments with artifacts were discarded (1.79% of the data on average; SD = 2.51, range: 0 to 11%). For technical validation, we re-referenced the LFPs using a bipolar referencing scheme by subtracting signals from neighbouring electrode contacts within each hemisphere in order to focus on local neural activity[15].

Minimal pre-processing included a 1 Hz high-pass filter to remove low-frequency noise and slow drift, as well as down-sampling the data from 2000 to 200 Hz. The power spectral density of the EMG signals from the hand performing the task was computed using Welch's method in the frequency range from 2 to 45 Hz[16]. For computing resting-state MEG-LFP coupling, we created fixed-length epochs lasting 2-s with a 1-s overlap. The epochs were convolved with 7 Slepian tapers, and coherence between MEG and LFP was computed using the *spectral_connectivity_epochs* function of the MNE Python toolbox in the frequency range from 13 to 30 Hz[17].

Electrode placement was assessed using LeadDBS, a Matlab toolbox for reconstructing the location of DBS electrodes from their characteristic CT artifacts and visualizing them in a common template brain[18]. This step required an individual pre-surgical MR and a post-surgical CT scan.

Data Records

The dataset adheres to the Brain Imaging Data Structure (BIDS) v1.6.0 standard and was transformed into BIDS format using the MNE-BIDS tool (https://github.com/mne-tools/mne-bids) version 0.10[19,20]. It is publicly accessible at https://openneuro.org/datasets/ds004998[21] and has a total size of 162GB. The dataset's structure is outlined in Fig. 3.

The directory structure consists of a root folder containing general meta-information and the individual subject folders (e.g., sub-0cGdk9). Each subject-folder contains one session-folder called *ses-PeriOp* with the raw data and session-specific meta-information. All electrophysiological recordings are contained in the.fif files (MEG, LFP, EOG and EMG). Rest and motor task (either HOLD or MOVE) are part of the same file, unless the patient had only undergone resting-state recordings. Each.fif file has a size of approx. 1.5GB, comprising 204 gradiometers, 102 magnetometers, 8 LFP channels (prefix "EEG"), 4 EMG channels, 2 EOG channels and 3 "stimulus channels". The latter can be used to record external triggers, but were not used here.

In order to epoch the data into rest, forearm extension, and fist-clenching, we provide both the epoch start and end times <*events.tsv*> and code for epoching (https://github.com/Fayed-Rsl/RHM_preprocessing). In addition, we provide a list of bad channels <*channels.tsv*> and epochs containing artifacts <*events.tsv*>, which should be removed in pre-preprocessing. Typical reasons for marking a channel/epoch as bad are SQUID jumps (MEG) or strong high-frequency noise caused by muscle contractions. The mapping from LFP channel labels, as contained in the raw data, to interpretable DBS electrode contact names is provided in <*montage.tsv*>. This is useful for re-referencing the LFP data, which is commonly done to focus on local voltage changes.

Overview of root folder.

- *./dataset_description.json* contains information about the dataset, including title, authors, and study details.
- *./participants.tsv* stores subject identifiers, age, sex, disease and disease duration.
- ./participants_updrs_<on/off>.tsv provides raw, non-aggregated UPDRS scores for each item of part III.
- ./template_sourcemodel.mat contains the template grid (source locations).

```
RestHoldMove/
├── README
├── dataset_description.json
├── participants.json
├── participants.tsv
├── participants_updrs_off.tsv
├── participants_updrs_on.tsv
├── template_sourcemodel.mat
└── sub-0cGdk9/
    ├── ses-PeriOp/
    │   ├── sub-0cGdk9_ses-PeriOp_scans.tsv
    │   ├── meg/
    │   │   ├── sub-0cGdk9_ses-PeriOp_acq-MedOff_coordsystem.json
    │   │   ├── sub-0cGdk9_ses-PeriOp_acq-MedOn_coordsystem.json
    │   │   ├── sub-0cGdk9_ses-PeriOp_task-HoldL_acq-MedOff_run-1_channels.tsv
    │   │   ├── sub-0cGdk9_ses-PeriOp_task-HoldL_acq-MedOff_run-1_events.tsv
    │   │   ├── sub-0cGdk9_ses-PeriOp_task-HoldL_acq-MedOff_run-1_meg.fif
    │   │   ├── sub-0cGdk9_ses-PeriOp_task-HoldL_acq-MedOff_run-1_meg.json
    │   │   └── ...
    │   ├── headmodel/
    │   │   └── sub-0cGdk9_ses-PeriOp_headmodel.mat
    │   ├── sourcemodel/
    │   │   └── sub-0cGdk9_ses-PeriOp_sourcemodel.mat
    │   └── montage/
    │       └── sub-0cGdk9_ses-montage.tsv
    └── sub-FYbcap/
        └── ...
```

Fig. 3 Dataset structure. Brain Imaging Data Structure (BIDS) showcasing the hierarchical arrangement of files.

Overview of session folder.

- *<ses>/meg/* encompasses the raw data, including sensor and anatomical landmark coordinates, channel information and event details.
- *<ses>/headmodel/* contains the head model (.mat).
- *<ses>/sourcemodel/* contains the individual MNI-aligned grid (.mat).
- *<ses>/montage/* holds montage-related information for re-referencing LFP data.

Technical Validation

We used the BIDS-Validator to ensure that the dataset conforms to the standardised brain imaging data structure (https://github.com/bids-standard/bids-validator). To further validate the technical quality of the dataset, we verified that the medication indeed improved motor symptoms. As expected, administration of levodopa led to a significant reduction in symptom scores in the medication ON state compared to the OFF state ($p < 0.01$, paired t-test, Fig. 4a).

Furthermore, we confirmed that the event times we provide correctly reflect the patients' motor state. To do so, we epoched the data based on the events provided and plotted the forearm EMG both in the time (Fig. 4c) and in the frequency domain (Fig. 4d), revealing distinct patterns corresponding to the different movements. As expected, REST exhibited the lowest EMG power. The spectral peaks around 5 Hz and its harmonics are due to Parkinsonian rest tremor. HOLD was characterized by intermediate power levels with prominent peaks reflecting postural tremor. MOVE had the highest power overall and lacked discernible tremor peaks in the group average.

In addition, we verified that resting-state functional connectivity between STN and cortex displays the hemispheric laterality described by several groups[4,22,23]. Specifically, the left STN is expected to couple to the left motor cortex in the beta band (13–35 Hz) while the right STN is connected to the right motor cortex. Figure 4b illustrates the topographical organization of beta-band coherence averaged over all left-hemispheric electrode contacts and all right-hemispheric electrode contacts, respectively. Coupling was clearly lateralized.

Figure 5 illustrates the reconstructed locations of all electrodes in relation to the STN in MNI space. All electrodes in this dataset appear to be correctly placed. Nonetheless, there is inter-subject variability with respect to contact location.

Usage Notes

The data is available under a CC0 license and can be retrieved with open access from openneuro.org (https://openneuro.org/datasets/ds004998). To help interested researchers get started with analyzing these data, we provide Python code for loading, epoch creation, artifact rejection and LFP re-referencing on our GitHub repository (https://github.com/Fayed-Rsl/RHM_preprocessing). In this code, we make use of the MNE Python

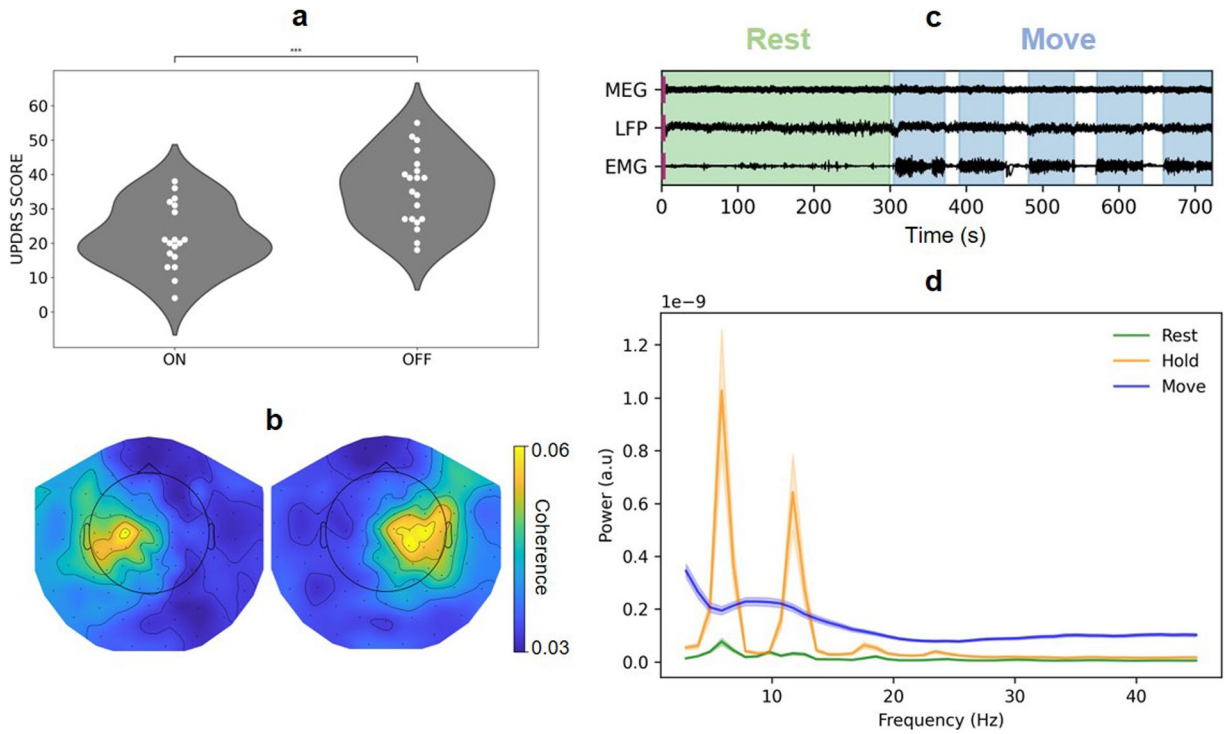

Fig. 4 Technical validation. (**a**) Unified Parkinson's Disease Rating Scale (UPDRS) Part III scores in medication ON and medication OFF. ***$p < 0.01$, paired t-test. (**b**) Topographical maps of MEG-LFP beta-band coherence, averaged over all left-hemispheric and all right-hemispheric electrode contacts, respectively. (**c**) Example of MEG, LFP, and EMG time-domain data (subject QZTsn6), REST (green), and MOVE (blue) highlighted. (**d**) Group-average power spectral density of EMG signals for REST (green), HOLD (orange), and MOVE (blue).

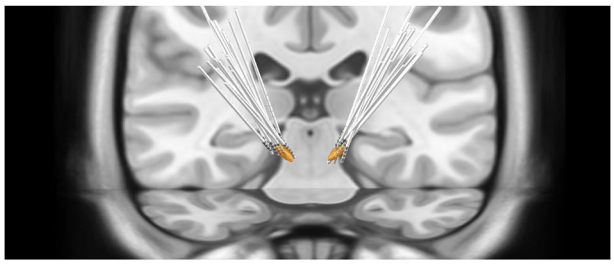

Fig. 5 Electrode reconstructions in Montreal Neurological Institute Space. The subthalamic nucleus is shown in orange.

toolbox for MEG data analysis[17]. Note that there are several alternatives, which are equally well suited for this dataset, such as FieldTrip[24], Brainstorm[25], or SPM[26]. We additionally provide examples for source reconstruction, based on the FieldTrip toolbox.

For those who have worked with MEG data of healthy participants before, we note that the data quality might be worse than what they are used to. Our data were recorded one day after brain surgery in patients severely affected by PD, off their usual medication. Movement disorders patients cannot be expected to minimize movement the way healthy participants can, resulting in more movement-related artifacts. Rest tremor and postural tremor occurred frequently, for example. The head position was measured at the start of each recording, not continuously.

Moreover, these patients had brain implants, further affecting signal quality. While the custom-made, non-ferromagnetic extensions used here mitigated most of the severe artifacts related to DBS hardware[27], the connections were not completely free of ferromagnetic material. This resulted in signal distortions in right parietal and right temporal MEG sensors, reflecting the path of the extensions (Fig. 6). These rather mild artifacts can be dealt with by standard analysis steps such as temporal signal space separation[28], computing condition contrasts or relating the MEG signal to a non-distorted reference, e.g. by computing LFP-MEG coherence. Please note that artifacts also occur in the LFP data, and noisy LFP channels are common. Hence, screening for artifacts and the removal of bad channels is essential when analysing these data. We provide information and code to assist with this.

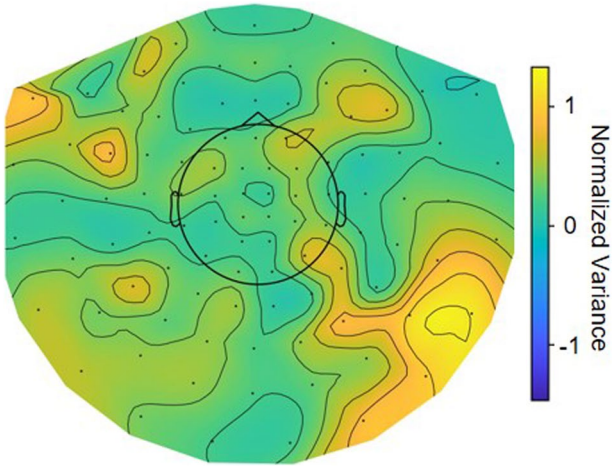

Fig. 6 Map of signal distortions caused by electrode extensions. The topographical map represents the group average normalized variance of MEG sensors. We removed sensors with strong noise (>2 SD) and divided each individual variance topography by its mean before averaging over subjects.

Further, we strongly recommend re-referencing the LFP signal, e.g. by subtracting the signals from adjacent contacts (the shared data are nor re-referenced yet). Otherwise, the LFP signal is dominated by muscle activity recorded at the mastoid reference. In this context, please note that the LFP channel labels in the raw data (EEG001, EEG002, …) are not meaningful, but need to be renamed as indicated in the montage.tsv files. The channel labels in these files contain information about the position of each contact along the electrode. LFP-left-0, for example, would indicate the lowermost contact of the electrode in the left hemisphere. Note, however, that we do not provide information about the anatomical position of the contacts, e.g. with respect to the boundaries of the STN or compartments of the STN, due to uncertainty in the electrode reconstruction and the uncertain spatial coverage of LFP recordings. In case an analysis requires contact selection, we recommend a functional criterion such as a threshold on task- or symptom-related activity.

Lastly, we note that the time we waited to reach the OFF state is insufficient for the drugs to lose their effects completely[29]. Thus, the medication OFF state is to be understood as a relative OFF which can be further attenuated due to the surgery-related stun effect.

Code availability

All custom code used for pre-processing and technical validation is available at https://github.com/Fayed-Rsl/RHM_preprocessing.

Received: 15 March 2024; Accepted: 8 August 2024;
Published online: 15 August 2024

References

1. Poewe, W. *et al*. Parkinson disease. *Nat Rev Dis Primers* **3**, 17013 (2017).
2. Hollunder, B. *et al*. Mapping dysfunctional circuits in the frontal cortex using deep brain stimulation. *Nat Neurosci* 1–14 https://doi.org/10.1038/s41593-024-01570-1 (2024).
3. Goetz, C. G. *et al*. Movement Disorder Society-sponsored revision of the Unified Parkinson's Disease Rating Scale (MDS-UPDRS): scale presentation and clinimetric testing results. *Mov Disord* **23**, 2129–2170 (2008).
4. Litvak, V. *et al*. Resting oscillatory cortico-subthalamic connectivity in patients with Parkinson's disease. *Brain* **134**, 359–374 (2011).
5. van Wijk, B. C. M. *et al*. Subthalamic nucleus phase–amplitude coupling correlates with motor impairment in Parkinson's disease. *Clin Neurophysiol* **127**, 2010–2019 (2016).
6. Sharma, A., Vidaurre, D., Vesper, J., Schnitzler, A. & Florin, E. Differential dopaminergic modulation of spontaneous cortico-subthalamic activity in Parkinson's disease. *Elife* **10**, e66057 (2021).
7. Hirschmann, J. *et al*. Distinct oscillatory STN-cortical loops revealed by simultaneous MEG and local field potential recordings in patients with Parkinson's disease. *Neuroimage* **55**, 1159–1168 (2011).
8. Hirschmann, J. *et al*. A direct relationship between oscillatory subthalamic nucleus–cortex coupling and rest tremor in Parkinson's disease. *Brain* **136**, 3659–3670 (2013).
9. Hirschmann, J. *et al*. Differential modulation of STN-cortical and cortico-muscular coherence by movement and levodopa in Parkinson's disease. *Neuroimage* **68**, 203–213 (2013).
10. Hirschmann, J. *et al*. Parkinsonian Rest Tremor Is Associated With Modulations of Subthalamic High-Frequency Oscillations. *Movement Disorders* **31**, 1551–1559 (2016).
11. Hirschmann, J., Schoffelen, J. M., Schnitzler, A. & van Gerven, M. A. J. Parkinsonian rest tremor can be detected accurately based on neuronal oscillations recorded from the subthalamic nucleus. *Clinical Neurophysiology* **128**, 2029–2036 (2017).
12. Todorov, D., Schnitzler, A. & Hirschmann, J. Parkinsonian rest tremor can be distinguished from voluntary hand movements based on subthalamic and cortical activity. *Clinical Neurophysiology* **157**, 146–155 (2024).
13. Hirschmann, J., Steina, A., Vesper, J., Florin, E. & Schnitzler, A. Neuronal oscillations predict deep brain stimulation outcome in Parkinson's disease. *Brain Stimulation* **15**, 792–802 (2022).
14. Nolte, G. The magnetic lead field theorem in the quasi-static approximation and its use for magnetoencephalography forward calculation in realistic volume conductors. *Phys Med Biol* **48**, 3637–3652 (2003).

15. Li, G. *et al*. Optimal referencing for stereo-electroencephalographic (SEEG) recordings. *Neuroimage* **183**, 327–335 (2018).
16. Welch, P. The use of fast Fourier transform for the estimation of power spectra: A method based on time averaging over short, modified periodograms. *IEEE Transactions on Audio and Electroacoustics* **15**, 70–73 (1967).
17. Gramfort, A. *et al*. MEG and EEG data analysis with MNE-Python. *Frontiers in Neuroscience* **7** (2013).
18. Horn, A. & Kühn, A. A. Lead-DBS: A toolbox for deep brain stimulation electrode localizations and visualizations. *NeuroImage* **107**, 127–135 (2015).
19. Appelhoff, S. *et al*. MNE-BIDS: Organizing electrophysiological data into the BIDS format and facilitating their analysis. *J. Open Source Softw* **4**, 1896 (2019).
20. Niso, G. *et al*. MEG-BIDS, the brain imaging data structure extended to magnetoencephalography. *Sci Data* **5**, 180110 (2018).
21. Rassoulou, F. *et al*. Exploring the electrophysiology of Parkinson's disease - magnetoencephalography combined with deep brain recordings from the subthalamic nucleus. *OpenNeuro* https://doi.org/10.18112/openneuro.ds004998.v1.2.1 (2024).
22. van Wijk, B. C. M. *et al*. Functional connectivity maps of theta/alpha and beta coherence within the subthalamic nucleus region. *NeuroImage* **257**, 119320 (2022).
23. Damborská, A. *et al*. Resting-State Phase-Amplitude Coupling Between the Human Subthalamic Nucleus and Cortical Activity: A Simultaneous Intracranial and Scalp EEG Study. *Brain Topogr* **34**, 272–282 (2021).
24. Oostenveld, R., Fries, P., Maris, E. & Schoffelen, J.-M. FieldTrip: Open source software for advanced analysis of MEG, EEG, and invasive electrophysiological data. *Comput Intell Neurosci* **2011**, 156869 (2011).
25. Tadel, F., Baillet, S., Mosher, J. C., Pantazis, D. & Leahy, R. M. Brainstorm: a user-friendly application for MEG/EEG analysis. *Comput Intell Neurosci* **2011**, 879716 (2011).
26. *Statistical Parametric Mapping: The Analysis of Funtional Brain Images*. (Elsevier/Academic Press, Amsterdam; Boston, 2007).
27. Litvak, V. *et al*. Optimized beamforming for simultaneous MEG and intracranial local field potential recordings in deep brain stimulation patients. *Neuroimage* **50**, 1578–1588 (2010).
28. Taulu, S. & Simola, J. Spatiotemporal signal space separation method for rejecting nearby interference in MEG measurements. *Phys Med Biol* **51**, 1759–1768 (2006).
29. Hauser, R. A., Ellenbogen, A., Khanna, S., Gupta, S. & Modi, N. B. Onset and duration of effect of extended-release carbidopa-levodopa in advanced Parkinson's disease. *Neuropsychiatr Dis Treat* **14**, 839–845 (2018).

Acknowledgements

The original project was funded by ERA-NET Neuron (01EW0903). Data curation and publication was supported by Brunhilde Moll Stiftung. The authors would like to thank Lydia Rassoulou for help with Fig. 2.

Author contributions

F.R. performed data curation, technical validation of the dataset and wrote the manuscript. A.St. helped with the data preparation and pre-processing. C.J.H. acquired clinical data and recruited participants. J.V. performed the surgery. M.B. recorded MEG data and helped design the experiment. A.Sch. designed the experiment, acquired the funding and supervised the original study. J.H. recorded MEG data, revised the manuscript and supervised data curation and publication. All authors read the manuscript and provided feedback.

Funding

Open Access funding enabled and organized by Projekt DEAL.

Competing interests

The authors declare no competing interests.

Additional information

Correspondence and requests for materials should be addressed to J.H.

3. Study 2: Electrophysiological signatures predict the therapeutic window of deep brain stimulation electrode contacts

npj | digital medicine

Article

Published in partnership with Seoul National University Bundang Hospital

https://doi.org/10.1038/s41746-025-02089-w

Electrophysiological signatures predict the therapeutic window of deep brain stimulation electrode contacts

Fayed Rassoulou[1], Abhinav Sharma[2,3], Alexandra Steina[1], Markus Butz[1], Christian J. Hartmann[1,4], Bahne H. Bahners[1,4], Jan Vesper[5], Alfons Schnitzler[1,4] & Jan Hirschmann[1] ✉

Deep brain stimulation (DBS) is an effective treatment for Parkinson's disease. Identifying the optimal parameters is a complex task. Here, we investigated whether electrophysiology, combined with machine learning, can support contact selection. We applied tree learning to resting-state magnetoencephalographic and local field potential recordings from the subthalamic nucleus (STN). STN power and STN-cortex coherence in various frequency bands served to predict the therapeutic window. The model successfully predicted therapeutic windows in the original ($r = 0.45$, $p < 0.001$, $N = 45$) and in an independent cohort ($r = 0.30$, $p < 0.001$, $N = 8$). It relied mostly on fast (>35 Hz) subthalamic activity and on STN-cortex coherence in several bands. Furthermore, it was able to order contacts such that the optimal contact can be found faster. Our study demonstrates the feasibility of predicting therapeutic windows from electrophysiological features and could contribute to automated contact selection in the future.

Deep brain stimulation (DBS) is a well-established therapy for neurological movement disorders such as Parkinson's disease (PD)[1]. PD is characterized by degeneration of dopaminergic neurons in the midbrain, leading to motor impairment and to pathological oscillatory patterns in the basal ganglia[2]. Among these structures, the subthalamic nucleus (STN), a key regulator of motor function[3], has become an established target for DBS[4].

Although stimulation of the STN is effective, achieving optimal symptom relief can be challenging in some patients, due to the anatomical complexity of the midbrain. Choosing a suboptimal contact for stimulation, for example, might lead to the activation of non-target brain areas, causing side effects. These, in turn, forbid the usage of amplitudes high enough to fully suppress motor symptoms, i.e, they limit the therapeutic window. Accordingly, one major aim in DBS programming is to find the electrode contact with the largest therapeutic window, to be used for chronic stimulation. This is achieved through the so-called monopolar review, a clinical procedure involving incremental increases of stimulation amplitude while assessing symptom relief as well as side effects[5].

Monopolar reviews are both time-consuming and tedious because each patient requires a tailored approach[6–8]. The complexity of this task has increased further with the development of advanced DBS systems that allow for thousands of possible parameter combinations[9,10]. As decision-support systems are increasingly being adopted across clinical domains[11], it is logical to explore how machine learning techniques could help speed up the identification of optimal DBS settings. These techniques have already started to show promise in the DBS field (see refs. 12,13 for a review).

The majority of machine learning studies addressing DBS programming come from the imaging domain[14–16]. A landmark study by Roediger et al., for example, demonstrated the validity of automated programming in a clinical trial[7]. The authors developed and evaluated the so-called StimFit algorithm, which models the relationship between electrode location and DBS settings on the one hand and clinical outcome on the other hand through linear mixed effect models, and selects optimal DBS settings by means of gradient descent optimization[10]. Applying this strategy to PD patients in a randomized, double-blinded trial, the authors demonstrated non-inferiority of automated programming compared to conventional programming. Other studies applied machine learning to kinematic measurements to improve DBS programming[17–20]. Sarikhani and colleagues, for example, have recently optimized DBS programming for tremor suppression based on smartwatch-accelerometery[19]. Automated parameter

[1]Institute of Clinical Neuroscience and Medical Psychology, Medical Faculty and University Hospital Düsseldorf, Heinrich Heine University Düsseldorf, Düsseldorf, Germany. [2]MRC Brain Networks Dynamics Unit, University of Oxford, Oxford, UK. [3]Nuffield Department of Clinical Neurosciences, University of Oxford, Oxford, UK. [4]Center for Movement Disorders and Neuromodulation, Department of Neurology, Medical Faculty and University Hospital Düsseldorf, Heinrich Heine University Düsseldorf, Düsseldorf, Germany. [5]Department of Functional Neurosurgery and Stereotaxy, Medical Faculty and University Hospital Düsseldorf, Heinrich Heine University Düsseldorf, Düsseldorf, Germany. ✉e-mail: Jan.Hirschmann@med.uni-duesseldorf.de

Table 1 | Patient information for the cohort used for leave-one-out cross-validation

Id	Study	Age [y]	Sex	Electrode type	Monopolar review [day after surgery]	Disease duration
S01	1	75	f	MDT 3389	36	21
S02	1	70	m	MDT 3389	6	11
S03	1	64	f	MDT 3389	8	14
S04	1	62	f	MDT 3389	6	15
S05	1	54	f	MDT 3389	16	10
S06	1	47	m	MDT 3389	5	10
S07	1	68	m	MDT 3389	6	11
S08	1	66	m	MDT 3389	6	8
S09	1	69	m	MDT 3389	6	6
S10	1	70	m	MDT 3389	12	11
S11	1	60	m	MDT 3389	6	6
S12	1	69	m	MDT 3389	6	1
S13	1	67	m	MDT 3389	6	6
S14	1	53	m	MDT 3389	6	11
S15	1	61	f	MDT 3389	9	10
S16	1	52	m	BSC Vercise Standard	7	9
S17	1	53	m	BSC Vercise Standard	8	6
S18	1	44	m	MDT 3389	6	5
S19	1	50	m	MDT 3389	10	18
S20	1	44	f	MDT 3389	372	9
S21	1	65	m	MDT 3389	6	4
S22	1	69	m	MDT 3389	7	12
S23	1	61	f	MDT 3389	6	3
S24	1	72	m	MDT 3389	6	14
S25	1	66	m	MDT 3389	6	12
S26	1	75	f	MDT 3389	7	14
S27	2	69	m	ABI 6662	113	12
S28	2	65	m	ABI 6662	6	6
S29	2	56	m	ABI 6662	498	13
S30	2	62	f	ABI 6662	6	13
S31	2	70	m	ABI 6662	671	11
S32	2	45	m	ABI 6662	125	13
S33	2	60	f	ABI 6662	419	6
S34	2	59	f	ABI 6662	100	9
S35	2	66	f	ABI 6662	6	10
S36	2	72	f	ABI 6662	6	3
S37	2	69	m	ABI 6662	103	10
S38	2	54	m	ABI 6662	5	3
S39	2	55	f	ABI 6662	50	4
S40	2	41	m	ABI 6662	6	7
S41	2	46	m	ABI 6662	357	6
S42	2	59	m	ABI 6662	225	15
S43	2	58	m	ABI 6662	49	8
S44	2	62	f	ABI 6662	6	2
S45	2	59	m	ABI 6662	58	10
mean	—	61	—	—	75	9
median	—	62	—	—	7	10
sd	—	9	—	—	149	4

Age refers to the date of measurement.
MDT Medtronic, *BSC* Boston Scientific, *ABI* Abbott Infinity, *m* male, *f* female.

selection by means of Gaussian process regression achieved similar tremor suppression as expert clinicians.

Besides imaging and kinematics, electrophysiology has been a major focus of this research. Neural oscillations, as obtained via electroencephalography, magnetoencephalography (MEG) or local field potential (LFPs) recordings, are of particular interest to the field because they encompass relevant neural signatures associated with Parkinsonian symptoms. STN beta power, for example, is well known to correlate with bradykinesia and rigidity[21–24]. Due to this robust relationship, it is commonly used as a feedback signal for automated DBS parameter adjustments in closed-loop stimulation[25–27]. Moreover, it has recently been validated for contact selection[28,29].

However, STN beta power is not the only signal related to PD symptoms. In fact, the literature bears a wealth of candidate markers, many of which are symptom or state-specific. This includes finely-tuned and broadband gamma oscillations[30–33], oscillations in the tremor range (4–8 Hz)[34–36] and high-frequency oscillations[37–39], just to name a few. Given this rich set of potentially informative signals, it seems suboptimal to base decisions on a single marker. A more holistic approach would be to leverage multivariate tools that base decisions on a large set of variables.

Here, we use such a strategy to predict therapeutic windows from various electrophysiological markers. Based on the STN's fundamental contribution to PD pathophysiology, we take an STN-centric view and consider STN power in various frequency bands. Subthalamic activity alone, however, might not be sufficient for optimizing DBS parameters. Recent research suggests that cortical signals are a major asset when inferring clinical parameters of interest[40]. Thus, we further include STN-cortex coherence, a functional connectivity metric capturing subthalamo-cortical interactions.

Results

We analysed resting-state data from two prior studies[41–43], which involved 26 and 19 PD patients, respectively (Table 1). All patients were implanted with externalized DBS electrodes, allowing for simultaneous MEG-LFP measurements. Recordings took place the day following DBS electrode implantation and after an overnight withdrawal from dopaminergic medication. The data from this combined cohort were used to train an extreme gradient boosting model[44] predicting the clinical utility of each electrode contact based on the neural oscillations recorded at this contact, and their synchrony with cortical oscillations. Clinical utility was quantified by the normalized therapeutic window, i.e., the difference between clinical effect and side effect threshold, as obtained from monopolar review (see Methods). Model performance was assessed using a leave-one-electrode-out (LOEO) cross-validation scheme. Subsequently, we validated the model in an independent cohort (Table 2).

Model performance

The model's ability to predict the therapeutic window was quantified by the correlation between actual and predicted values. As shown in Fig. 1A, the LOEO validation yielded a positive correlation ($r = 0.45$, $p < 0.001$), indicating that the model successfully captured the relationship between neural oscillations and therapeutic windows. To account for repeated measures per electrode, we also fitted a linear mixed effect model as an alternative

Table 2 | Patient information for the independent cohort

Id	Study	Age [y]	Sex	Electrode type	Monopolar review [day after surgery]	Disease duration
S01	3	68	m	ABI 6662	6	13
S02	3	57	m	MDT SenSight	6	6
S03	3	66	m	BSC Vercise Cartesia	6	4
S04	3	68	m	ABI 6662	51	9
S05	3	58	m	ABI 6662	7	7
S06	3	64	f	BSC Vercise Cartesia	51	5
S07	3	81	m	ABI 6662	82	7
S08	3	49	m	ABI 6662	57	11
mean	—	64	—	—	33	8
median	—	65	—	—	29	7
sd	—	9	—	—	28	3

Age refers to the date of measurement.
MDT Medtronic, *BSC* Boston Scientific, *ABI* Abbott Infinity, *m* male, *f* female.

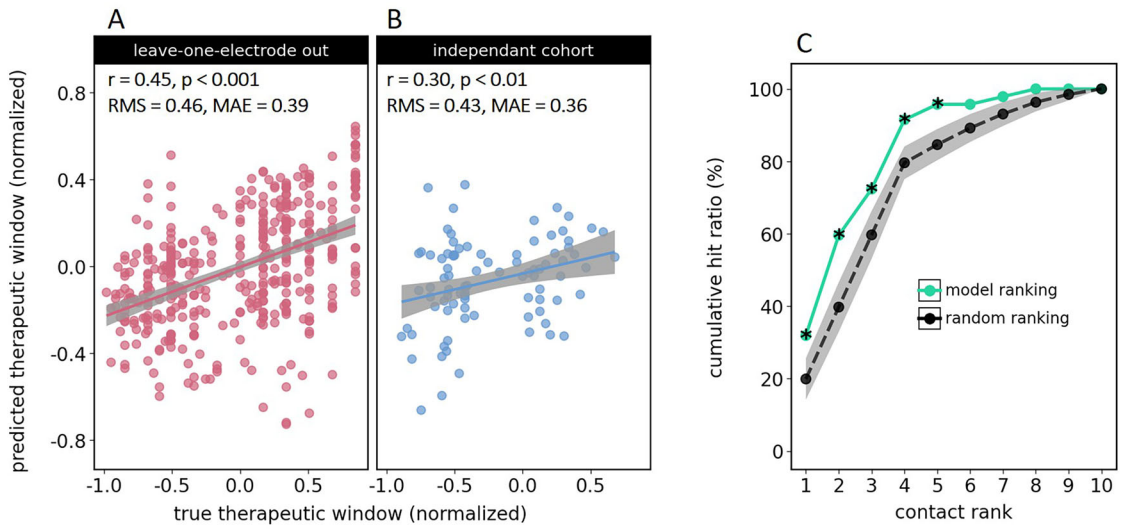

Fig. 1 | Model performance. A Scatter plots displaying the relationship between actual and predicted therapeutic windows for the leave-one-electrode-out approach. Gray shaded areas represent 95% confidence intervals. **B** Same as (**A**), but showing predictions generated for the independent cohort. **C** Cumulative hit ratio for the model's ranking of DBS electrode contacts (green) and the average hit ratio resulting from random ranking (black). The gray shaded area represents the mean ± 1 standard deviation. Asterisks (*) indicate above-chance performance ($p < 0.05$).

performance measure, yielding similar results ($\beta = 0.312$, CI = [0.093, 0.532], $p < 0.01$; Supplementary Table S3). When we applied a model trained on the entire original cohort to a new set of patients, the positive correlation remained ($r = 0.30$, $p < 0.01$), demonstrating the model's ability to generalize to unseen data (Fig. 1B). This model used the features most frequently selected in the LOEO procedure (Fig. 2A).

Figure 1C demonstrates the model's effectiveness in ranking electrode contacts according to their therapeutic window. It compares two scenarios in which the electrode contacts are first ordered, either randomly or according to the predicted therapeutic window (model-based), followed by a sequential search for the "optimal" contact, i.e., the contact chosen by the clinician. The cumulative hit ratio quantifies, for each rank *i*, the fraction of electrodes for which the optimal contact got ranked *i*th or better. The steepness of the curve thus indicates how fast one would find the optimal contact using a given ranking. The model-based ranking outperformed the vast majority of random rankings ($p < 0.05$), confirming the model's ability to inform the search for the optimal contact. These results indicate practical utility in guiding DBS programming decisions.

Feature importance

Full model. Feature importance analysis was conducted to identify the frequency bands and brain regions most relevant for predicting the therapeutic window. Using the Boruta algorithm during each iteration of the LOEO cycle (see Methods), we aimed to retain only the features that contributed significantly to model predictions. Thus, the number of times a feature got selected is indicative of its importance. Here, we used this quantity to assess feature importance for the full model, considering both STN power and STN-cortex coherence features.

From the initial set of 217 features (31 brain regions * 7 frequency bands), a total of 36 were selected consistently across iterations. Figure 2 illustrates the selection frequency for different features, grouped by frequency band (θ, α, β, γ, and HFO) and brain region. STN power features were particularly influential, particularly in higher frequency bands (γ and HFO). When applied to the subset of patients exhibiting one or more prominent beta peaks, STN beta power emerged as an important feature, indicating that subthalamic beta power is helpful when present (Supplementary Fig. S5).

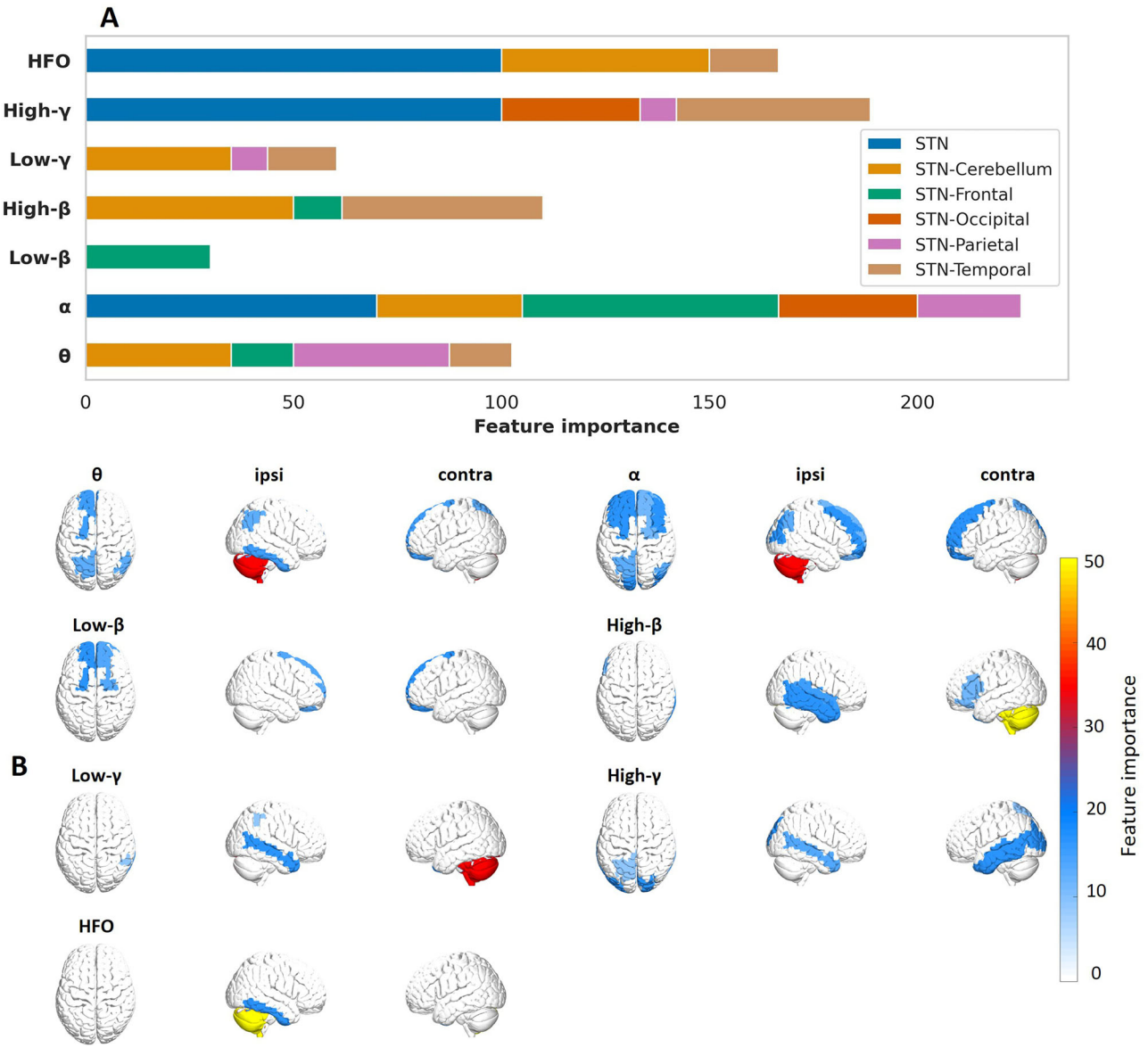

Fig. 2 | Distribution of feature importance across brain regions and frequency bands. A The bar plot illustrates the importance of each feature, grouped by brain region (indicated by colors) and frequency band (θ, α, β, γ, HFO). The length of each bar represents the relative contribution of each feature. Feature importance was quantified by selection frequency across leave-one-out cycles, normalized by the number of brain areas per lobe. **B** 3D topography of STN-cortex coherence features (parcellated).

Regarding STN-cortex coherence, the features spanned a broad spectrum, indicating that STN connectivity to multiple regions, in various frequency bands, contributed to the prediction of therapeutic windows. Notably, STN connectivity with the cerebellum, the temporal lobe, the superior frontal and superior parietal cortex were among the most important predictors.

Reduced feature sets. An alternative way of addressing feature importance is to exclude a subset of features and to reassess prediction performance. Here, we used this strategy to investigate the contribution of STN power vs. STN-cortex coherence, the importance of the cerebellum, and the possibility of obtaining accurate predictions when using only subthalamic and primary sensorimotor features.

A model trained on STN power alone yielded a lower performance than the full model ($r = 0.22$, $p < 0.001$; Supplementary Fig. S1A). In contrast, a model trained on STN-cortex coherence achieved a correlation comparable to that of the full model ($r = 0.40$, $p < 0.001$; Supplementary Fig. S1C). Despite the relatively strong performance, the cumulative hit ratio analysis did not indicate any ability to speed up the search for the optimal contact (Supplementary Fig. S1D), emphasizing the advantage of combining STN power with STN-cortex coherence.

Excluding the cerebellum from the feature set (Supplementary Figs. S2A, B and S3), or all cortical areas except sensorimotor cortex (Supplementary Fig. S2C, D), worsened predictions, but still yielded significant correlations between predicted and actual therapeutic windows ($r \geq 0.32$, $p < 0.001$).

Enhanced feature set. In order to test whether the addition of anatomical information would improve predictions we tested an enhanced feature set that included the best-performing electrophysiological features (Fig. 2A) and the distance of the contacts' center to a published anatomical sweet spot for STN DBS (x = 12.58, y = −13.41, z = −5.87[45]). We tested both feature sets in the LOEO framework and found that the anatomical information improved both the prediction performance and

the cumulative hit ratio (Supplementary Fig. S4), highlighting the merits of combining electrophysiology and anatomy.

Discussion

In this proof-of-concept study, we show that STN power and STN-cortex coherence allow for predicting a contact's therapeutic window, demonstrating the potential of electrophysiological markers for contact selection. No single feature dominated the prediction; rather, a combination of features across different brain regions and frequency bands—particularly in the alpha, high-gamma, and HFO range— facilitated the prediction of therapeutic windows. Predictions could be improved by adding anatomical information. Overall, these results highlight the importance of integrating information from multiple sources rather than relying on isolated markers.

Using electrophysiological features, we could successfully predict therapeutic windows in both the original and the independent cohort. The generalization to a new set of patients is particularly important for any future application to be developed based on this study, because the overarching goal is to gain a time advantage, requiring that predictions are based on previously recorded data. This sort of generalization is difficult to achieve in clinical neuroscience, due to the high between-subject and between-study variability of electrophysiological recordings[46] and due to the numerous methodological caveats, that can lead to overfitting[47]. Our model likely profited from the fact that the original cohort included two distinct datasets[41–43], forcing the model to focus on robust feature-outcome relationships. In addition, the features themselves appear to be rather robust. The basic, frequency-dependent layout of STN-cortex coherence has been replicated in numerous studies, indicating stability[41,48–51]. Accordingly, we observed a high similarity between the original cohort and the independent cohort in this study (Fig. 4).

The main value of machine learning in medicine is to provide clinically useful tools. For the current study, the utility lies in the time advantage that our approach might bring to the tedious, trial-and-error search for the best DBS contact. Our study sets the ground for such a tool by demonstrating that predicting therapeutic windows from electrophysiological signatures is possible in principle. Moreover, we provide evidence of an advantage over random search, which is the current standard, in our cumulative hit ratio analysis. Whether or not the approach really saves time in practice, however, needs to be established in a prospective study.

Besides producing useful tools, machine learning in medicine has the potential to uncover previously unknown relationships between measured signals and clinical outcomes. A machine learning model monitors a vast number of variables simultaneously and, unlike humans, is not biased by expectations[52]. Hence, investigating the features important to a successful machine learning model can provide scientific insights. In this context, it is important to keep in mind that the term "importance" refers to the model's internal computations, not to the process of interest. Accordingly, a model might rely on features that are unrelated to the underlying causal mechanisms[53]. That being said, we continue with discussing the most important features identified in this study.

In general, STN power was important to the model, particularly in the alpha, high-gamma and HFO range. This result tallies with a study by Shah et al., who used Lasso-regression to predict therapeutic windows from LFPs recorded intraoperatively in the resting-state. Matching the current results, the authors identified STN high-gamma and HFO power as the most predictive features[54]. The importance of fast STN oscillations is further corroborated by recent studies on adaptive DBS at home, which found that stimulation-entrained gamma oscillations best reflect motor symptom fluctuations[32,55]. Our previous study, which aimed at predicting the motor symptom improvement achieved with the optimal contact, lends further support to the current findings: in the STN power model, STN alpha power ranked second, and HFO power ranked third[56]. The best STN feature in that study, however, was high-beta power, in line with previous reports[57,58], prompting the question of why STN beta power did not emerge as a dominant feature here.

The reasons could be methodological, as both the target variable (therapeutic window vs. UPDRS sum score improvement) and the method for feature selection (BORUTA vs. Shapley values) differed across studies. Further, subthalamic beta and gamma power are anti-correlated[59], and feature selection in a set of correlated features is arbitrary to some degree. Beyond that, there might also be neurobiological reasons. STN beta power is primarily related to akinesia and rigidity[23]. For the monopolar review, however, tremor is usually the preferred target symptom, if present, because it is an easy readout. Thus, the review data might be less related to beta power than clinical scores with a stronger emphasis on akinesia and rigidity, such as the UPDRS. Further, in this particular dataset, there were many contacts lacking a clear beta power peak, presumably due to the stun effect[46]. This raises the question whether beta power is helpful when present. Indeed, we found STN beta power to be important in the set of patients exhibiting a clear beta peak.

In line with our previous work[56], we find that STN-cortex connectivity provides valuable information for predicting DBS effects. The coherence-only model performed better than the STN-only model and both performed worse than the combined model, indicating that STN power and STN-cortex coherence are complementary sources of information. With respect to STN-cortex coherence, our model mostly relied on low-frequency coupling (theta to low-beta) to bilaterally symmetric, medial, fronto-parietal regions. Further, it relied on coherence with the ipsilateral temporal cortex, and on coherence with the contralateral cerebellum (both not frequency-specific). In the following, we briefly discuss each of these couplings.

Low-frequency coherence with medial frontal areas was particularly important to the model. This is interesting because the STN has dense structural connections with the medial frontal cortex[60]. Structural connectivity forms the basis of functional connectivity. Accordingly, recent studies demonstrate that structural connectivity and STN-cortex coherence correlate in a frequency- and area-specific fashion[61,62]. Structural connectivity is also a major predictor of the DBS effect[63], with the set of important fibers varying systematically across diseases[60] and symptoms[64]. Taken together, these considerations suggest that STN-cortex coherence might be useful for contact selection because it contains information about the structural connections within reach of a given contact. Some of these connections might be critical to the DBS effect, as they convey clinically relevant, cortical afferents[65,66] or because they mediate remote cortical effects of DBS[67–69]. Finally, coherence and power might be indicative of fibers or regions that should be avoided, such as the pyramidal tract[70]. Despite being closely related, electrophysiology and anatomy are distinct sources of information. As demonstrated here, their combination can improve predictions—a finding that might inspire future applications.

The ipsilateral temporal lobe is known to be one of the hot spots of STN-cortex coherence, primarily in the alpha band[41,48,49]. This coupling is not STN-specific, but has been reported for numerous DBS targets, such as the ventral thalamus[71], the internal pallidum[72] and the nucleus basalis of Meynert[73]. Neither the anatomical underpinnings nor the functional significance are well understood to date. Yet, its occurrence in a number of different diseases suggests a physiological rather than a pathological nature.

The strong contribution of the cerebellum is likely based on structural connections between the STN and cerebellum, which are reciprocally connected via a disynaptic pathway involving the pontine nuclei[74]. As expected, due to fiber decussation, we observed the strongest contribution from the cerebellar hemisphere contralateral to the STN. Both, the basal ganglia and cerebellum, are important hubs for motor learning[75] and tremor[76]. Modulating their functional interactions might thus be a critical aspect of DBS, and contacts allowing for this modulation might be better suited than others. In line with this idea, we observed that removing cerebellar features from the input impaired model performance.

Interestingly, there appears to be some segregation between the areas with the strongest coherence (Fig. 4) and the areas with the most informative coherence (Fig. 2), most strikingly in the beta band. The ipsilateral sensorimotor cortex is strongly coupled to the STN in the beta band, but that coupling does not seem to be very useful for predicting the therapeutic

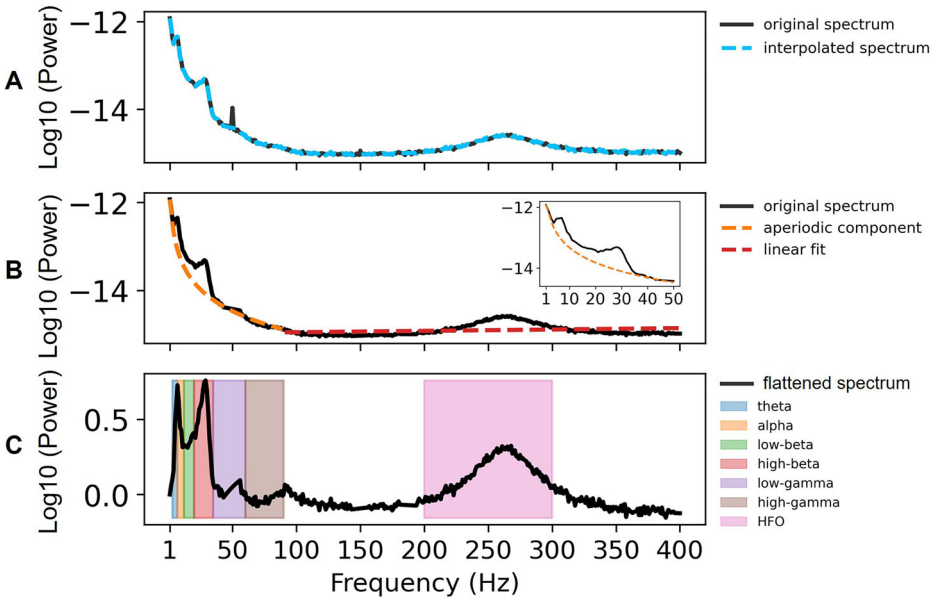

Fig. 3 | Subthalamic nucleus power feature extraction. A Power spectrum before (black) and after removing power line noise (blue). **B** Removal of the aperiodic component (1–90 Hz) and the linear trend (>90 Hz). **C** Preprocessed power spectrum. Frequency bands are color-coded.

window (current study), nor for predicting the UPDRS improvement[56]. This finding aligns with a study on DBS effects on STN-cortex coherence. Standard 130 Hz DBS markedly reduced beta-band coherence between sensorimotor cortex and STN, but this reduction did not correlate with the concurrent reduction of symptoms[50], suggesting that these two consequences of DBS are largely independent.

With respect to the time delay between electrophysiological measurements and clinical assessment, our study demonstrates that recordings obtained 1 day after surgery can predict the contact selected during monopolar reviews conducted between 5 and 671 days post-surgery, suggesting relative stability of neural oscillations over time. This perspective is supported by work from Garcia et al., who reported that subthalamic oscillations recorded intraoperatively can predict clinically effective contacts up to 27 months later[28]. Although these and similar findings[77] indicate that early recordings can be useful for guiding future programming decisions, it is to be expected that prediction performance improves with decreasing the delay between electrophysiological recording and monopolar review, as more immediate measurements better capture the neural dynamics predominating at the time of clinical assessment. Here, most of the reviews were performed <30 days after surgery, ensuring temporal proximity between the electrophysiological recordings and the monopolar review. Using early reviews, however, comes at the disadvantage of the stun effect masking some of the clinical effects. This is the reason why we observed many negative therapeutic windows, indicating the presence of side effects in the absence of clinical effects (Fig. 1). Ideally, reducing the delay between recording and review should be achieved by shifting the recordings to a later stage. This is not possible when using externalized leads, but can be achieved with intracranial sensing[78].

We acknowledge that MEG is not widely available, limiting the translation of our approach. Alternative setups, such as combining sensing-capable DBS stimulators with EEG or electrocorticography[55,62,79] might be better suited for clinical application. This would require training a new model in a new cohort due to the differences with respect to channels and signal-to-noise ratio. Irrespective of the hardware, the procedure would involve obtaining a short electrophysiological measurement, feature computation and the prediction of therapeutic windows based on a pre-trained group model, rather than an individualized model. Contacts scoring very low might be omitted in the monopolar review, saving valuable time. Alternatively, contacts that were not initially expected to be useful, e.g., because they rarely yield good outcomes, might be explored with more rigor when scoring high. In this sense, our approach, the feasibility of which we demonstrated here, has the potential to speed up and improve the standard monopolar review.

In conclusion, this study demonstrates that STN power and STN-cortex coherence can be used to predict the width of the therapeutic window, the key criterion for contact selection. Our approach has the potential to reduce the duration of DBS programming. Moreover, our study confirms the utility of synchronized oscillations for generating clinically relevant predictions.

Methods

Patients

We analysed resting-state data from two prior studies conducted at the University Hospital Düsseldorf[41–43], which involved 26 and 19 PD patients, respectively, with an average age of 60.73 years (SD = 9; Table 1). All patients were implanted with DBS electrodes, following standard clinical procedures, and took part with written informed consent according to the Declaration of Helsinki. Recordings took place the day following DBS electrode implantation and after overnight withdrawal from dopaminergic medication (Med OFF). The data from this combined cohort were used to train a machine learning model predicting the therapeutic window for each electrode contact based on the neural oscillations recorded at this contact, and their synchrony with cortical oscillations. The performance of this model was assessed using a leave-one-electrode-out (LOEO) cross-validation scheme. Subsequently, we validated our model in an independent cohort (Table 2) consisting of eight PD patients (M = 64; SD = 9), measured for the current study. Resting-state recording durations varied across cohorts (LOEO cohort 1: M = 263 s, SD = 56 s; LOEO cohort 2: M = 540 s, SD = 68 s; independent cohort: M = 385 s, SD = 106 s).

The experimental protocols were approved by the Ethics Committee of the Medical Faculty of Heinrich Heine University Düsseldorf for both the original cohort (no. 3209 and 5608) and the independent cohort (no. 2021-1587—Andere Forschung, Erstvotierend).

Electrophysiology

Patients were recorded using a 306-channel MEG system (VectorView, MEGIN), while simultaneously measuring LFPs from the STN via externalized leads. The DBS electrodes were connected to the integrated EEG amplifier via non-ferromagnetic extension cables, minimizing magnetic interference. In addition to LFPs, we recorded vertical and horizontal electro-oculograms and electromyograms of the extensor and flexor muscles of both forearms. In our analyses, these were solely used for artifact detection. All signals were sampled by the same acquisition system, at a rate

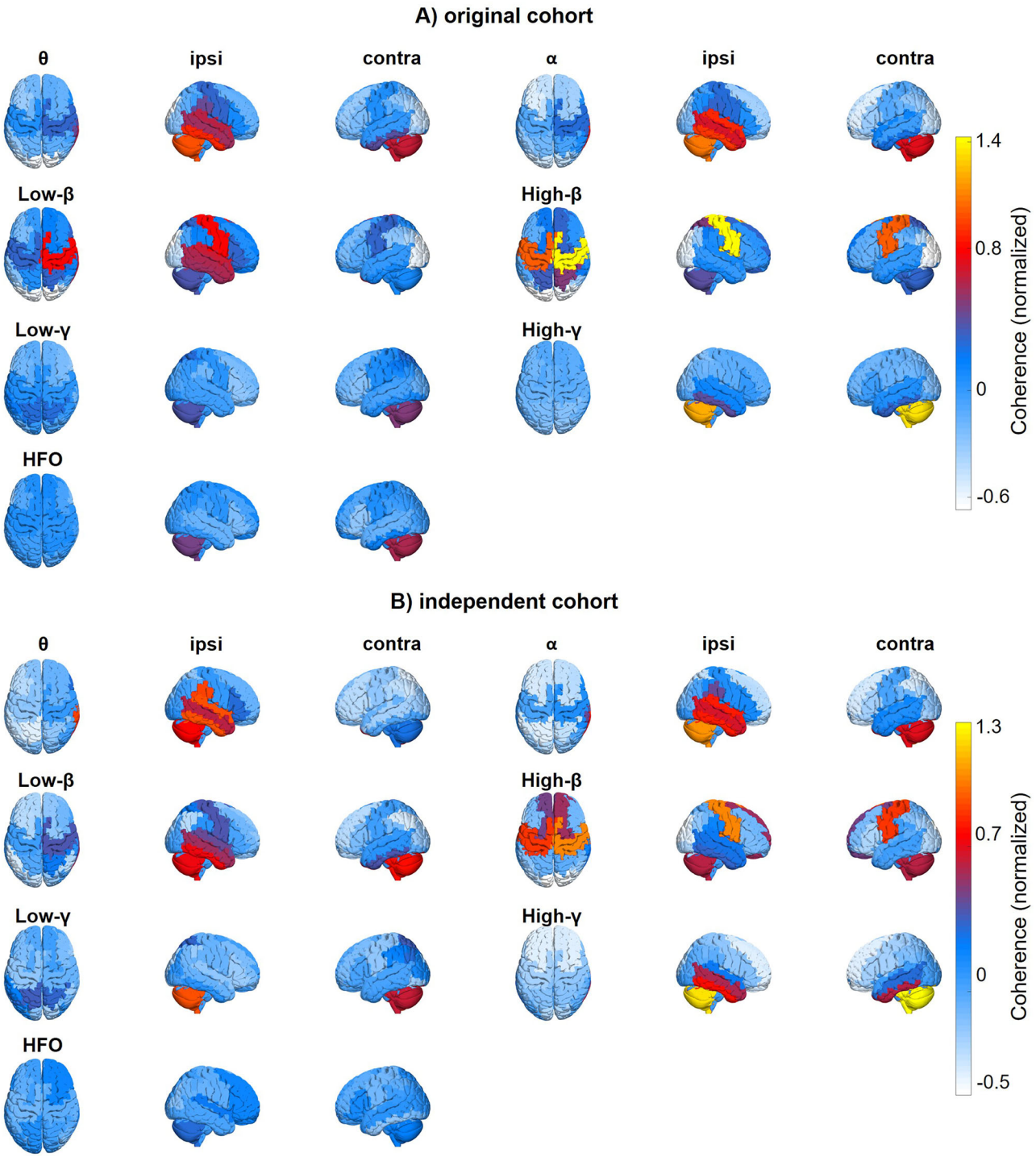

Fig. 4 | STN-cortex coherence. Source-reconstructed STN-cortex coherence for different frequency bands (θ, α, low-β, high-β, low-γ, high-γ, and HFO), projected onto a 3D template brain (parcellated). The topographies were normalized by means of spatial z-scoring before computing the group average. **A** Original cohort. **B** Independent cohort. The terms ipsilateral (ipsi) and contralateral (contra) refer to the DBS electrode.

of 2 kHz [LOEO cohort 1 and independent cohort; **42**] and 2.4 kHz [LOEO cohort 2, **43**], respectively.

LFP signals were referenced to a surface electrode on the left mastoid and re-referenced post-hoc according to an average reference scheme. Within each electrode, we computed the mean across LFP channels and subtracted it from each signal.

Preprocessing. LFP and MEG data underwent visual artifact screening. Channels with a very low signal-to-noise ratio were marked as bad channels. On average, this led to the exclusion of 6.26 ± 6.67 (SD) MEG channels and 1.67 ± 1.81 electrode contacts per patient. Segments containing movement artifacts were likewise excluded from analysis. On average, this led to the exclusion of 13.66 s ± 24.80 s of data per patient. Data were segmented into 2 s windows with 50% overlap, resulting in a frequency resolution of 0.5 Hz.

Feature extraction. Feature extraction details have been described in ref. 56. In brief, STN power features were computed for each integer

Table 3 | Therapeutic window normalization

Before normalization					After normalization			
Contact	SET [mA]	TET [mA]	TW [mA]		SET [mA]	TET [mA]	TW [mA]	TW (z) [mA]
1	3	1	2	→	3	1	2	0,34
2	—	1	—	→	**6**	1	**5**	**0,85**
3	4	—	—	→	4	**6**	**-2**	**-0,34**
4	2,5	1	1,5	→	2,5	1	1,5	0,25

The table illustrates monopolar review data before (left) and after normalization (right). First, we replaced missing values by the maximum amplitude tested (6 mA in this case). Next, we divided all windows by the range of amplitudes tested (5.9 mA in this case).
SET side-effect threshold, *TET* therapeutic effect threshold, *TW* therapeutic window, *TW(z)* normalized therapeutic window.

frequency from 1 to 300 Hz using Welch's method. To remove line noise (50 Hz) and its harmonics, power within ±7 Hz from the harmonics were replaced with surrogate values obtained through linear interpolation (Fig. 3A). The aperiodic (1/f) component of the LFP power spectra was removed using the fitting oscillations and one-over-f algorithm (FOOOF)[80], applied up to 90 Hz. For frequencies above 90 Hz, we applied linear de-trending (Fig. 3B). The periodic component was retained, and power was averaged within eight frequency bands of interest: theta (3–7 Hz), alpha (8–12 Hz), low-beta (13–20 Hz), high-beta (21–35 Hz), low-gamma (36–60 Hz), high-gamma (60–90 Hz), and high-frequency oscillations (HFO; 200–300 Hz). The band definitions include the upper and the lower limit. LFP-MEG coherence was calculated for each frequency band using the multitaper method[81] and source-localized through Dynamic Imaging of Coherent Sources[82]. The beamformer grid comprised 567 locations on the cortical surface, which were subsequently subdivided into 30 regions of interest based on the automatic anatomic labeling (AAL) atlas[83] (Supplementary Table S2). We spatially normalized coherence by z-scoring across parcels. We used all available data for feature computation to maximize feature quality.

When constructing group-average maps of coherence (Fig. 4), we mirrored coherence maps for electrodes implanted in the left STN across the mid-sagittal plane, aligning the hemisphere ipsilateral to the LFP recording site to the right hemisphere of the brain template.

Monopolar review. The aim of the monopolar review is to identify the optimal electrode contact for chronic stimulation. During the monopolar review, an experienced movement disorder neurologist tested each electrode contact in a monopolar configuration, i.e., with the contact as cathode and the neurostimulator case as anode. Stimulation amplitude was gradually increased in steps of 0.5 or 1 mA until reaching either the highest amplitude tolerated by the patient (side-effect threshold) or the highest amplitude considered safe (5 or 6 mA). At each step, the therapeutic and side effects of DBS were documented. The minimum amplitude required for a sustained clinical benefit was defined as the therapeutic effect threshold, and the electrode contact with the widest therapeutic window, defined as the difference between the side-effect threshold and therapeutic effect threshold, was chosen for chronic stimulation. Frequency and pulse width were kept constant at 130 Hz and 60 µs, respectively, and adapted later if required.

For each patient, the monopolar review was performed between 5 and 7 days after surgery for initial treatment and repeated between 4 and 13 weeks after surgery. Not all reviews encompassed the complete set of electrode contacts, including all contacts, all segments and ring modes. Accordingly, the number of contacts tested varied across patients (training cohort: median: 8, SD: 4.4, minimum 3, maximum 20; independent cohort: median: 13, SD: 6, minimum 8, maximum 20). In case several reviews were available per patient, we included the review with the highest number of contacts tested to maximize the amount of training data.

Some of the monopolar reviews contained clinical data for segmented contacts used in ring mode. In this case, we estimated the corresponding electrophysiological features by averaging band-limited power and coherence across ring segments.

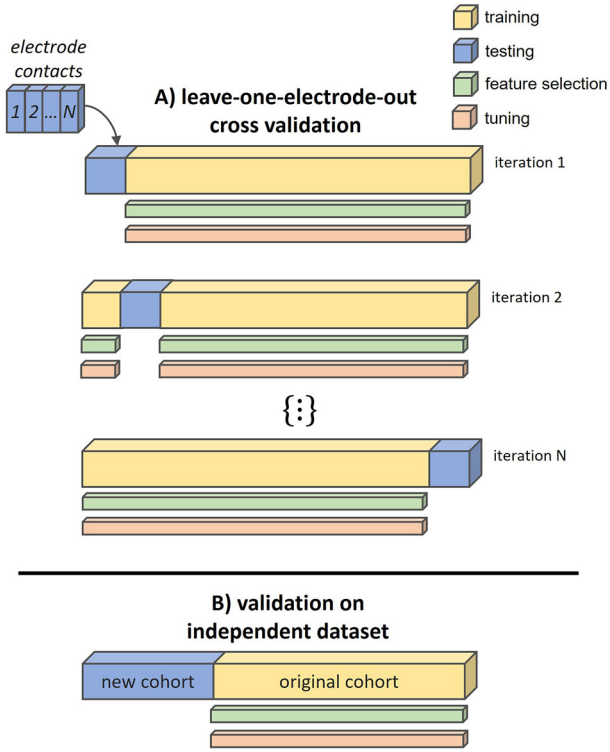

Fig. 5 | Model evaluation pipeline. A Leave-one-electrode-out cross-validation. For each iteration, one electrode from the original cohort (blue) is left out for testing, while the remaining electrodes (yellow) are used for training, including nested feature selection and hyperparameter tuning. This process is repeated for every electrode ($N = 82$) in the dataset. Once all electrodes are evaluated, the performance metrics are aggregated to assess the model's overall performance. **B** Validation in an independent cohort. A model trained on the entire original cohort (yellow) is applied to a new cohort (blue).

Therapeutic window. To account for variability in the review procedure, such as variable step-size and maximum amplitude, we normalized the therapeutic window such that it ranged between −1 and 1, with 1 describing the best-case scenario (clinical effects at lowest amplitude, first side effects at highest amplitude or not at all) and −1 describing the worst-case scenario (side effects at lowest amplitude, first clinical effects at highest amplitude or not at all). This was achieved by dividing the therapeutic window by the range of amplitudes tested. Missing values, indicating that no effect occurred up to the highest amplitude tested, were replaced by the maximum amplitude tested. The procedure is illustrated in Table 3. Using higher values than the maximum amplitude tested for replacement did not impair model performance (Supplementary Table S4).

Model. We used extreme gradient boosting, as implemented in the XGBoost package for Python[44], to predict the therapeutic window of each electrode contact based on STN power and STN-cortex coherence. This machine learning approach has been widely used and proven effective in analysing electrophysiological datasets[56,84]. As illustrated in Fig. 5A, predictions were iteratively generated for each electrode using a LOEO cross-validation approach, wherein each electrode served as the test set once while being included in the train set for all other iterations. In terms of hyperparameters, we first selected the number of trees by means of 10-fold cross-validation and then applied the Hyperopt package[85]. Tuning was nested, i.e., restricted to the train set. The

selected hyperparameters, averaged across LOEO cycles, are reported in Supplementary Table S1.

Feature selection. During each iteration of the LOEO cycle, we utilized the Boruta method for nested feature selection[86]. Boruta works by first creating a copy of the original features, called "shadow features", with values randomly shuffled to destroy any correlation with the target. A Random Forest model is then trained on the combined set of original and shadow features, producing an importance metric for each feature. Original features scoring significantly lower ($p < 0.05$ in a binomial test) than the most important shadow feature are removed. Boruta repeats this process for a maximum of 100 iterations or until all features are either confirmed or rejected, removing more unimportant features in each iteration. To ensure a robust set of features across iterations, we resampled from the train set and applied the Boruta method 10 times, keeping only features that were selected ≥7 times. The selection frequency, i.e., the fraction of LOEO cycles preserving a feature, served as our feature importance metric.

Model evaluation. The model's performance was quantified by Pearson's correlation between the predicted and actual therapeutic windows. Additionally, we assessed the model's ability to rank electrode contacts by clinical utility—a potential use case for our method. Specifically, we ranked the contacts electrode by electrode based on their predicted therapeutic window, assigning higher ranks to contacts with higher predicted windows. We then computed the cumulative hit ratio, quantifying how often the active contact, i.e., the clinician's choice, coincided with contact ranked first, was among the top two ranks, the top three ranks and so forth. As more and more contacts are considered, the cumulative hit ratio increases, eventually reaching 100% because the active contact must be among the set of all available contacts. Next, we computed an empirical null distribution by randomly ranking contacts 10,000 times and re-computing the cumulative hit ratio. Ratios exceeding the upper 95th percentile of the null distribution were deemed significant. Note that we limited this analysis to electrodes with data for at least four contacts ($N = 47$), to ensure a reasonable number of unique within-electrode permutations.

To further test the generalizability of our model, we re-trained it on the entire, original cohort (45 patients), including feature selection, and applied it to the independent cohort of eight PD patients, not available to the model during training. The selected hyperparameters of this model are summarized in Supplementary Table S1.

Data availability

The data from LOEO cohort 1 are available at OpenNeuro.org with the accession number ds004998 (https://doi.org/10.18112/openneuro.ds004998.v1.2.2). The remaining data were not publicly available because patients did not consent to data sharing.

Code availability

The code for this study is publicly available at https://github.com/Fayed-Rsl/DBS_Prediction_TW.

Received: 12 May 2025; Accepted: 11 October 2025;
Published online: 29 October 2025

References

1. Perlmutter, J. S. & Mink, J. W. Deep brain stimulation. *Annu. Rev. Neurosci.* **29**, 229–257 (2006).
2. Poewe, W. et al. Parkinson disease. *Nat. Rev. Dis. Prim.* **3**, 17013 (2017).
3. Alexander, G. E., DeLong, M. R. & Strick, P. L. Parallel organization of functionally segregated circuits linking basal ganglia and cortex. *Annu, Rev. Neurosci.* **9**, 357–381 (1986).
4. Lachenmayer, M. L. et al. Subthalamic and pallidal deep brain stimulation for Parkinson's disease—meta-analysis of outcomes. *npj Parkinsons Dis.* **7**, 1–10 (2021).
5. Volkmann, J., Herzog, J., Kopper, F. & Deuschl, G. Introduction to the programming of deep brain stimulators. *Mov. Disord.* **17**, S181–S187 (2002).
6. Hunka, K., Suchowersky, O., Wood, S., Derwent, L. & Kiss, Z. H. T. Nursing time to program and assess deep brain stimulators in movement disorder patients. *J. Neurosci. Nurs.* **37**, 204 (2005).
7. Roediger, J. et al. Automated deep brain stimulation programming based on electrode location: a randomised, crossover trial using a data-driven algorithm. *Lancet Digital Health* **5**, e59–e70 (2023).
8. Bahners, B. H. et al. Evoked response signatures explain deep brain stimulation outcomes. Preprint at https://doi.org/10.1101/2024.10.04.24314308 (2024).
9. Wagle Shukla, A., Zeilman, P., Fernandez, H., Bajwa, J. A. & Mehanna, R. DBS programming: an evolving approach for patients with Parkinson's disease. *Parkinsons Dis.* **2017**, 8492619 (2017).
10. Roediger, J. et al. StimFit—a data-driven algorithm for automated deep brain stimulation programming. *Mov. Disord.* **37**, 574–584 (2022).
11. Rajkomar, A., Dean, J. & Kohane, I. Machine learning in medicine. *N. Engl. J. Med*. **380**, 1347–1358 (2019).
12. Chandrabhatla, A. S., Pomeraniec, I. J., Horgan, T. M., Wat, E. K. & Ksendzovsky, A. Landscape and future directions of machine learning applications in closed-loop brain stimulation. *npj Digit. Med.* **6**, 79 (2023).
13. Cole, E. R. & Miocinovic, S. Are we ready for automated deep brain stimulation programming? *Parkinsonism Relat. Disord.* **134**, 107347 (2025).
14. Boutet, A. et al. Predicting optimal deep brain stimulation parameters for Parkinson's disease using functional MRI and machine learning. *Nat. Commun.* **12**, 3043 (2021).
15. Malekmohammadi, M. et al. Automated optimization of deep brain stimulation parameters for modulating neuroimaging-based targets. *J. Neural Eng.* https://doi.org/10.1088/1741-2552/ac7e6c (2022).
16. Lange, F. et al. Machine versus physician-based programming of deep brain stimulation in isolated dystonia: a feasibility study. *Brain Stimul.* **16**, 1105–1111 (2023).
17. Heldman, D. A. et al. Computer-guided deep brain stimulation programming for Parkinson's disease. *Neuromodulation* **19**, 127–132 (2016).
18. Malekmohammadi, M. et al. Kinematic adaptive deep brain stimulation for resting tremor in Parkinson's disease. *Mov. Disord.* **31**, 426–428 (2016).
19. Sarikhani, P. et al. Automated deep brain stimulation programming with safety constraints for tremor suppression in patients with Parkinson's disease and essential tremor. *J. Neural. Eng.* **19**, (2022).
20. Fekri Azgomi, H. et al. Modeling and optimizing deep brain stimulation to enhance gait in Parkinson's disease: personalized treatment with neurophysiological insights. *npj Parkinsons Dis.* **11**, 173 (2025).
21. Kühn, A. A. et al. Pathological synchronisation in the subthalamic nucleus of patients with Parkinson's disease relates to both bradykinesia and rigidity. *Exp. Neurol.* **215**, 380–387 (2009).
22. Neumann, W.-J. et al. Subthalamic synchronized oscillatory activity correlates with motor impairment in patients with Parkinson's disease. *Mov. Disord.* **31**, 1748–1751 (2016).
23. Neumann, W.-J. & Kühn, A. A. Subthalamic beta power-unified Parkinson's disease rating scale III correlations require akinetic symptoms. *Mov. Disord.* **32**, 175–176 (2017).
24. Beudel, M. et al. Oscillatory beta power correlates with akinesia-rigidity in the Parkinsonian subthalamic nucleus. *Mov. Disord.* **32**, 174–175 (2017).
25. Little, S. et al. Adaptive deep brain stimulation in advanced Parkinson disease. *Ann. Neurol.* **74**, 449–457 (2013).

26. Tinkhauser, G. et al. The modulatory effect of adaptive deep brain stimulation on beta bursts in Parkinson's disease. *Brain* **140**, 1053–1067 (2017).
27. He, S. et al. Beta-triggered adaptive deep brain stimulation during reaching movement in Parkinson's disease. *Brain* **146**, 5015–5030 (2023).
28. Fernández-García, C. et al. Long-term directional deep brain stimulation: monopolar review vs. local field potential guided programming. *Brain Stimul.* **15**, 727–736 (2022).
29. Binder, T. et al. Feasibility of local field potential-guided programming for deep brain stimulation in Parkinson's disease: a comparison with clinical and neuro-imaging guided approaches in a randomized, controlled pilot trial. *Brain Stimul.* **16**, 1243–1251 (2023).
30. Swann, N. C. et al. Gamma oscillations in the hyperkinetic state detected with chronic human brain recordings in Parkinson's disease. *J. Neurosci.* **36**, 6445–6458 (2016).
31. Wiest, C. et al. Subthalamic deep brain stimulation induces finely-tuned gamma oscillations in the absence of levodopa. *Neurobiol. Dis.* **152**, 105287 (2021).
32. Colombo, A. et al. Finely tuned γ tracks medication cycles in Parkinson's disease: an ambulatory Brain-sense study. *Mov. Disord.* https://doi.org/10.1002/mds.30160 (2025).
33. Olaru, M. et al. Deep brain stimulation-entrained gamma oscillations in chronic home recordings in Parkinson's disease. *Brain Stimul.* **18**, 132–141 (2025).
34. Hirschmann, J. et al. A direct relationship between oscillatory subthalamic nucleus–cortex coupling and rest tremor in Parkinson's disease. *Brain* **136**, 3659–3670 (2013).
35. Muthuraman, M. et al. Oscillating central motor networks in pathological tremors and voluntary movements. What makes the difference? *Neuroimage* **60**, 1331–1339 (2012).
36. Steina, A. et al. Oscillatory coupling between thalamus, cerebellum, and motor cortex in essential tremor. *Mov. Disord.* https://doi.org/10.1002/mds.30165 (2025).
37. Hirschmann, J. et al. Parkinsonian rest tremor is associated with modulations of subthalamic high-frequency oscillations. *Mov. Disord.* **31**, 1551–1559 (2016).
38. Özkurt, T. E. et al. High frequency oscillations in the subthalamic nucleus: a neurophysiological marker of the motor state in Parkinson's disease. *Exp. Neurol.* **229**, 324–331 (2011).
39. Wang, J. et al. High-frequency oscillations in Parkinson's disease: Spatial distribution and clinical relevance. *Mov. Disord.* **29**, 1265–1272 (2014).
40. Herron, J. et al. Challenges and opportunities of acquiring cortical recordings for chronic adaptive deep brain stimulation. *Nat. Biomed. Eng.* https://doi.org/10.1038/s41551-024-01314-3 (2024).
41. Hirschmann, J. et al. Distinct oscillatory STN-cortical loops revealed by simultaneous MEG and local field potential recordings in patients with Parkinson's disease. *Neuroimage* **55**, 1159–1168 (2011).
42. Sharma, A., Vidaurre, D., Vesper, J., Schnitzler, A. & Florin, E. Differential dopaminergic modulation of spontaneous cortico-subthalamic activity in Parkinson's disease. *Elife* **10**, e66057 (2021).
43. Rassoulou, F. et al. Exploring the electrophysiology of Parkinson's disease with magnetoencephalography and deep brain recordings. *Sci. Data* **11**, 889 (2024).
44. Chen, T. & Guestrin, C. XGBoost: A scalable tree boosting system. In *Proc. 22nd ACM SIGKDD International Conference on Knowledge Discovery and Data Mining* 785–794 (Association for Computing Machinery, 2016).
45. Horn, A., Neumann, W., Degen, K., Schneider, G. & Kühn, A. A. Toward an electrophysiological "sweet spot" for deep brain stimulation in the subthalamic nucleus. *Hum. Brain Mapp.* **38**, 3377–3390 (2017).
46. Gerster, M. et al. Beyond beta: aperiodic broadband power reflects Parkinson's disease severity–a multicenter study. Preprint at *bioRxiv* https://doi.org/10.1101/2025.03.11.642600 (2025).
47. Goetz, L., Seedat, N., Vandersluis, R. & van der Schaar, M. Generalization—a key challenge for responsible AI in patient-facing clinical applications. *npj Digit. Med.* **7**, 1–4 (2024).
48. Litvak, V. et al. Resting oscillatory cortico-subthalamic connectivity in patients with Parkinson's disease. *Brain* **134**, 359–374 (2011).
49. Oswal, A., Brown, P. & Litvak, V. Movement related dynamics of subthalmo-cortical alpha connectivity in Parkinson's disease. *Neuroimage* **70**, 132–142 (2013).
50. Oswal, A. et al. Deep brain stimulation modulates synchrony within spatially and spectrally distinct resting state networks in Parkinson's disease. *Brain* **139**, 1482–1496 (2016).
51. van Wijk, B. C. M. et al. Functional connectivity maps of theta/alpha and beta coherence within the subthalamic nucleus region. *Neuroimage* **257**, 119320 (2022).
52. McSweeney, B. Fooling ourselves and others: confirmation bias and the trustworthiness of qualitative research—Part 1 (the threats). *J. Organ. Change Manag.* **34**, 1063–1075 (2021).
53. Glaser, J. I., Benjamin, A. S., Farhoodi, R. & Kording, K. P. The roles of supervised machine learning in systems neuroscience. *Prog. Neurobiol.* **175**, 126–137 (2019).
54. Shah, A. et al. Combining multimodal biomarkers to guide deep brain stimulation programming in Parkinson disease. *Neuromodulation* **26**, 320–332 (2023).
55. Oehrn, C. R. et al. Chronic adaptive deep brain stimulation versus conventional stimulation in Parkinson's disease: a blinded randomized feasibility trial. *Nat. Med*. **30**, 3345–3356 (2024).
56. Hirschmann, J., Steina, A., Vesper, J., Florin, E. & Schnitzler, A. Neuronal oscillations predict deep brain stimulation outcome in Parkinson's disease. *Brain Stimul.* **15**, 792–802 (2022).
57. Chen, P.-L. et al. Subthalamic high-beta oscillation informs the outcome of deep brain stimulation in patients with Parkinson's disease. *Front. Hum. Neurosci*. **16**, 958521 (2022).
58. Averna, A. et al. Spectral topography of the subthalamic nucleus to inform next-generation deep brain stimulation. *Mov. Disord.* **38**, 818–830 (2023).
59. Fogelson, N. et al. Reciprocal interactions between oscillatory activities of different frequencies in the subthalamic region of patients with Parkinson's disease. *Eur. J. Neurosci.* **22**, 257–266 (2005).
60. Hollunder, B. et al. Mapping dysfunctional circuits in the frontal cortex using deep brain stimulation. *Nat. Neurosci*. https://doi.org/10.1038/s41593-024-01570-1 (2024).
61. Oswal, A. et al. Neural signatures of hyperdirect pathway activity in Parkinson's disease. *Nat. Commun.* **12**, 5185 (2021).
62. Binns, T. S. et al. Shared pathway-specific network mechanisms of dopamine and deep brain stimulation for the treatment of Parkinson's disease. *Nat. Commun.* **16**, 3587 (2025).
63. Horn, A. et al. Connectivity predicts deep brain stimulation outcome in Parkinson disease. *Ann. Neurol.* **82**, 67–78 (2017).
64. Rajamani, N. et al. Deep brain stimulation of symptom-specific networks in Parkinson's disease. *Nat. Commun.* **15**, 4662 (2024).
65. Gradinaru, V., Mogri, M., Thompson, K. R., Henderson, J. M. & Deisseroth, K. Optical deconstruction of parkinsonian neural circuitry. *Science* **324**, 354–359 (2009).
66. Haynes, W. I. A. & Haber, S. N. The organization of prefrontal-subthalamic inputs in primates provides an anatomical substrate for both functional specificity and integration: implications for basal ganglia models and deep brain stimulation. *J. Neurosci.* **33**, 4804–4814 (2013).
67. Li, Q. et al. Therapeutic deep brain stimulation in Parkinsonian rats directly influences motor cortex. *Neuron* **76**, 1030–1041 (2012).

68. Johnson, L. A. et al. Direct activation of primary motor cortex during subthalamic but not pallidal deep brain stimulation. *J. Neurosci.* **40**, 2166–2177 (2020).
69. Valverde, S. et al. Deep brain stimulation-guided optogenetic rescue of parkinsonian symptoms. *Nat. Commun.* **11**, 2388 (2020).
70. Mahlknecht, P. et al. Pyramidal tract activation due to subthalamic deep brain stimulation in Parkinson's disease. *Mov. Disord.* **32**, 1174–1182 (2017).
71. Steina, A. et al. Mapping subcortico-cortical coupling-a comparison of thalamic and subthalamic oscillations. *Mov. Disord.* **39**, 684–693 (2024).
72. Neumann, W.-J. et al. Cortico-pallidal oscillatory connectivity in patients with dystonia. *Brain* **138**, 1894–1906 (2015).
73. Gratwicke, J. et al. Resting state activity and connectivity of the nucleus basalis of Meynert and globus pallidus in Lewy body dementia and Parkinson's disease dementia. *Neuroimage* **221**, 117184 (2020).
74. Bostan, A. C., Dum, R. P. & Strick, P. L. The basal ganglia communicate with the cerebellum. *Proc. Natl Acad. Sci. USA* **107**, 8452–8456 (2010).
75. Bostan, A. C. & Strick, P. L. The basal ganglia and the cerebellum: nodes in an integrated network. *Nat. Rev. Neurosci.* **19**, 338–350 (2018).
76. Helmich, R. C., Hallett, M., Deuschl, G., Toni, I. & Bloem, B. R. Cerebral causes and consequences of parkinsonian resting tremor: a tale of two circuits? *Brain* **135**, 3206–3226 (2012).
77. Fasano, A. et al. Subthalamic nucleus local field potential stability in patients with Parkinson's disease. *Neurobiol. Dis.* **199**, 106589 (2024).
78. Stanslaski, S. et al. Sensing data and methodology from the adaptive DBS algorithm for personalized therapy in Parkinson's disease (ADAPT-PD) clinical trial. *npj Parkinsons Dis.* **10**, 1–11 (2024).
79. Köhler, R. M. et al. Dopamine and deep brain stimulation accelerate the neural dynamics of volitional action in Parkinson's disease. *Brain* **147**, 3358–3369 (2024).
80. Donoghue, T. et al. Parameterizing neural power spectra into periodic and aperiodic components. *Nat. Neurosci.* **23**, 1655–1665 (2020).
81. Thomson, D. J. Spectrum estimation and harmonic analysis. *Proc. IEEE* **70**, 1055–1096 (1982).
82. Gross, J. et al. Dynamic imaging of coherent sources: Studying neural interactions in the human brain. *Proc. Natl Acad. Sci. USA* **98**, 694–699 (2001).
83. Tzourio-Mazoyer, N. et al. Automated anatomical labeling of activations in SPM using a macroscopic anatomical parcellation of the MNI MRI single-subject brain. *Neuroimage* **15**, 273–289 (2002).
84. Merk, T. et al. Electrocorticography is superior to subthalamic local field potentials for movement decoding in Parkinson's disease. *eLife* **11**, e75126 (2022).
85. Bergstra, J., Yamins, D. & Cox, D. D. Making a science of model search: hyperparameter optimization in hundreds of dimensions for vision architectures. In: *Proc. 30th International Conference on Machine Learning* 115–123 (JMLR.org., 2013).
86. Kursa, M. B. & Rudnicki, W. R. Feature Selection with the Boruta Package. *J. Stat. Softw.* **36**, 1–13 (2010).

Acknowledgements

This study was funded by Brunhilde Moll Stiftung. The funder played no role in study design, data collection, analysis and interpretation of data, or the writing of this manuscript.

Author contributions

F.R. collected data, analysed the data, interpreted the results, and wrote the manuscript. A.St. helped with the data preparation and pre-processing. A.Sh. provided tools for statistical analysis. M.B. collected data. C.J.H. acquired clinical data and recruited participants. B.H.B. helped draft the manuscript. J.V. performed the surgery. A.Sch. acquired the funding and supervised the original study. J.H. collected data, designed the study, supervised data analysis and revised the manuscript. All authors read the manuscript and provided feedback.

Funding

Open Access funding enabled and organized by Projekt DEAL.

Competing interests

The authors declare no competing interests.

Additional information

Supplementary information The online version contains supplementary material available at https://doi.org/10.1038/s41746-025-02089-w.

Correspondence and requests for materials should be addressed to Jan Hirschmann.

Electrophysiological signatures predict the therapeutic window of deep brain stimulation electrode contacts

Supplementary Material

Fayed Rassoulou[1], Abhinav Sharma[2,3], Alexandra Steina[1], Markus Butz[1], Christian J. Hartmann[1, 4], Bahne H. Bahners[1,4], Jan Vesper[5], Alfons Schnitzler[1, 4], Jan Hirschmann[1]

Author affiliations

1. Institute of Clinical Neuroscience and Medical Psychology, Medical Faculty and University Hospital Düsseldorf, Heinrich Heine University Düsseldorf, Germany
2. MRC Brain Networks Dynamics Unit, University of Oxford
3. Nuffield Department of Clinical Neurosciences, University of Oxford
4. Center for Movement Disorders and Neuromodulation, Department of Neurology, Medical Faculty and University Hospital Düsseldorf, Heinrich Heine University Düsseldorf, Germany
5. Department of Functional Neurosurgery and Stereotaxy, Medical Faculty and University Hospital Düsseldorf, Heinrich Heine University Düsseldorf, Germany

Hyperparameter tuning

Table S1 summarizes the hyperparameters used in the leave-one-electrode-out (LOEO) cycle and for predicting the therapeutic windows of an independent cohort. Parameters in orange were tuned using the Hyperopt package within a nested, 3-fold cross-validation framework. For the LOEO cycle, the table provides the hyperparameters averaged across iterations. For the independent cohort, the hyperparameters were found through a cross-validated search in the entire original cohort. Parameters not tuned (black) remained at their default settings.

Table S1. Optimized hyperparameters for XGBoost.

	LOEO cycle	**indep. cohort**
parameter name	**value [average]**	**value**
objective	reg:squarederror	reg:squarederror
base_score	0.5	0.5
booster	gbtree	gbtree
colsample_bylevel	1	1
colsample_bynode	1	1
colsample_bytree	0.93	0.81
gamma	0.08	0.07
learning_rate	0.05	0.05
max_delta_step	0	0
max_depth	7	7
min_child_weight	4	4
missing	None	None
n_estimators	315	286
reg_alpha	0.18	0.19
reg_lambda	0.61	0.62
scale_pos_weight	1	1
subsample	0.62	0.51

Parcellation

Table S2 lists the labels of the cortical parcels used in this study, along with the x, y and z coordinates of the grid point cloud centroids in MNI space.

Table S2. ***Details on cortical areas***.

area	x	y	z
SensorimotorR	38.28	-14.42	54.59
FrontalSupR	17.78	33.48	41.75
FrontalMedR	36.35	38.63	20.92
FrontalInfR	52.30	31.11	1.94
ParietalSupR	23.00	-60.67	64.84
ParietalInfR	52.73	-47.50	47.29
TemporalSupR	63.47	-13.85	3.22
TemporalMidR	59.85	-23.91	-11.06
TemporalInfR	58.30	-35.63	-24.14
OccipitalSupR	19.94	-94.60	24.55
OccipitalMidR	39.38	-85.00	17.80
OccipitalInfR	29.33	-95.00	-9.09
AngularR	47.81	-65.00	39.75
SupraMarginalR	61.83	-32.50	34.73
CerebellumR	33.90	-61.22	-46.50
SensorimotorL	-39.35	-12.95	54.26
FrontalSupL	-14.80	44.73	30.35
FrontalMedL	-32.91	40.96	24.72
FrontalInfL	-50.60	29.52	3.11
ParietalSupL	-17.14	-61.76	64.62
ParietalInfL	-49.08	-51.11	46.36
TemporalSupL	-59.66	-8.18	-1.40
TemporalMidL	-61.87	-31.36	-5.78
TemporalInfL	-59.29	-28.33	-25.71
OccipitalSupL	-8.64	-97.80	21.46
OccipitalMidL	-33.41	-91.75	10.92
OccipitalInfL	-24.92	-91.83	-10.07
AngularL	-48.73	-66.00	36.52
SupraMarginalL	-61.99	-33.33	30.51
CerebellumL	-31.65	-61.54	-46.86

Reduced Feature Sets

One way of addressing feature importance is to exclude a subset of features and to re-assess prediction performance. Here, we used this strategy to investigate the contribution of STN power vs.

STN-cortex coherence, the importance of the cerebellum, and the possibility to obtain accurate predictions when using only subthalamic and primary sensorimotor features.

A model trained on STN power alone yielded a lower performance than the full model (r = 0.22, p < 0.001; **Fig. S1A**). In contrast, the STN-cortex coherence model achieved a correlation comparable to the full model (r = 0.40, p < 0.001; **Fig. S1C**). Despite the relatively good prediction, the cumulative hit ratio analysis did not indicate any ability to speed up the search for the optimal contact (**Fig S1D**), emphasizing the advantage of combining STN power with STN-cortex coherence.

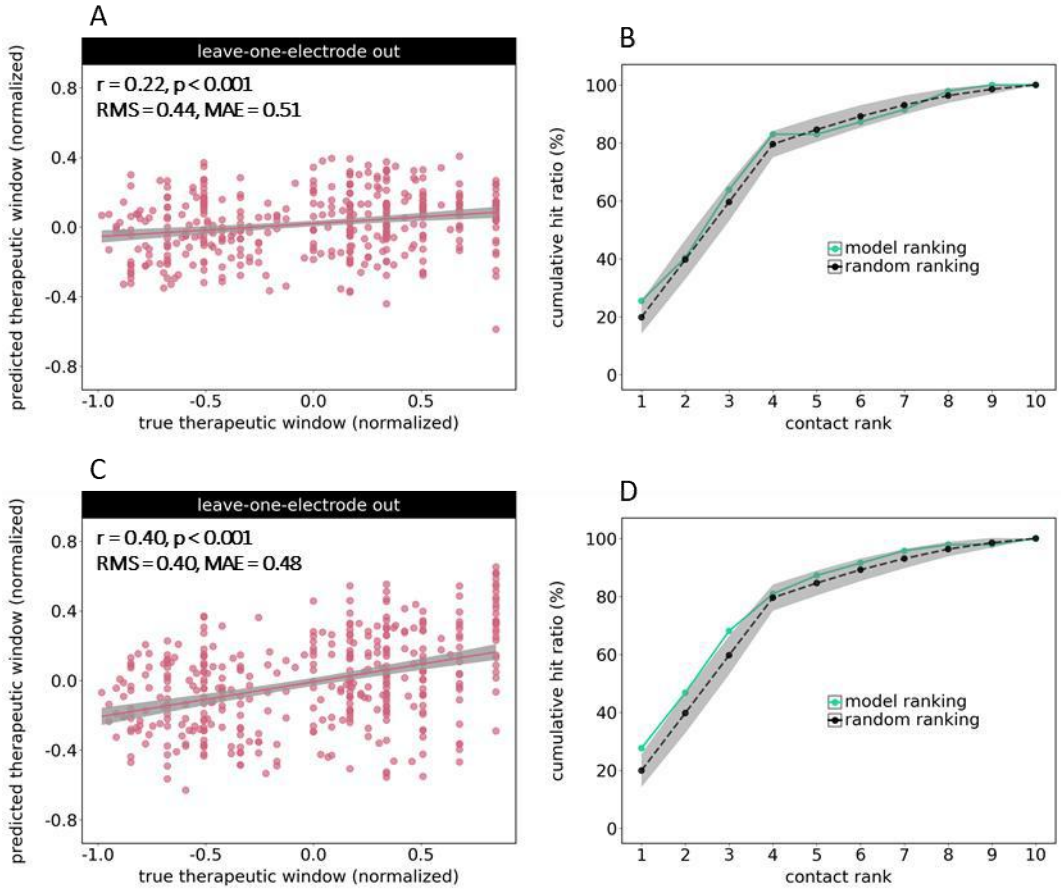

Figure S1. STN-power-only and STN-cortex-coherence-only feature sets. **A)** STN-only set. Scatter plots displaying the relationship between actual and predicted therapeutic windows for the leave-one-electrode-out approach. Grey shaded areas represent 95% confidence intervals. **B)** STN-only set. Cumulative hit ratio for the model's ranking of DBS electrode contacts (green) and the average hit ratio resulting from random ranking (black). The hit ratio at any rank, say 3, reflects the fraction of electrodes for which the active contact got ranked 3rd or better. Grey shaded area represents mean ± 1 standard deviation. Asterisks (*) indicate above-chance performance (p < 0.05). **C)** Scatter plot for coherence-only feature set. **D)** Cumulative hit ratio for coherence-only feature set.

We tested two further reduced feature sets that lacked some of the brain areas included in the original analysis. The first area-reduced feature set included all brain areas except the cerebellum (**Fig. S2A**). Feature selection was switched on, as in the original analysis. The second feature set, termed "ECoG" set, comprised only STN power and STN-sensorimotor coherence (all frequency bands). We used it to estimate the predictive power of a spatially restricted setup, mimicking the combination of STN electrodes and motor cortical electrocorticography (**Fig. S2B**). Automated feature selection was switched off. In both cases, the predicted therapeutic windows correlated significantly with the actual therapeutic windows, but the hit ratio analysis did not indicate a capacity to accelerate the search for the optimal contact (**Fig. S2**).

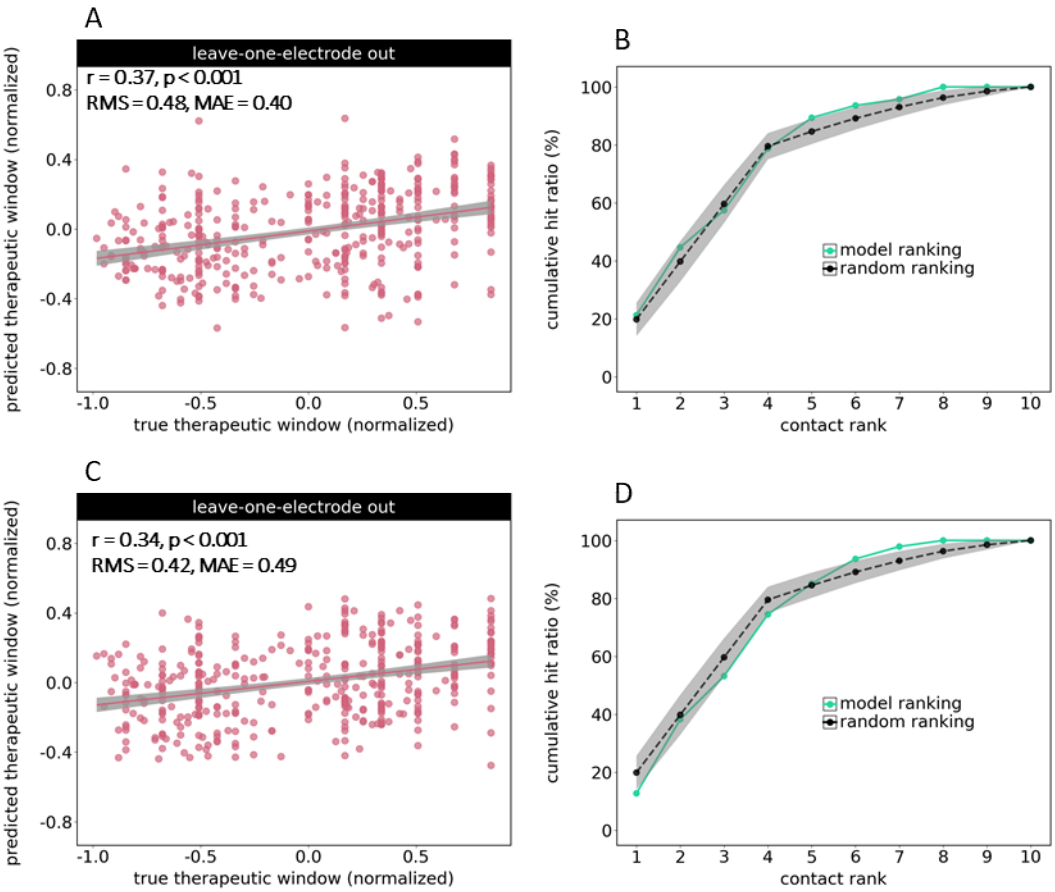

Figure S2. Area-reduced feature sets. **A,B)** All features except cerebellum. **C,D) "**ECoG" feature set (STN and sensorimotor cortex). See Fig. S1 for more explanations.

Interestingly, the algorithm relied much more on STN power features when excluding the cerebellum (**Fig. S3**).

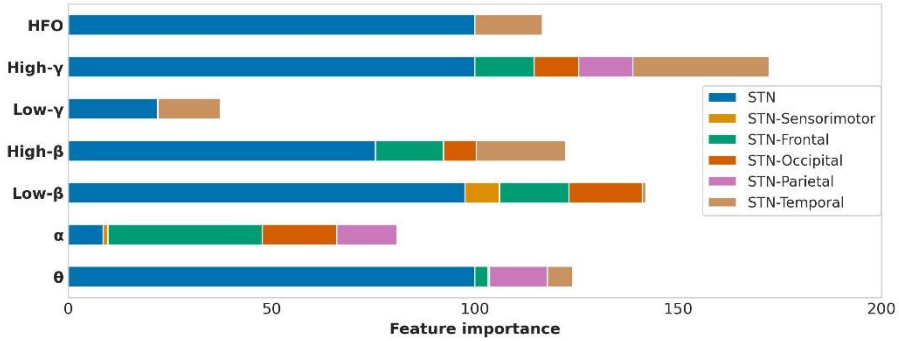

Figure S3. Feature importance for the feature set lacking the cerebellum. The bar plot illustrates the importance of each feature, grouped by brain region (indicated by colors) and frequency band (θ, α, β, γ, HFO). The height of each bar represents the relative contribution of each feature. Feature importance was quantified by selection frequency across leave-one-out cycles, normalized by the number of brain areas per lobe. Compare to Fig. 2 of the main paper.

Enhanced Feature Set

In order to test whether the addition of anatomical information would improve predictions we tested an enhanced feature set that included the best-performing electrophysiological features (main paper, **Fig. 2A**) and the distance of the contacts' centre to a published anatomical sweet spot for STN DBS (x = 12.58, y = -13.41, z = -5.87; Horn et al., Hum Brain Mapp **38**, 3377–3390, 2017). This required electrode reconstruction, conducted with LeadDBS (Horn & Kühn, Neuroimage 107:127–135, 2015), based on presurgical T1 and T2 MRI scans and postsurgical CT.

Fig. S4 illustrates the correlation between predicted and actual therapeutic windows without (**Fig. S4A**) and with (**Fig. S4C**) the additional anatomical feature, as well as the cumulative hit ratios (**Fig. S4B and S4D**).

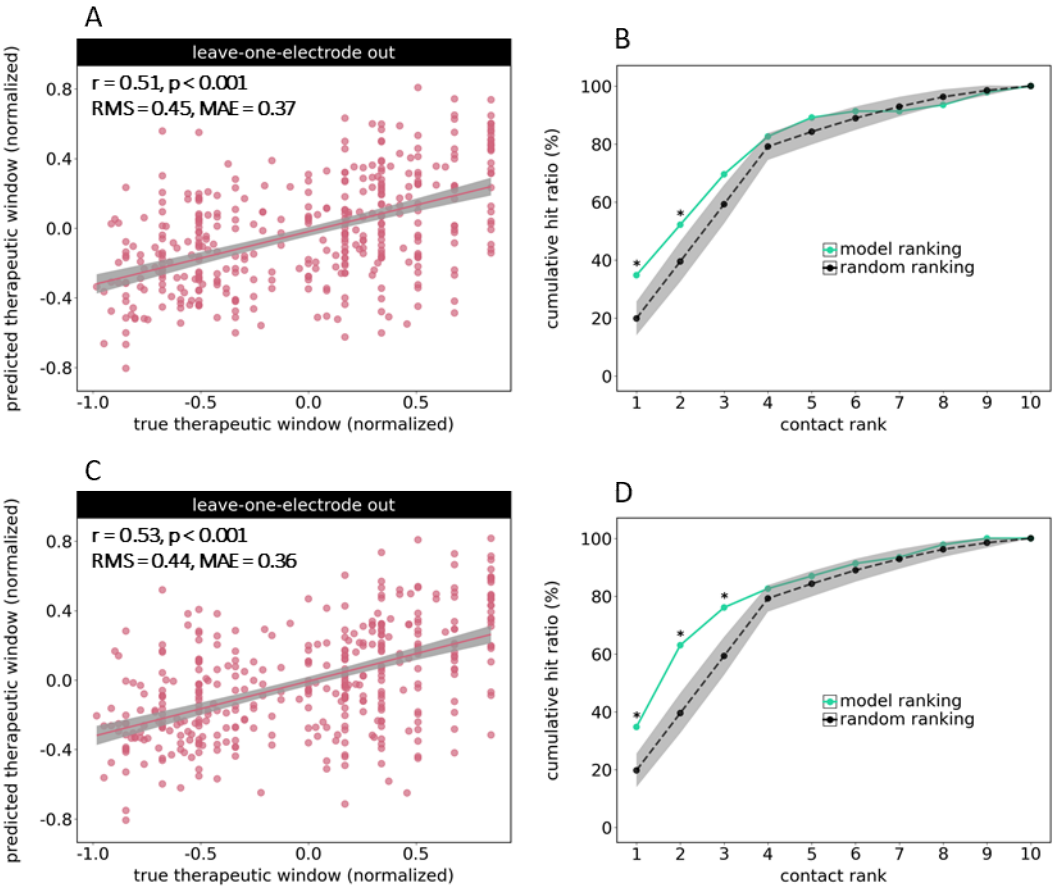

Figure S4. Enhanced feature set. **A,B)** Best-performing electrophysiological features. **C,D)** Best-performing electrophysiological features plus distance to sweet-spot. See Fig. S1 for more explanations.

Linear Mixed Model

Pearson correlation, as used in the main performance analysis, treats the contacts as independent samples and neglects their hierarchical structure. To confirm that this limitation does not confound our interpretation, we used a Linear Mixed Model as an alternative performance measure, with the following formula:

$$true \sim pred + (1|hemisphere)$$

where:

- **true** represents the actual therapeutic window.
- **pred** corresponds to the predicted therapeutic window.
- **(1|hemisphere)** is a random intercept for each hemisphere. Hemispheres are assumed to be independent samples randomly drawn from a large population.

The results presented in **Table S3** demonstrate a significant relationship between predicted and actual values (β = 0.312, *p* = 0.005), while accounting for repeated measures across hemispheres/electrodes.

Table S3. Fit results for the Linear Mixed Model estimating the relationship between predicted and actual therapeutic window. The positive coefficient for *pred* indicates a significant relationship between predictions and actual values.

fixed effects	coefficient (β)	std. error	*z*-value	*p*-value	95% CI (lower)	95% CI (upper)
intercept	-0.012	0.048	-0.250	0.802	-0.106	0.082
pred	0.312	0.112	2793	0.005	0.093	0.532

random effects	variance	std. dev.
hemisphere (intercept)	0.171	0.130

Reduced samples

In our train dataset, only 28 of 45 patients exhibited clear subthalamic power peaks in the beta range. To investigate whether and how the presence of such a peak influences automated feature selection, we repeated the feature selection process in the subset of patients exhibiting clear beta peaks. As depicted in Fig. S5, this led to the selection of STN alpha and low-beta power instead of gamma and HFO power, which were the most important STN features in the entire dataset.

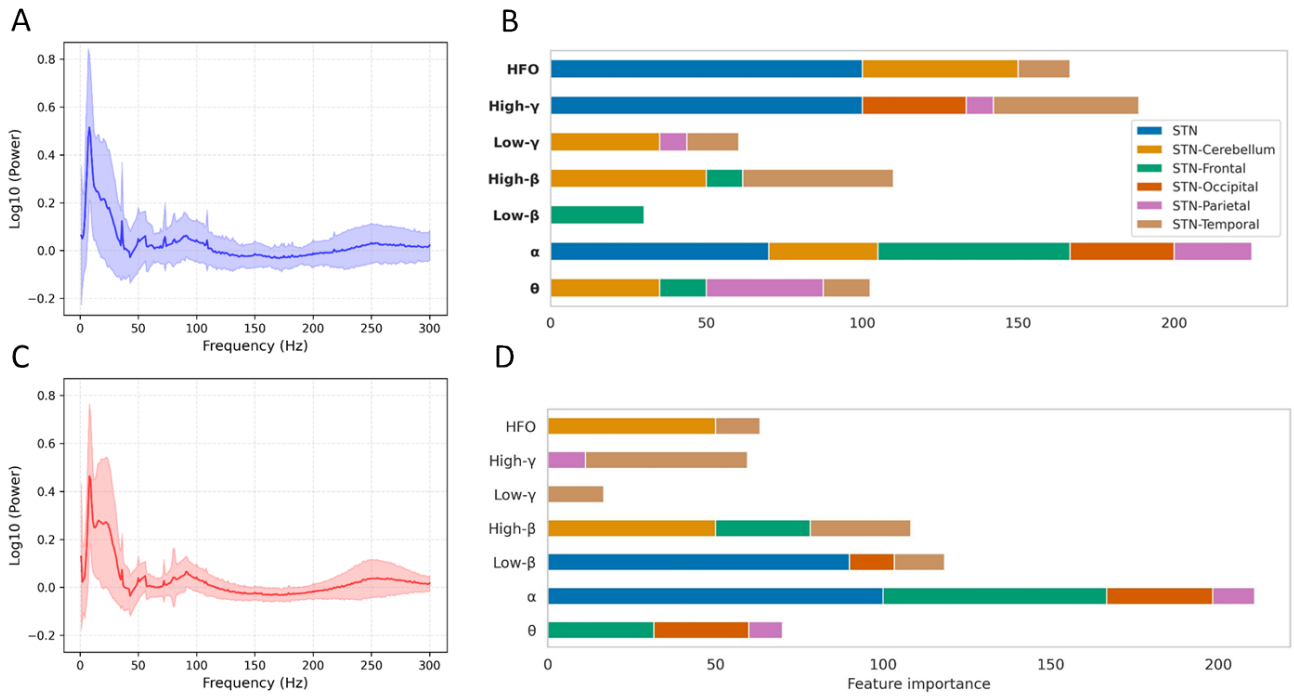

***Figure S5. Feature importance depends on peak availability*. A)** Group-mean subthalamic power spectrum and standard deviation (shading). All patients included. **B)** Feature importance. All patients included. **C)** As A), but includes only patients with a clear subthalamic power peak. **D)** As B), but includes only patients with a clear subthalamic power peak.

Data Imputation

In this study, we replaced missing clinical or side-effect thresholds with the highest amplitude tested to indicate that no side-effect or no clinical effect was observed up to that point. We acknowledge that the true thresholds are not known in these cases, but we do know that they must actually be larger than the highest amplitude tested. In order to investigate whether assuming higher thresholds would affect our conclusions, we systematically increased the imputed values by 2mA in steps of 0.5mA and re-evaluated model performance in leave-one-electrode-out cross-validation. The correlation between predicted and actual therapeutic windows was hardly affected by this change, indicating that the exact value used for replacing missing values is not critical to model performance.

Table S4. Increasing the value used in data imputation did affect model performance. The correlation coefficient quantifies the correlation between actual and predicted therapeutic windows in leave-one-electrode-out cross-validation.

value used for replacement	**Pearson correlation**
max. amplitude tested	0.44
max. amplitude tested + 0.5mA	0.43
max. amplitude tested + 1.0mA	0.44
max. amplitude tested + 1.5mA	0.44
max. amplitude tested + 2.0mA	0.43

4. Discussion

This dissertation addressed three interconnected objectives: demonstrating that electrophysiological signatures can predict therapeutic windows from DBS electrode contacts, curating a unique dataset to enable this analysis and validating the findings in an independent cohort. Here I discuss the key findings and their implications, acknowledge limitations of the current approach, and outline future directions for translating these findings toward clinical application.

This dissertation presents a comprehensive investigation of electrophysiological signatures in PD and their application for optimizing DBS therapy through machine learning approaches. The work addresses the critical translational challenge of transforming mechanistic understanding of parkinsonian network dysfunction into practical tools for clinical decision-making. By leveraging simultaneous MEG and LFP recordings from the STN, this research establishes that perioperative electrophysiological recordings contain sufficient information to guide electrode contact selection.

Key Findings

The foundation of this work lies in the systematic curation of electrophysiological data. Study 1 established a high-quality publicly accessible repository of simultaneous MEG and LFP recordings from twenty PD patients during rest and motor tasks, in both medication-on and medication-off states. The dataset is organized according to the BIDS standard with comprehensive metadata and preprocessing pipelines (Rassoulou et al., 2024). This addresses a fundamental challenge in the field: simultaneous cortical and subcortical recordings are available in only a handful of specialized centers worldwide, and datasets of sufficient quality for machine learning applications have been scarce. Beyond serving as the foundation for the predictive modelling in Study 2, this dataset enables the broader neuroscience community to investigate subcortico-cortical network dynamics, test hypotheses about connectivity patterns, and develop analytical methods without requiring access to the rare recording infrastructure. The dataset has already been used in two independent studies (Kohl et al., 2025; Gerster et al., 2025), demonstrating its value that extend beyond the scope of this thesis.

Building on this foundation, Study 2 provided the central proof-of-concept for this thesis: that machine learning algorithms can predict the therapeutic window of individual electrode contacts based on resting-state electrophysiological features. The model yielded reasonable predictions, correlating with the actual outcomes in both the original cohort ($r = 0.45$, $p < 0.001$) and an independent validation cohort ($r = 0.30$, $p < 0.001$) (Rassoulou et al., 2025). Importantly, the model successfully ranked electrode contacts such that the optimal contact could be identified more efficiently than through random search, as demonstrated by cumulative hit ratio analysis. This demonstrates that contact-specific neural signatures measured from a brief resting-state recording contain information about therapeutic

windows that can be extracted through machine learning without requiring systematic stimulation testing.

A central finding from this work is the highly localized nature of these predictive signatures. Our machine learning model using STN-power and STN–cortex coherence shows that neighboring contacts only a few millimeters apart differ in predictive value for the therapeutic window, indicating fine-grained spatial variation in oscillatory profiles and connectivity along the electrode (Averna et al., 2023). Rather than merely confirming that DBS depends on precise spatial targeting (Horn et al., 2017), these results demonstrate that the functional "sweet spot" is also encoded in highly localized dynamics that can vary significantly even within a correctly placed lead. The specific neural signatures at a given contact may reflect its position relative to functionally distinct STN territories or its proximity to white matter tracts that mediate therapeutic effects (Hacker et al., 2023; Arroyave et al., 2016, Lin et al., 2020). Regardless of the precise mechanism, the contact-to-contact variability in electrophysiological features provides a basis for data-driven contact selection that complements anatomical targeting approaches.

A key neurophysiological insight emerging from this predictive modelling is the dissociation between biomarkers of disease severity and biomarkers of therapeutic efficacy. Although STN beta oscillations (13–30 Hz) are widely recognized as the hallmark of Parkinsonian akinesia and rigidity (Neumann et al.; 2016; Neumann et al., 2017; Beudel et al., 2017), our feature importance analysis revealed that they were not the primary drivers of the therapeutic window prediction. Instead, the model relied heavily on STN high-frequency activity, specifically in the high-gamma (60–90 Hz) and high-frequency oscillation (>200 Hz) bands. Beta power is spatially broad and reflects the general pathological state of the motor network (Bosboom et al., 2006). The therapeutic window, however, is determined by the electrode's spatial proximity to the dorsolateral STN motor territory also known as the "sweet spot" for stimulation (Horn et al.; 2017). High-frequency signals are more spatially confined than lower-frequency rhythms (Maris et al., 2011), which probably makes them a superior localization marker for the optimal stimulation site. This suggests that even though beta is an excellent marker of the motor state, high-gamma and high-frequency oscillations are more useful when it comes to determining the optimal target location (Colombo et al., 2025; Olaru et al., 2025; Oehrn et al., 2024).

A key neurophysiological insight emerging from this predictive modeling is the dissociation between biomarkers of disease severity and biomarkers of therapeutic efficacy. Although STN beta oscillations (13–30 Hz) are widely recognized as the hallmark of PD motor symptoms (Neumann et al., 2016; Beudel et al., 2017), our feature importance analysis revealed that they were not the primary drivers of the therapeutic window prediction.

Several factors likely explain this lower predictive ranking. First, beta power is spatially broad and reflects a network-wide pathological state rather than a contact-specific anatomical position. In contrast, the therapeutic window is determined by the electrode’s

spatial proximity to the dorsolateral STN motor territory, often referred to as the "sweet spot" (Horn et al., 2017). Because high-frequency signals are more spatially confined than lower-frequency rhythms, they appear to be superior localization markers for the optimal stimulation site (Maris et al., 2011; Colombo et al., 2025).

Second, the postoperative "stun effect" can temporarily reduce beta power during the perioperative window, potentially masking its predictive value in some of our recordings. Finally, the utility of beta as a predictor may be patient-dependent; in the subset of patients with prominent, stable beta peaks, it did emerge as a more significant feature. Collectively, these findings suggest that while beta is an excellent marker of the global motor state, high-frequency oscillations provide the localized functional information required to determine the optimal target location (Olaru et al., 2025; Oehrn et al., 2024).

Furthermore, the predictive power of the model was significantly enhanced by the inclusion of network-level features, specifically STN-cortex coherence. This underscores that PD is fundamentally a network disorder and that the efficacy of DBS relies on modulating distributed circuits rather than solely suppressing local firing in the STN (Neumann et al., 2023). The model identified functional connectivity between the STN and the cerebellum, as well as the medial frontal cortex and temporal lobe as critical predictors. The involvement of the cerebellum is particularly intriguing and aligns with the growing recognition of the cerebello-basal ganglia loop in motor adaptation and parkinsonian tremor (Steina et al., 2025). The fact that removing cerebellar features degraded the model’s performance suggests that optimal DBS outcomes depend on how local stimulation propagates to, or interacts with, broader motor control loops. This supports a view of DBS as a therapy that restores functional equilibrium across a brain-wide network, rather than simply inhibiting a focal pathological nucleus (Deniau et al., 2010; McIntyre & Hahn, 2010). Consequently, the best contact would be the one that best engages and normalizes this broad, distributed network (Kringelbach et al., 2011, Bai et al., 2022).

The integration of anatomical data further refined the predictions based on electrophysiology. In Study 2, combining the distance to the anatomical sweet spot with electrophysiological features yielded better performance than either modality alone. This highlights that anatomy and physiology provide complementary information. Anatomical imaging tells us where the electrode is located in physical space, while electrophysiology tells us how the neurons at that location are functioning. The latter signal serves as a critical functional indicator, especially in cases where brain shift or individual anatomical variability renders traditional targeting ambiguous. Furthermore, oscillations may mark specific sub-regions of the STN that are most affected by the disease process, such as areas with the greatest dopamine depletion. Because these pathological hot spots may differ across patients, electrophysiology remains a valuable asset for contact selection even when anatomical information is technically perfect. Combining these multi-modal data streams within a generalizable machine learning framework, which utilizes the same model for all patients,

will enable a transition toward the identification of optimal stimulation sites across diverse individuals.

Implications

The primary implication of this work is establishing proof-of-concept that electrophysiological signatures can inform DBS contact selection. This challenges the traditional reliance on purely trial-and-error programming and demonstrates the feasibility of data-driven approaches. However, it is important to emphasize what has and has not been demonstrated. This thesis shows that prediction is possible and that validation in an independent cohort suggests generalizability. It does not demonstrate clinical implementation, nor does it prove that electrophysiology-guided programming outperforms expert clinical programming in prospective trials. Such validation would require randomized controlled trials comparing outcomes between standard and biomarker-guided approaches.

The finding that beta power was not the primary predictor in this dataset has implications for contact selection strategies. While beta power has proven valuable for adaptive DBS applications where real-time modulation tracks symptom fluctuations (Little et al., 2013), it may be less informative for identifying optimal electrode locations. Future work should investigate whether beta power becomes more predictive when measured later after surgery, once the stun effect has resolved.

The machine learning approach is designed to capture robust patterns that generalize across patient heterogeneity. Rather than requiring the development of individualized models for every new case, our approach utilizes a single, generalizable model that has learned to weight diverse electrophysiological features based on universal patterns identified in the training data. This "one-model-fits-all" framework is particularly advantageous given the clinical heterogeneity of PD, where patients differ in symptom profiles, disease duration, and anatomical variability. By integrating multi-modal features rather than relying on a single biomarker threshold, the model remains robust across these individual differences. This transition from a rigid, threshold-based protocol toward a flexible, data-driven framework enables a more precise identification of optimal stimulation sites that remains effective across a diverse patient population.

4.1 Outlook

The findings presented in this dissertation open several promising avenues for the evolution of DBS therapy, ranging from immediate changes in clinical workflow to the development of next-generation adaptive stimulation protocols.

The most immediate translational avenue for this work lies in the development of algorithmic decision-support systems for neurologists. In this envisioned clinical workflow, a patient’s perioperative recordings would be processed automatically to generate a ranked list of

electrode contacts. The clinician would then begin testing with the highest-ranked contact. If this contact proves satisfactory, the programming session could be concluded significantly earlier, sparing the patient from exhaustive testing of suboptimal contacts. Otherwise, the neurologist would proceed with the next contact in the list. Importantly, this approach does not seek to replace clinical judgment or the neurologist's expertise. Instead, it functions as a triage tool, filtering the immense parameter space down to a manageable subset of options thus reducing the time burden on patients and healthcare systems.

A critical step for widespread adoption will be transferring these predictive signatures from complex MEG setups to more accessible recording modalities. MEG provided the whole-brain resolution necessary for identifying relevant cortical nodes and showed promise in optimizing DBS programming but it is not a standard clinical tool available only in specialized research centers (Kariv et al., 2025). Future research must determine whether coherence features derived from simultaneous STN-LFP and EEG carry predictive value comparable to those obtained with MEG. Notably, Kato et al. (2015) already suggested that EEG-based coherence can approximate MEG-derived measures, supporting the feasibility of such an approach. Given that EEG is less expensive and widely available in neurological clinics, it might facilitate a wider adoption.

Furthermore, the technological landscape of DBS is increasingly characterized by a transition toward sensing-enabled pulse generators. This shift is currently spearheaded by the Medtronic Percept, which remains the only commercially available system capable of chronic LFP recording in a clinical setting (Goyal et al., 2021).

While the predictive models in this thesis were developed using perioperative externalized electrodes, their clinical translation is intrinsically linked to the adoption of sensing-enabled pulse generators. Crucially, the vast majority of DBS centers worldwide do not employ externalization as part of their surgical workflow. In these standard clinical settings, sensing-enabled devices represent the primary and often the only means of acquiring the electrophysiological signals required for an initial data-driven contact selection. Validating these signatures on data streaming from implanted devices is therefore the necessary bridge to translate static contact selection into dynamic, long-term therapy management. By confirming that these electrophysiological predictors remain stable over months or years, we can enable the development of "auto-programming" features that not only select the optimal contact at the start of therapy but also suggest parameter re-optimization as the patient's disease state or medication requirements evolve. Ultimately, this would transform the DBS system from a passive stimulator into an intelligent, longitudinal clinical monitor.

Beyond spatial optimization, the biomarkers identified in this work hold significant promise for temporal optimization through adaptive DBS. Current adaptative DBS trials largely rely on beta power as a control variable to adapt the amplitude of ongoing stimulation (Meidahl et al., 2017; Neumann et al., 2023). However, our findings suggest that beta is not the only, nor always the most reliable marker for defining the parameters required for maximal

symptom relief. Although the ability of the features identified in this thesis to guide real-time amplitude modulation cannot be directly inferred from this work, high-frequency STN activity has been identified as a robust marker for adaptative DBS in other studies (Olaru et al., 2025). For example, recent research on home-based adaptative DBS found that stimulation-entrained gamma oscillations accurately reflect motor symptom fluctuations (Oehrn et al. 2024). Consequently, an adaptive system could potentially be trained to maintain the network in a state of high physiological coherence or to maximize specific gamma dynamics, potentially offering superior symptom control compared to simple beta-suppression strategies.

Additionally, future research should aim to refine the granularity of these predictions. The current model predicts a composite therapeutic window, which effectively balances efficacy against side effects. However, different patients prioritize different outcomes; for some, tremor suppression is paramount, while others may prioritize the alleviation of rigidity. Future iterations of this work could develop symptom-specific models, training separate algorithms to predict the best contact for tremor versus rigidity. This would require larger datasets with detailed symptom-specific outcome measures from monopolar reviews.

To further investigate the role of STN-cortex connectivity, I conducted a post-hoc analysis to test whether the raw magnitude of coherence could differentiate between contacts with the widest and narrowest therapeutic windows. This was motivated by the common hypothesis that higher connectivity might serve as a straightforward, linear marker for optimal stimulation sites. However, this comparison did not reveal significant differences in raw coherence magnitude between the highest- and lowest-ranked contacts.

This finding suggests that the relationship between neural connectivity and clinical utility is multi-variate and frequency-specific, rather than a simple linear correlation where "more" coherence always equals a "better" contact. While this result does not allow for direct inferences regarding the mechanism of action of DBS, it highlights that the information predicting the therapeutic window is encoded in a complex functional signature that cannot be captured by simple magnitude-based comparisons. The model’s success in utilizing these features, despite the absence of raw magnitude differences, underscores the necessity of using non-linear computational approaches to decode the functional state of the STN and its surrounding networks.

Finally, the methodological pipeline established in this thesis is disease-agnostic. Similar frameworks could be applied to other DBS therapy for disorders such as essential tremor, dystonia, or obsessive-compulsive disorder (Herrington et al., 2016). By isolating the specific network signatures predictive of efficacy in each condition, it would be possible to move toward a generalized data-driven predictions guide neuromodulation across the entire spectrum of brain disorders treated by DBS.

4.2 Limitations

This work establishes a strong proof-of-concept for data-driven DBS contact selection, yet several limitations must be acknowledged regarding the interpretability of the data.

The therapeutic window, while clinically important, does not comprehensively capture treatment success. It reflects acute symptom response and side effect thresholds during monopolar review but does not measure long-term quality of life, subjective patient satisfaction, or effects on specific symptom domains like freezing of gait or speech. A contact with a wide window for rigidity may not optimally address other symptoms. Future studies should aim to predict long-term multidimensional outcomes rather than acute thresholds alone.

From a machine learning perspective, the sample size was relatively small. Training non-linear models on limited data increases overfitting risk, necessitating careful feature selection and validation strategies. The successful validation on an independent cohort significantly mitigates concerns that findings resulted from overfitting, but larger multi-center datasets would enable more robust models with better generalization. Feature importance rankings should be interpreted cautiously, as small datasets can be sensitive to noise. The choice to use a relatively simple model (XGBoost) rather than deep learning approaches was deliberate, favoring interpretability and avoiding overfitting given the available sample size.

Machine learning models, particularly ensemble methods like XGBoost, are less interpretable than simple linear models. Feature importance analysis reveals which signals contribute to predictions but does not fully explain how the algorithm weighs complex nonlinear interactions. This black box nature poses challenges for mechanistic understanding and clinical trust (Köhler et al., 2025). However, the goal of this work was predictive utility rather than mechanistic explanation of the algorithm. The model's value lies in demonstrating that prediction is possible. Future work could explore more interpretable model architectures or develop post-hoc explanation methods to enhance clinical acceptance.

4.3 Conclusions

This thesis demonstrates the feasibility of predicting DBS therapeutic windows from electrophysiological signatures. By curating a high-quality dataset of simultaneous MEG and LFP recordings, applying machine learning to identify predictive features, and validating predictions in an independent cohort, this work establishes proof-of-concept for data-driven contact selection. The findings show that brief resting-state recordings contain information about therapeutic potential that can be extracted computationally, providing an objective complement to trial-and-error programming approaches.

These findings challenge the traditional reliance on beta power as the sole biomarker of interest, demonstrating that a multi-feature approach provides a more comprehensive view of the therapeutic landscape. More importantly, they provide the proof-of-principle that these physiological signatures can be translated into predictive clinical tools. By validating that machine learning can reliably identify useful contacts from brain recordings, this work lays the foundation for a transition from empirical DBS programming to a data-driven precision medicine. Ultimately, transforming these neural signals into clinical decisions promises to make DBS more efficient, more precise, and ensuring that every patient receives the maximum benefit from this effective therapy.

5. Bibliography

Abbasi, O., Hirschmann, J., Storzer, L., Özkurt, T. E., Elben, S., Vesper, J., Wojtecki, L., Schmitz, G., Schnitzler, A., & Butz, M. (2018). Unilateral deep brain stimulation suppresses *alpha* and *beta* oscillations in sensorimotor cortices. *NeuroImage*, *174*, 201–207. https://doi.org/10.1016/j.neuroimage.2018.03.026

Ahlskog, J. E., & Muenter, M. D. (2001). Frequency of levodopa-related dyskinesias and motor fluctuations as estimated from the cumulative literature. *Movement Disorders: Official Journal of the Movement Disorder Society*, *16*(3), 448–458. https://doi.org/10.1002/mds.1090

Alexander, G. E., & Crutcher, M. D. (1990). Functional architecture of basal ganglia circuits: Neural substrates of parallel processing. *Trends in Neurosciences*, *13*(7), 266–271. https://doi.org/10.1016/0166-2236(90)90107-L

Alexander, G. E., DeLong, M. R., & Strick, P. L. (1986). Parallel organization of functionally segregated circuits linking basal ganglia and cortex. *Annual Review of Neuroscience*, *9*, 357–381. https://doi.org/10.1146/annurev.ne.09.030186.002041

Ambrosanio, M., Lopez, E. T., Autorino, M. M., Franceschini, S., Micco, R. D., Tessitore, A., Vettoliere, A., Granata, C., Sorrentino, G., Sorrentino, P., Baselice, F., Ambrosanio, M., Lopez, E. T., Autorino, M. M., Franceschini, S., Micco, R. D., Tessitore, A., Vettoliere, A., Granata, C., … Baselice, F. (2025). Analyzing Information Exchange in Parkinson's Disease via Eigenvector Centrality: A Source-Level Magnetoencephalography Study. *Journal of Clinical Medicine*, *14*(3). https://doi.org/10.3390/jcm14031020

Anumanchipalli, G. K., Chartier, J., & Chang, E. F. (2019). Speech synthesis from neural decoding of spoken sentences. *Nature*, *568*(7753), 493–498. https://doi.org/10.1038/s41586-019-1119-1

Ascherio, A., & Schwarzschild, M. A. (2016). The epidemiology of Parkinson's disease: Risk factors and prevention. *The Lancet. Neurology*, *15*(12), 1257–1272. https://doi.org/10.1016/S1474-4422(16)30230-7

Averna, A., Debove, I., Nowacki, A., Peterman, K., Duchet, B., Sousa, M., Bernasconi, E., Alva, L., Lachenmayer, M. L., Schuepbach, M., Pollo, C., Krack, P., Nguyen, T.-A. K., & Tinkhauser, G. (2023). Spectral Topography of the Subthalamic Nucleus to Inform Next-Generation Deep Brain Stimulation. *Movement Disorders: Official Journal of the Movement Disorder Society*, *38*(5), 818–830. https://doi.org/10.1002/mds.29381

Bai, Y., Diao, Y., Gan, L., Zhuo, Z., Yin, Z., Hu, T., Cheng, D., Xie, H., Wu, D., Fan, H., Zhang, Q., Duan, Y., Meng, F., Liu, Y., Jiang, Y., & Zhang, J. (2022). Deep Brain Stimulation Modulates Multiple Abnormal Resting-State Network Connectivity in Patients With Parkinson's Disease. *Frontiers in Aging Neuroscience*, *14*. https://doi.org/10.3389/fnagi.2022.794987

Baillet, S. (2017). Magnetoencephalography for brain electrophysiology and imaging. *Nature Neuroscience*, *20*(3), 327–339. https://doi.org/10.1038/nn.4504

Baillet, S., Mosher, J. C., & Leahy, R. M. (2001). Electromagnetic brain mapping. *IEEE Signal Processing Magazine*, *18*(6), 14–30. https://doi.org/10.1109/79.962275

Bandres-Ciga, S., Diez-Fairen, M., Kim, J. J., & Singleton, A. B. (2020). Genetics of Parkinson disease: An introspection of its journey towards precision medicine. *Neurobiology of Disease*, *137*, 104782. https://doi.org/10.1016/j.nbd.2020.104782

Bastos, A. M., & Schoffelen, J.-M. (2016). A Tutorial Review of Functional Connectivity Analysis Methods and Their Interpretational Pitfalls. *Frontiers in Systems Neuroscience*, *9*. https://doi.org/10.3389/fnsys.2015.00175

Benabid, A. L., Chabardes, S., Mitrofanis, J., & Pollak, P. (2009). Deep brain stimulation of the subthalamic nucleus for the treatment of Parkinson's disease. *The Lancet. Neurology*, *8*(1), 67–81. https://doi.org/10.1016/S1474-4422(08)70291-6

Berg, D., Postuma, R. B., Adler, C. H., Bloem, B. R., Chan, P., Dubois, B., Gasser, T., Goetz, C. G., Halliday, G., Joseph, L., Lang, A. E., Liepelt-Scarfone, I., Litvan, I., Marek, K., Obeso, J., Oertel, W., Olanow, C. W., Poewe, W., Stern, M., & Deuschl, G. (2015). MDS research criteria for prodromal Parkinson's disease. *Movement Disorders*, *30*(12), 1600–1611. https://doi.org/10.1002/mds.26431

Beudel, M., Oswal, A., Jha, A., Foltynie, T., Zrinzo, L., Hariz, M., Limousin, P., & Litvak, V. (2017). Oscillatory Beta Power Correlates With Akinesia-Rigidity in the Parkinsonian Subthalamic Nucleus. *Movement Disorders: Official Journal of the Movement Disorder Society*, *32*(1), 174–175. https://doi.org/10.1002/mds.26860

Binder, T., Lange, F., Pozzi, N., Musacchio, T., Daniels, C., Odorfer, T., Fricke, P., Matthies, C., Volkmann, J., & Capetian, P. (2023). Feasibility of local field potential-guided programming for deep brain stimulation in Parkinson's disease: A comparison with clinical and neuro-imaging guided approaches in a randomized, controlled pilot trial. *Brain Stimulation*, *16*(5), 1243–1251. https://doi.org/10.1016/j.brs.2023.08.017

Bishop, C. M. (2006). *Pattern recognition and machine learning*. Springer.

Bloem, B. R., Okun, M. S., & Klein, C. (2021). Parkinson's disease. *The Lancet*, *397*(10291), 2284–2303. https://doi.org/10.1016/S0140-6736(21)00218-X

Bonnefond, M., Kastner, S., & Jensen, O. (2017). Communication between Brain Areas Based on Nested Oscillations. *eNeuro*, *4*(2). https://doi.org/10.1523/ENEURO.0153-16.2017

Bosboom, J. L. W., Stoffers, D., Stam, C. J., van Dijk, B. W., Verbunt, J., Berendse, H. W., & Wolters, E. C. (2006). Resting state oscillatory brain dynamics in Parkinson's disease: An MEG study. *Clinical Neurophysiology: Official Journal of the International Federation of Clinical Neurophysiology*, *117*(11), 2521–2531. https://doi.org/10.1016/j.clinph.2006.06.720

Breiman, L. (2001). Random Forests. *Mach. Learn.*, *45*(1), 5–32. https://doi.org/10.1023/A:1010933404324

Bronstein, J. M., Tagliati, M., Alterman, R. L., Lozano, A. M., Volkmann, J., Stefani, A., Horak, F. B., Okun, M. S., Foote, K. D., Krack, P., Pahwa, R., Henderson, J. M., Hariz, M. I., Bakay, R. A., Rezai, A., Marks, W. J., Jr, Moro, E., Vitek, J. L., Weaver, F. M., … DeLong, M. R. (2011). Deep Brain Stimulation for Parkinson Disease: An Expert Consensus and Review of Key Issues. *Archives of Neurology*, *68*(2), 165. https://doi.org/10.1001/archneurol.2010.260

Bronte-Stewart, H. M., Beudel, M., Ostrem, J. L., Little, S., Almeida, L., Ramirez-Zamora, A., Fasano, A., Hassell, T., Mitchell, K. T., Moro, E., Gostkowski, M., Chattree, G., De Bie, R. M. A., De Neeling, M., Piña-Fuentes, D., Swinnen, B., Starr, P. A., Hammer, L. H., Foote, K. D., … Sarangmat, N. (2025). Long-Term Personalized Adaptive Deep Brain Stimulation in Parkinson Disease: A Nonrandomized Clinical Trial. *JAMA Neurology*, *82*(11), 1171. https://doi.org/10.1001/jamaneurol.2025.2781

Brookes, M. J., Vrba, J., Robinson, S. E., Stevenson, C. M., Peters, A. M., Barnes, G. R., Hillebrand, A., & Morris, P. G. (2008). Optimising experimental design for MEG beamformer imaging. *NeuroImage*, *39*(4), 1788–1802. https://doi.org/10.1016/j.neuroimage.2007.09.050

Brown, P. (2003). Oscillatory nature of human basal ganglia activity: Relationship to the pathophysiology of Parkinson's disease. *Movement Disorders: Official Journal of the Movement Disorder Society*, *18*(4), 357–363. https://doi.org/10.1002/mds.10358

Brown, P., Oliviero, A., Mazzone, P., Insola, A., Tonali, P., & Di Lazzaro, V. (2001). Dopamine Dependency of Oscillations between Subthalamic Nucleus and Pallidum in Parkinson's Disease. *The Journal of Neuroscience*, *21*(3), 1033–1038. https://doi.org/10.1523/JNEUROSCI.21-03-01033.2001

Burré, J., Sharma, M., Tsetsenis, T., Buchman, V., Etherton, M. R., & Südhof, T. C. (2010). Alpha-synuclein promotes SNARE-complex assembly in vivo and in vitro. *Science*, *329*(5999), 1663–1667. https://doi.org/10.1126/science.1195227

Bustos, G., Abarca, J., Campusano, J., Bustos, V., Noriega, V., & Aliaga, E. (2004). Functional interactions between somatodendritic dopamine release, glutamate receptors and brain-derived neurotrophic factor expression in mesencephalic structures of the brain. *Brain Research Reviews, Chemical and Electrical Synapses*, *47*(1), 126–144. https://doi.org/10.1016/j.brainresrev.2004.05.002

Buzsáki, G. (2006). *Rhythms of the Brain*. Oxford University Press. https://doi.org/10.1093/acprof:oso/9780195301069.001.0001

Buzsáki, G., Anastassiou, C. A., & Koch, C. (2012). The origin of extracellular fields and currents—EEG, ECoG, LFP and spikes. *Nature Reviews Neuroscience*, *13*(6), 407–420. https://doi.org/10.1038/nrn3241

Carvey, P. M., Punati, A., & Newman, M. B. (2006). Progressive Dopamine Neuron Loss in Parkinson's Disease: The Multiple Hit Hypothesis. *Cell Transplantation*, *15*(3), 239–250. https://doi.org/10.3727/000000006783981990

Cassidy, M., Mazzone, P., Oliviero, A., Insola, A., Tonali, P., Lazzaro, V. D., & Brown, P. (2002). Movement-related changes in synchronization in the human basal ganglia. *Brain*, *125*(6), 1235–1246. https://doi.org/10.1093/brain/awf135

Castrioto, A., Lozano, A. M., Poon, Y.-Y., Lang, A. E., Fallis, M., & Moro, E. (2011). Ten-year outcome of subthalamic stimulation in Parkinson disease: A blinded evaluation. *Archives of Neurology*, *68*(12), 1550–1556. https://doi.org/10.1001/archneurol.2011.182

Chartier, J., Anumanchipalli, G. K., Johnson, K., & Chang, E. F. (2018). Encoding of Articulatory Kinematic Trajectories in Human Speech Sensorimotor Cortex. *Neuron*, *98*(5), 1042-1054.e4. https://doi.org/10.1016/j.neuron.2018.04.031

Chaudhuri, K. R., Healy, D. G., & Schapira, A. H. (2006). Non-motor symptoms of Parkinson's disease: Diagnosis and management. *The Lancet Neurology*, *5*(3), 235–245. https://doi.org/10.1016/S1474-4422(06)70373-8

Chen, C. C., Pogosyan, A., Zrinzo, L. U., Tisch, S., Limousin, P., Ashkan, K., Yousry, T., Hariz, M. I., & Brown, P. (2006). Intra-operative recordings of local field potentials can help localize the subthalamic nucleus in Parkinson's disease surgery. *Experimental Neurology*, *198*(1), 214–221. https://doi.org/10.1016/j.expneurol.2005.11.019

Cheyne, D., Bells, S., Ferrari, P., Gaetz, W., & Bostan, A. C. (2008). Self-paced movements induce high-frequency gamma oscillations in primary motor cortex. *NeuroImage*, *42*(1), 332–342. https://doi.org/10.1016/j.neuroimage.2008.04.178

Chiken, S., & Nambu, A. (2016). Mechanism of Deep Brain Stimulation: Inhibition, Excitation, or Disruption? *The Neuroscientist: A Review Journal Bringing Neurobiology, Neurology and Psychiatry*, *22*(3), 313–322. https://doi.org/10.1177/1073858415581986

Cimbalnik, J., Kucewicz, M. T., & Worrell, G. (2016). Interictal high-frequency oscillations in focal human epilepsy. *Current Opinion in Neurology*, *29*(2), 175–181. https://doi.org/10.1097/WCO.0000000000000302

Cohen, M. X. (2014). *Analyzing Neural Time Series Data: Theory and Practice*. The MIT Press. https://doi.org/10.7551/mitpress/9609.001.0001

Cole, E. R., & Miocinovic, S. (2025). Are we ready for automated deep brain stimulation programming? *Parkinsonism & Related Disorders*, *134*, 107347. https://doi.org/10.1016/j.parkreldis.2025.107347

Colombo, A., Bernasconi, E., Alva, L., Sousa, M., Debove, I., Nowacki, A., Serquet, C., Petermann, K., Nguyen, T. A. K., Magalhães, A. D., Lachenmayer, L., Waskönig, J., Nef, T., Schuepbach, M., Pollo, C., Krack, P., Averna, A., & Tinkhauser, G. (2025). Finely Tuned γ Tracks Medication Cycles in Parkinson's Disease: An Ambulatory Brain-Sense Study. *Movement Disorders: Official Journal of the Movement Disorder Society*. https://doi.org/10.1002/mds.30160

Colosimo, C., & Michele, M. D. (1999). Motor fluctuations in Parkinson's disease: Pathophysiology and treatment. *European Journal of Neurology*, *6*(1), 1–21. https://doi.org/10.1046/j.1468-1331.1999.610001.x

Cotzias, G. C., Papavasiliou, P. S., & Gellene, R. (1969). Modification of Parkinsonism—Chronic Treatment with L-Dopa. *New England Journal of Medicine*, *280*(7), 337–345. https://doi.org/10.1056/NEJM196902132800701

Dalal, S. S., Baillet, S., Adam, C., Ducorps, A., Schwartz, D., Jerbi, K., Bertrand, O., Garnero, L., Martinerie, J., & Lachaux, J.-P. (2009). Simultaneous MEG and intracranial EEG recordings during attentive reading. *NeuroImage*, *45*(4), 1289–1304. https://doi.org/10.1016/j.neuroimage.2009.01.017

Dayan, P., & Abbott, L. F. (2001). *Theoretical neuroscience: Computational and mathematical modeling of neural systems*. MIT Press.

DeLong, M., & Wichmann, T. (2009). Update on models of basal ganglia function and dysfunction. *Parkinsonism & Related Disorders*, *15*(0 3), S237–S240. https://doi.org/10.1016/S1353-8020(09)70822-3

Dembek, T. A., Reker, P., Visser-Vandewalle, V., Wirths, J., Treuer, H., Klehr, M., Roediger, J., Dafsari, H. S., Barbe, M. T., & Timmermann, L. (2017). Directional DBS increases side-effect thresholds—A prospective, double-blind trial. *Movement Disorders*, *32*(10), 1380–1388. https://doi.org/10.1002/mds.27093

Deniau, J.-M., Degos, B., Bosch, C., & Maurice, N. (2010). Deep brain stimulation mechanisms: Beyond the concept of local functional inhibition. *European Journal of Neuroscience*, *32*(7), 1080–1091. https://doi.org/10.1111/j.1460-9568.2010.07413.x

Deo, R. C. (2015). Machine Learning in Medicine. *Circulation*, *132*(20), 1920–1930. https://doi.org/10.1161/CIRCULATIONAHA.115.001593

Deuschl, G., Schade-Brittinger, C., Krack, P., Volkmann, J., Schäfer, H., Bötzel, K., Daniels, C., Deutschländer, A., Dillmann, U., Eisner, W., Gruber, D., Hamel, W., Herzog, J., Hilker, R., Klebe, S., Kloss, M., Koy, J., Krause, M., Kupsch, A., … German Parkinson Study Group, Neurostimulation Section. (2006). A randomized trial of deep-brain stimulation for Parkinson's disease. *The New England Journal of Medicine*, *355*(9), 896–908. https://doi.org/10.1056/NEJMoa060281

Domingos, P. (2012). A few useful things to know about machine learning. *Communications of the ACM*, *55*(10), 78–87. https://doi.org/10.1145/2347736.2347755

D'Onofrio, V., Weis, L., Rigon, L., Ciprietti, D., Grassi, L. L., Landi, A., Porcaro, C., Tinkhauser, G., Antonini, A., & Guerra, A. (2025). Local field potentials survey to guide DBS programming in Parkinson's disease: A clinical-neurophysiological longitudinal study. *Npj Parkinson's Disease*, *12*(1), 1. https://doi.org/10.1038/s41531-025-01208-4

Dorsey, E. R., Sherer, T., Okun, M. S., & Bloem, B. R. (n.d.). The Emerging Evidence of the Parkinson Pandemic. *Journal of Parkinson's Disease*, *8*(Suppl 1), S3–S8. https://doi.org/10.3233/JPD-181474

Einevoll, G. T., Kayser, C., Logothetis, N. K., & Panzeri, S. (2013). Modelling and analysis of local field potentials for studying the function of cortical circuits. *Nature Reviews Neuroscience*, *14*(11), 770–785. https://doi.org/10.1038/nrn3599

Esteva, A., Kuprel, B., Novoa, R. A., Ko, J., Swetter, S. M., Blau, H. M., & Thrun, S. (2017). Dermatologist-level classification of skin cancer with deep neural networks. *Nature*, *542*(7639), 115–118. https://doi.org/10.1038/nature21056

Fasano, A., & Lozano, A. M. (2015). Deep brain stimulation for movement disorders: 2015 and beyond. *Current Opinion in Neurology*, *28*(4), 423–436. https://doi.org/10.1097/WCO.0000000000000226

Fearnley, J. M., & Lees, A. J. (1991). Ageing and Parkinson's disease: Substantia nigra regional selectivity. *Brain: A Journal of Neurology*, *114 (Pt 5)*, 2283–2301. https://doi.org/10.1093/brain/114.5.2283

Feingold, J., Gibson, D. J., DePasquale, B., & Graybiel, A. M. (2015). Bursts of beta oscillation differentiate postperformance activity in the striatum and motor cortex of

monkeys performing movement tasks. *Proceedings of the National Academy of Sciences*, *112*(44), 13687–13692. https://doi.org/10.1073/pnas.1517629112

Fenoy, A. J., & Simpson, R. K. (2014). Risks of common complications in deep brain stimulation surgery: Management and avoidance. *Journal of Neurosurgery*, *120*(1), 132–139. https://doi.org/10.3171/2013.10.JNS131225

Fernández-García, C., Monje, M. H. G., Gómez-Mayordomo, V., Foffani, G., Herranz, R., Catalán, M. J., González-Hidalgo, M., Matias-Guiu, J., & Alonso-Frech, F. (2022). Long-term directional deep brain stimulation: Monopolar review vs. local field potential guided programming. *Brain Stimulation: Basic, Translational, and Clinical Research in Neuromodulation*, *15*(3), 727–736. https://doi.org/10.1016/j.brs.2022.04.015

Frank, M. J. (2005). Dynamic dopamine modulation in the basal ganglia: A neurocomputational account of cognitive deficits in medicated and nonmedicated Parkinsonism. *Journal of Cognitive Neuroscience*, *17*(1), 51–72. https://doi.org/10.1162/0898929052880093

Friedman, J. H. (2001). Greedy function approximation: A gradient boosting machine. *The Annals of Statistics*, *29*(5), 1189–1232. https://doi.org/10.1214/aos/1013203451

Friston, K. J., Bastos, A. M., Pinotsis, D., & Litvak, V. (2015). LFP and oscillations—What do they tell us? *Current Opinion in Neurobiology, SI: Brain Rhythms and Dynamic Coordination*, *31*, 1–6. https://doi.org/10.1016/j.conb.2014.05.004

Gerfen, C. R., & Surmeier, D. J. (2011). Modulation of striatal projection systems by dopamine. *Annual Review of Neuroscience*, *34*, 441–466. https://doi.org/10.1146/annurev-neuro-061010-113641

Gerster, M., Waterstraat, G., Binns, T. S., Darcy, N., Wiest, C., Köhler, R. M., Vanhoecke, J., West, T. O., Sure, M., Todorov, D., Radzinski, L., Habets, J., Busch, J. L., Feldmann, L. K., Krause, P., Faust, K., Schneider, G.-H., Ashkan, K., Pereira, E., … Nikulin, V. (2025). Beyond beta rhythms: Subthalamic aperiodic broadband power scales with Parkinson's disease severity–a cross-sectional multicentre study. *eBioMedicine*, 105988. https://doi.org/10.1016/j.ebiom.2025.105988

Glaser, J. I., Benjamin, A. S., Chowdhury, R. H., Perich, M. G., Miller, L. E., & Kording, K. P. (2020). Machine Learning for Neural Decoding. *eNeuro*, *7*(4). https://doi.org/10.1523/ENEURO.0506-19.2020

Glaser, J. I., Benjamin, A. S., Farhoodi, R., & Kording, K. P. (2019). The roles of supervised machine learning in systems neuroscience. *Progress in Neurobiology*, *175*, 126–137. https://doi.org/10.1016/j.pneurobio.2019.01.008

Goedert, M., Spillantini, M. G., Del Tredici, K., & Braak, H. (2013). 100 years of Lewy pathology. *Nature Reviews. Neurology*, *9*(1), 13–24. https://doi.org/10.1038/nrneurol.2012.242

Goyal, A., Goetz, S., Stanslaski, S., Oh, Y., Rusheen, A. E., Klassen, B., Miller, K., Blaha, C. D., Bennet, K. E., & Lee, K. (2021). The development of an implantable deep brain stimulation device with simultaneous chronic electrophysiological recording and stimulation in humans. *Biosensors & Bioelectronics*, *176*, 112888. https://doi.org/10.1016/j.bios.2020.112888

Gross, J. (2019). Magnetoencephalography in Cognitive Neuroscience: A Primer. *Neuron*, *104*(2), 189–204. https://doi.org/10.1016/j.neuron.2019.07.001

Guerra, A., Asci, F., D'Onofrio, V., Sveva, V., Bologna, M., Fabbrini, G., Berardelli, A., & Suppa, A. (2020). Enhancing Gamma Oscillations Restores Primary Motor Cortex Plasticity in Parkinson's Disease. *Journal of Neuroscience*, *40*(24), 4788–4796. https://doi.org/10.1523/JNEUROSCI.0357-20.2020

Guyon, I., & Elisseeff, A. (2003). An introduction to variable and feature selection. *Journal of Machine Learning Research*, *3*(7–8), 1157–1182. https://doi.org/10.1162/153244303322753616

Hacker, M. L., Rajamani, N., Neudorfer, C., Hollunder, B., Oxenford, S., Li, N., Sternberg, A. L., Davis, T. L., Konrad, P. E., Horn, A., & Charles, D. (2023). Connectivity Profile for Subthalamic Nucleus Deep Brain Stimulation in Early Stage Parkinson Disease. *Annals of Neurology*, *94*(2), 271–284. https://doi.org/10.1002/ana.26674

Hämäläinen, M., Hari, R., Ilmoniemi, R. J., Knuutila, J., & Lounasmaa, O. V. (1993). Magnetoencephalography—Theory, instrumentation, and applications to noninvasive studies of the working human brain. *Reviews of Modern Physics*, *65*(2), 413–497. https://doi.org/10.1103/RevModPhys.65.413

Hastie, T., Tibshirani, R., & Friedman, J. (2009). *The Elements of Statistical Learning*. Springer New York. https://doi.org/10.1007/978-0-387-84858-7

Herreras, O. (2016). Local Field Potentials: Myths and Misunderstandings. *Frontiers in Neural Circuits*, *10*. https://www.frontiersin.org/articles/10.3389/fncir.2016.00101

Herrington, T. M., Cheng, J. J., & Eskandar, E. N. (2016). Mechanisms of deep brain stimulation. *Journal of Neurophysiology*, *115*(1), 19–38. https://doi.org/10.1152/jn.00281.2015

Hikosaka, O., Takikawa, Y., & Kawagoe, R. (2000). Role of the basal ganglia in the control of purposive saccadic eye movements. *Physiological Reviews*, *80*(3), 953–978. https://doi.org/10.1152/physrev.2000.80.3.953

Hillebrand, A., & Barnes, G. R. (2002). A Quantitative Assessment of the Sensitivity of Whole-Head MEG to Activity in the Adult Human Cortex. *NeuroImage*, *16*(3, Part A), 638–650. https://doi.org/10.1006/nimg.2002.1102

Hirschmann, J., Butz, M., Hartmann, C. J., Hoogenboom, N., Özkurt, T. E., Vesper, J., Wojtecki, L., & Schnitzler, A. (2016). Parkinsonian Rest Tremor Is Associated With Modulations of Subthalamic High-Frequency Oscillations. *Movement Disorders*, *31*(10), 1551–1559. https://doi.org/10.1002/mds.26663

Hirschmann, J., Hartmann, C. J., Butz, M., Hoogenboom, N., Özkurt, T. E., Elben, S., Vesper, J., Wojtecki, L., & Schnitzler, A. (2013). A direct relationship between oscillatory subthalamic nucleus–cortex coupling and rest tremor in Parkinson's disease. *Brain*, *136*(12), 3659–3670. https://doi.org/10.1093/brain/awt271

Hirschmann, J., Özkurt, T. E., Butz, M., Homburger, M., Elben, S., Hartmann, C. J., Vesper, J., Wojtecki, L., & Schnitzler, A. (2011). Distinct oscillatory STN-cortical loops revealed by simultaneous MEG and local field potential recordings in patients with

Parkinson's disease. *NeuroImage*, *55*(3), 1159–1168. https://doi.org/10.1016/j.neuroimage.2010.11.063

Hirschmann, J., Özkurt, T. E., Butz, M., Homburger, M., Elben, S., Hartmann, C. J., Vesper, J., Wojtecki, L., & Schnitzler, A. (2013). Differential modulation of STN-cortical and cortico-muscular coherence by movement and levodopa in Parkinson's disease. *NeuroImage*, *68*, 203–213. https://doi.org/10.1016/j.neuroimage.2012.11.036

Hirschmann, J., Steina, A., Vesper, J., Florin, E., & Schnitzler, A. (2022). Neuronal oscillations predict deep brain stimulation outcome in Parkinson's disease. *Brain Stimulation*, *15*(3), 792–802. https://doi.org/10.1016/j.brs.2022.05.008

Hochberg, L. R., Serruya, M. D., Friehs, G. M., Mukand, J. A., Saleh, M., Caplan, A. H., Branner, A., Chen, D., Penn, R. D., & Donoghue, J. P. (2006). Neuronal ensemble control of prosthetic devices by a human with tetraplegia. *Nature*, *442*(7099), 164–171. https://doi.org/10.1038/nature04970

Holdgraf, C. R., Rieger, J. W., Micheli, C., Martin, S., Knight, R. T., & Theunissen, F. E. (2017). Encoding and Decoding Models in Cognitive Electrophysiology. *Frontiers in Systems Neuroscience*, *11*. https://doi.org/10.3389/fnsys.2017.00061

Horn, A., Kühn, A. A., Merkl, A., Shih, L., Alterman, R., & Fox, M. (2017). Probabilistic conversion of neurosurgical DBS electrode coordinates into MNI space. *NeuroImage*, *150*, 395–404. https://doi.org/10.1016/j.neuroimage.2017.02.004

Horn, A., Neumann, W., Degen, K., Schneider, G., & Kühn, A. A. (2017). Toward an electrophysiological "sweet spot" for deep brain stimulation in the subthalamic nucleus. *Human Brain Mapping*, *38*(7), 3377–3390. https://doi.org/10.1002/hbm.23594

Horn, A., Reich, M., Vorwerk, J., Li, N., Wenzel, G., Fang, Q., Schmitz-Hübsch, T., Nickl, R., Kupsch, A., Volkmann, J., Kühn, A. A., & Fox, M. D. (2017). Connectivity Predicts deep brain stimulation outcome in Parkinson disease. *Annals of Neurology*, *82*(1), 67–78. https://doi.org/10.1002/ana.24974

Ikemoto, S., Yang, C., & Tan, A. (2015). Basal ganglia circuit loops, dopamine and motivation: A review and enquiry. *Behavioural Brain Research*, *290*, 17–31. https://doi.org/10.1016/j.bbr.2015.04.018

Jankovic, J. (2025). Parkinson Disease. *Neurologic Clinics*, *43*(2), xiii–xv. https://doi.org/10.1016/j.ncl.2024.12.001

Kalia, L. V., & Lang, A. E. (2015). Parkinson's disease. *The Lancet*, *386*(9996), 896–912. https://doi.org/10.1016/S0140-6736(14)61393-3

Kanai, S., Daida, A., Zhang, Y., Ding, Y., Monsoor, T., Qiao, J. X., Salamon, N., Ronne, E., Ahn, S. S., Hussain, S. A., Sankar, R., Fallah, A., Speier, W., Roychowdhury, V., Engel, J., Staba, R. J., & Nariai, H. (2025). Optimizing responsive neurostimulation targeting based on interictal high-frequency oscillations and phase–amplitude coupling. *Epilepsia*, epi.18675. https://doi.org/10.1111/epi.18675

Kandel, E. R., Koester, J., Mack, S., & Siegelbaum, S. (Eds). (2021). *Principles of neural science* (Sixth edition). McGraw Hill.

Kariv, S., Choi, J. W., Benam, M., Chilukuri, S., Alijanpourotaghsara, A., & Pouratian, N. (2025). Using Magnetoencephalography to Advance the Science of Parkinson Disease: A Systematic Review. *Brain and Behavior*, *15*(9), e70889. https://doi.org/10.1002/brb3.70889

Kato, K., Yokochi, F., Taniguchi, M., Okiyama, R., Kawasaki, T., Kimura, K., & Ushiba, J. (2015). Bilateral coherence between motor cortices and subthalamic nuclei in patients with Parkinson's disease. *Clinical Neurophysiology*, *126*(10), 1941–1950. https://doi.org/10.1016/j.clinph.2014.12.007

Kirsch, A. (1988). Inverse Problems. In K.-H. Hoffmann, J. Zowe, J.-B. Hiriart-Urruty, & C. Lemarechal (Eds), *Trends in Mathematical Optimization: 4th French-German Conference on Optimization* (pp. 117–137). Birkhäuser. https://doi.org/10.1007/978-3-0348-9297-1_9

Kish, S. J., Shannak, K., & Hornykiewicz, O. (1988). Uneven pattern of dopamine loss in the striatum of patients with idiopathic Parkinson's disease. Pathophysiologic and clinical implications. *The New England Journal of Medicine*, *318*(14), 876–880. https://doi.org/10.1056/NEJM198804073181402

Kohl, O., Gohil, C., Sure, M., Schnitzler, A., & Florin, E. (2025). *Varying patterns of association between cortical large-scale networks and subthalamic nucleus activity in Parkinson's Disease*. Research Square. https://doi.org/10.21203/rs.3.rs-8222792/v1

Köhler, D., Rügamer, D., Boyle, L. J., Maloney, K. O., & Schmid, M. (2025). Achieving interpretable machine learning by functional decomposition of black-box models into explainable predictor effects. *Npj Artificial Intelligence*, *1*(1), 34. https://doi.org/10.1038/s44387-025-00033-7

Krack, P., Volkmann, J., Tinkhauser, G., & Deuschl, G. (2019). Deep Brain Stimulation in Movement Disorders: From Experimental Surgery to Evidence-Based Therapy. *Movement Disorders: Official Journal of the Movement Disorder Society*, *34*(12), 1795–1810. https://doi.org/10.1002/mds.27860

Kramer, M. A., Tort, A. B. L., & Kopell, N. J. (2008). Sharp edge artifacts and spurious coupling in EEG frequency comodulation measures. *Journal of Neuroscience Methods*, *170*(2), 352–357. https://doi.org/10.1016/j.jneumeth.2008.01.020

Kriegeskorte, N., & Douglas, P. K. (2019). Interpreting encoding and decoding models. *Current Opinion in Neurobiology, Machine Learning, Big Data, and Neuroscience*, *55*, 167–179. https://doi.org/10.1016/j.conb.2019.04.002

Kringelbach, M. L., Green, A. L., & Aziz, T. Z. (2011). Balancing the Brain: Resting State Networks and Deep Brain Stimulation. *Frontiers in Integrative Neuroscience*, *5*. https://doi.org/10.3389/fnint.2011.00008

Kuhlmann, L., Lehnertz, K., Richardson, M. P., Schelter, B., & Zaveri, H. P. (2018). Seizure prediction—Ready for a new era. *Nature Reviews Neurology*, *14*(10), 618–630. https://doi.org/10.1038/s41582-018-0055-2

Kühn, A. A., Tsui, A., Aziz, T., Ray, N., Brücke, C., Kupsch, A., Schneider, G.-H., & Brown, P. (2009). Pathological synchronisation in the subthalamic nucleus of patients with

Parkinson's disease relates to both bradykinesia and rigidity. *Experimental Neurology*, *215*(2), 380–387. https://doi.org/10.1016/j.expneurol.2008.11.008

Kühn, A. A., Williams, D., Kupsch, A., Limousin, P., Hariz, M., Schneider, G., Yarrow, K., & Brown, P. (2004). Event-related beta desynchronization in human subthalamic nucleus correlates with motor performance. *Brain*, *127*(4), 735–746. https://doi.org/10.1093/brain/awh106

Lanciego, J. L., Luquin, N., & Obeso, J. A. (2012). Functional Neuroanatomy of the Basal Ganglia. *Cold Spring Harbor Perspectives in Medicine*, *2*(12), a009621. https://doi.org/10.1101/cshperspect.a009621

Lau, L. M. de, & Breteler, M. M. (2006). Epidemiology of Parkinson's disease. *The Lancet Neurology*, *5*(6), 525–535. https://doi.org/10.1016/S1474-4422(06)70471-9

Lebedev, M. A., & Nicolelis, M. A. L. (2006). Brain–machine interfaces: Past, present and future. *Trends in Neurosciences*, *29*(9), 536–546. https://doi.org/10.1016/j.tins.2006.07.004

Lin, H., Na, P., Zhang, D., Liu, J., Cai, X., & Li, W. (2020). Brain connectivity markers for the identification of effective contacts in subthalamic nucleus deep brain stimulation. *Human Brain Mapping*, *41*(8), 2028–2036. https://doi.org/10.1002/hbm.24927

Little, S., & Brown, P. (2014). The functional role of beta oscillations in Parkinson's disease. *Parkinsonism & Related Disorders, Proceedings of XX World Congress on Parkinson's Disease and Related Disorders*, *20*, S44–S48. https://doi.org/10.1016/S1353-8020(13)70013-0

Little, S., Pogosyan, A., Neal, S., Zavala, B., Zrinzo, L., Hariz, M., Foltynie, T., Limousin, P., Ashkan, K., FitzGerald, J., Green, A. L., Aziz, T. Z., & Brown, P. (2013). Adaptive deep brain stimulation in advanced Parkinson disease. *Annals of Neurology*, *74*(3), 449–457. https://doi.org/10.1002/ana.23951

Litvak, V., Eusebio, A., Jha, A., Oostenveld, R., Barnes, G., Foltynie, T., Limousin, P., Zrinzo, L., Hariz, M. I., Friston, K., & Brown, P. (2012). Movement-Related Changes in Local and Long-Range Synchronization in Parkinson's Disease Revealed by Simultaneous Magnetoencephalography and Intracranial Recordings. *Journal of Neuroscience*, *32*(31), 10541–10553. https://doi.org/10.1523/JNEUROSCI.0767-12.2012

Litvak, V., & Friston, K. (2008). Electromagnetic source reconstruction for group studies. *NeuroImage*, *42*(4), 1490–1498. https://doi.org/10.1016/j.neuroimage.2008.06.022

Litvak, V., Jha, A., Eusebio, A., Oostenveld, R., Foltynie, T., Limousin, P., Zrinzo, L., Hariz, M. I., Friston, K., & Brown, P. (2011). Resting oscillatory cortico-subthalamic connectivity in patients with Parkinson's disease. *Brain*, *134*(2), 359–374. https://doi.org/10.1093/brain/awq332

Lofredi, R., Neumann, W.-J., Bock, A., Horn, A., Huebl, J., Siegert, S., Schneider, G.-H., Krauss, J. K., & Kühn, A. A. (2018). Dopamine-dependent scaling of subthalamic gamma bursts with movement velocity in patients with Parkinson's disease. *eLife*, *7*, e31895. https://doi.org/10.7554/eLife.31895

Lozano, A. M., & Lipsman, N. (2013). Probing and regulating dysfunctional circuits using deep brain stimulation. *Neuron*, *77*(3), 406–424. https://doi.org/10.1016/j.neuron.2013.01.020

Maris, E., van Vugt, M., & Kahana, M. (2011). Spatially distributed patterns of oscillatory coupling between high-frequency amplitudes and low-frequency phases in human iEEG. *NeuroImage*, *54*(2), 836–850. https://doi.org/10.1016/j.neuroimage.2010.09.029

Martinez-Nunez, A. E., Rozell, C. J., Little, S., Tan, H., Schmidt, S. L., Grill, W. M., Pajic, M., Turner, D. A., de Hemptinne, C., Machado, A., Schiff, N. D., Holt-Becker, A. S., Raike, R. S., Malekmohammadi, M., Pathak, Y. J., Himes, L., Greene, D., Krinke, L., Arlotti, M., … Wong, J. K. (2025). Proceedings of the 12th annual deep brain stimulation think tank: Cutting edge technology meets novel applications. *Frontiers in Human Neuroscience*, *19*, 1544994. https://doi.org/10.3389/fnhum.2025.1544994

Mathalon, D. H., & Sohal, V. S. (2015). Neural Oscillations and Synchrony in Brain Dysfunction and Neuropsychiatric Disorders: It's About Time. *JAMA Psychiatry*, *72*(8), 840–844. https://doi.org/10.1001/jamapsychiatry.2015.0483

McIntyre, C. C., & Hahn, P. J. (2010). Network perspectives on the mechanisms of deep brain stimulation. *Neurobiology of Disease, Frontiers in Brain Stimulation*, *38*(3), 329–337. https://doi.org/10.1016/j.nbd.2009.09.022

McIntyre, C. C., Savasta, M., Kerkerian-Le Goff, L., & Vitek, J. L. (2004). Uncovering the mechanism(s) of action of deep brain stimulation: Activation, inhibition, or both. *Clinical Neurophysiology: Official Journal of the International Federation of Clinical Neurophysiology*, *115*(6), 1239–1248. https://doi.org/10.1016/j.clinph.2003.12.024

Meidahl, A. C., Tinkhauser, G., Herz, D. M., Cagnan, H., Debarros, J., & Brown, P. (2017). Adaptive Deep Brain Stimulation for Movement Disorders: The Long Road to Clinical Therapy. *Movement Disorders*, *32*(6), 810–819. https://doi.org/10.1002/mds.27022

Merk, T., Köhler, R. M., Brotons, T. M., Vossberg, S. R., Peterson, V., Lyra, L. F., Vanhoecke, J., Chikermane, M., Binns, T. S., Li, N., Walton, A., Neudorfer, C., Bush, A., Sisterson, N., Busch, J., Lofredi, R., Habets, J., Huebl, J., Zhu, G., … Neumann, W.-J. (2025). Invasive neurophysiology and whole brain connectomics for neural decoding in patients with brain implants. *Nature Biomedical Engineering*, 1–18. https://doi.org/10.1038/s41551-025-01467-9

Merk, T., Peterson, V., Köhler, R., Haufe, S., Richardson, R. M., & Neumann, W.-J. (2022). Machine learning based brain signal decoding for intelligent adaptive deep brain stimulation. *Experimental Neurology*, *351*, 113993. https://doi.org/10.1016/j.expneurol.2022.113993

Middleton, F. A., & Strick, P. L. (2000). Basal ganglia and cerebellar loops: Motor and cognitive circuits. *Brain Research. Brain Research Reviews*, *31*(2–3), 236–250. https://doi.org/10.1016/s0165-0173(99)00040-5

Miller, K. J., Leuthardt, E. C., Schalk, G., Rao, R. P. N., Anderson, N. R., Moran, D. W., Miller, J. W., & Ojemann, J. G. (2007). Spectral Changes in Cortical Surface Potentials during Motor Movement. *Journal of Neuroscience*, *27*(9), 2424–2432. https://doi.org/10.1523/JNEUROSCI.3886-06.2007

Mitchell, T. M. (2013). *Machine learning* (Nachdr.). McGraw-Hill.

Mormann, F., Andrzejak, R. G., Elger, C. E., & Lehnertz, K. (2007). Seizure prediction: The long and winding road. *Brain*, *130*(2), 314–333. https://doi.org/10.1093/brain/awl241

Moro, E., Poon, Y.-Y. W., Lozano, A. M., Saint-Cyr, J. A., & Lang, A. E. (2006). Subthalamic nucleus stimulation: Improvements in outcome with reprogramming. *Archives of Neurology*, *63*(9), 1266–1272. https://doi.org/10.1001/archneur.63.9.1266

Moustafa, A. A., Chakravarthy, S., Phillips, J. R., Gupta, A., Keri, S., Polner, B., Frank, M. J., & Jahanshahi, M. (2016). Motor symptoms in Parkinson's disease: A unified framework. *Neuroscience & Biobehavioral Reviews*, *68*, 727–740. https://doi.org/10.1016/j.neubiorev.2016.07.010

Ms, H., & Rj, I. (1994). Interpreting magnetic fields of the brain: Minimum norm estimates. *Medical & Biological Engineering & Computing*, *32*(1). https://doi.org/10.1007/BF02512476

Muthuraman, M., Heute, U., Arning, K., Anwar, A. R., Elble, R., Deuschl, G., & Raethjen, J. (2012). Oscillating central motor networks in pathological tremors and voluntary movements. What makes the difference? *NeuroImage*, *60*(2), 1331–1339. https://doi.org/10.1016/j.neuroimage.2012.01.088

Nambu, A., Tokuno, H., & Takada, M. (2002). Functional significance of the cortico–subthalamo–pallidal 'hyperdirect' pathway. *Neuroscience Research*, *43*(2), 111–117. https://doi.org/10.1016/S0168-0102(02)00027-5

Naselaris, T., Kay, K. N., Nishimoto, S., & Gallant, J. L. (2011). Encoding and decoding in fMRI. *NeuroImage, Multivariate Decoding and Brain Reading*, *56*(2), 400–410. https://doi.org/10.1016/j.neuroimage.2010.07.073

Neumann, W.-J., Degen, K., Schneider, G.-H., Brücke, C., Huebl, J., Brown, P., & Kühn, A. A. (2016). Subthalamic synchronized oscillatory activity correlates with motor impairment in patients with Parkinson's disease. *Movement Disorders*, *31*(11), 1748–1751. https://doi.org/10.1002/mds.26759

Neumann, W.-J., Gilron, R., Little, S., & Tinkhauser, G. (2023). Adaptive Deep Brain Stimulation: From Experimental Evidence Toward Practical Implementation. *Movement Disorders*, *38*(6), 937–948. https://doi.org/10.1002/mds.29415

Neumann, W.-J., Staub-Bartelt, F., Horn, A., Schanda, J., Schneider, G.-H., Brown, P., & Kühn, A. A. (2017). Long term correlation of subthalamic beta band activity with motor impairment in patients with Parkinson's disease. *Clinical Neurophysiology: Official Journal of the International Federation of Clinical Neurophysiology*, *128*(11), 2286–2291. https://doi.org/10.1016/j.clinph.2017.08.028

Neumann, W.-J., Steiner, L. A., & Milosevic, L. (2023). Neurophysiological mechanisms of deep brain stimulation across spatiotemporal resolutions. *Brain*, *146*(11), 4456–4468. https://doi.org/10.1093/brain/awad239

Nichols, T. E., Das, S., Eickhoff, S. B., Evans, A. C., Glatard, T., Hanke, M., Kriegeskorte, N., Milham, M. P., Poldrack, R. A., Poline, J.-B., Proal, E., Thirion, B., Van Essen, D. C., White, T., & Yeo, B. T. T. (2017). Best practices in data analysis and sharing in

neuroimaging using MRI. *Nature Neuroscience*, *20*(3), 299–303. https://doi.org/10.1038/nn.4500

Norouzi, H., Ietswaart, M., Adair, J., & Learmonth, G. (2025). *A meta-analysis of periodic and aperiodic M/EEG components in Parkinson's disease* (p. 2025.07.07.663454). bioRxiv. https://doi.org/10.1101/2025.07.07.663454

Nunez, P. L., & Srinivasan, R. (2006). *Electric Fields of the Brain: The Neurophysics of EEG*. Oxford University Press.

Obeso, J. A., Marin, C., Rodriguez-Oroz, C., Blesa, J., Benitez-Temiño, B., Mena-Segovia, J., Rodríguez, M., & Olanow, C. W. (2008). The basal ganglia in Parkinson's disease: Current concepts and unexplained observations. *Annals of Neurology*, *64*(S2), S30–S46. https://doi.org/10.1002/ana.21481

Obeso, J. A., Olanow, C. W., & Nutt, J. G. (2000). Levodopa motor complications in Parkinson's disease. *Trends in Neurosciences*, *23*(10 Suppl), S2-7. https://doi.org/10.1016/s1471-1931(00)00031-8

Obeso, J. A., Rodríguez-Oroz, M. C., Benitez-Temino, B., Blesa, F. J., Guridi, J., Marin, C., & Rodriguez, M. (2008). Functional organization of the basal ganglia: Therapeutic implications for Parkinson's disease. *Movement Disorders: Official Journal of the Movement Disorder Society*, *23 Suppl 3*, S548-559. https://doi.org/10.1002/mds.22062

Obeso, J. A., Rodríguez-Oroz, M. C., Rodríguez, M., Arbizu, J., & Giménez-Amaya, J. M. (2002). The Basal Ganglia and Disorders of Movement: Pathophysiological Mechanisms. *Physiology*, *17*(2), 51–55. https://doi.org/10.1152/nips.01363.2001

Oehrn, C. R., Cernera, S., Hammer, L. H., Shcherbakova, M., Yao, J., Hahn, A., Wang, S., Ostrem, J. L., Little, S., & Starr, P. A. (2024). Chronic adaptive deep brain stimulation versus conventional stimulation in Parkinson's disease: A blinded randomized feasibility trial. *Nature Medicine*, 1–12. https://doi.org/10.1038/s41591-024-03196-z

Okun, M. S. (2012). Deep-Brain Stimulation for Parkinson's Disease. *New England Journal of Medicine*, *367*(16), 1529–1538. https://doi.org/10.1056/NEJMct1208070

Olanow, C. W. (2004). The Scientific Basis for the Current Treatment of Parkinson's Disease. *Annual Review of Medicine*, *55*(1), 41–60. https://doi.org/10.1146/annurev.med.55.091902.104422

Olaru, M., Hahn, A., Shcherbakova, M., Little, S., Neumann, W.-J., Abbasi-Asl, R., & Starr, P. A. (2025). Deep brain stimulation-entrained gamma oscillations in chronic home recordings in Parkinson's disease. *Brain Stimulation*, *18*(2), 132–141. https://doi.org/10.1016/j.brs.2025.01.011

Oliveira, A. M., Coelho, L., Carvalho, E., Ferreira-Pinto, M. J., Vaz, R., & Aguiar, P. (2023). Machine learning for adaptive deep brain stimulation in Parkinson's disease: Closing the loop. *Journal of Neurology*, *270*(11), 5313–5326. https://doi.org/10.1007/s00415-023-11873-1

Oswal, A., Beudel, M., Zrinzo, L., Limousin, P., Hariz, M., Foltynie, T., Litvak, V., & Brown, P. (2016). Deep brain stimulation modulates synchrony within spatially and

spectrally distinct resting state networks in Parkinson's disease. *Brain*, *139*(5), 1482–1496. https://doi.org/10.1093/brain/aww048

Oswal, A., Cao, C., Yeh, C.-H., Neumann, W.-J., Gratwicke, J., Akram, H., Horn, A., Li, D., Zhan, S., Zhang, C., Wang, Q., Zrinzo, L., Foltynie, T., Limousin, P., Bogacz, R., Sun, B., Husain, M., Brown, P., & Litvak, V. (2021). Neural signatures of hyperdirect pathway activity in Parkinson's disease. *Nature Communications*, *12*(1), 5185. https://doi.org/10.1038/s41467-021-25366-0

Oswal, A., Jha, A., Neal, S., Reid, A., Bradbury, D., Aston, P., Limousin, P., Foltynie, T., Zrinzo, L., Brown, P., & Litvak, V. (2016). Analysis of simultaneous MEG and intracranial LFP recordings during Deep Brain Stimulation: A protocol and experimental validation. *Journal of Neuroscience Methods*, *261*, 29–46. https://doi.org/10.1016/j.jneumeth.2015.11.029

Özkurt, T. E. (2024). Abnormally low sensorimotor α band nonlinearity serves as an effective EEG biomarker of Parkinson's disease. *Journal of Neurophysiology*, *131*(2), 435–445. https://doi.org/10.1152/jn.00272.2023

Özkurt, T. E., Butz, M., Homburger, M., Elben, S., Vesper, J., Wojtecki, L., & Schnitzler, A. (2011). High frequency oscillations in the subthalamic nucleus: A neurophysiological marker of the motor state in Parkinson's disease. *Experimental Neurology*, *229*(2), 324–331. https://doi.org/10.1016/j.expneurol.2011.02.015

Pandarinath, C., O'Shea, D. J., Collins, J., Jozefowicz, R., Stavisky, S. D., Kao, J. C., Trautmann, E. M., Kaufman, M. T., Ryu, S. I., Hochberg, L. R., Henderson, J. M., Shenoy, K. V., Abbott, L. F., & Sussillo, D. (2018). Inferring single-trial neural population dynamics using sequential auto-encoders. *Nature Methods*, *15*(10), 805–815. https://doi.org/10.1038/s41592-018-0109-9

Paninski, L., Pillow, J., & Lewi, J. (2007). Statistical models for neural encoding, decoding, and optimal stimulus design. *Progress in Brain Research*, *165*, 493–507. https://doi.org/10.1016/S0079-6123(06)65031-0

Parent, A., & Hazrati, L. N. (1995). Functional anatomy of the basal ganglia. II. The place of subthalamic nucleus and external pallidum in basal ganglia circuitry. *Brain Research. Brain Research Reviews*, *20*(1), 128–154. https://doi.org/10.1016/0165-0173(94)00008-d

Pauls, K. A. M., Korsun, O., Nenonen, J., Nurminen, J., Liljeström, M., Kujala, J., Pekkonen, E., & Renvall, H. (2022). Cortical beta burst dynamics are altered in Parkinson's disease but normalized by deep brain stimulation. *NeuroImage*, *257*, 119308. https://doi.org/10.1016/j.neuroimage.2022.119308

Pesaran, B., Vinck, M., Einevoll, G. T., Sirota, A., Fries, P., Siegel, M., Truccolo, W., Schroeder, C. E., & Srinivasan, R. (2018). Investigating large-scale brain dynamics using field potential recordings: Analysis and interpretation. *Nature Neuroscience*, *21*(7), 903–919. https://doi.org/10.1038/s41593-018-0171-8

Picillo, M., Lozano, A. M., Kou, N., Munhoz, R. P., & Fasano, A. (2016). Programming Deep Brain Stimulation for Parkinson's Disease: The Toronto Western Hospital Algorithms. *Brain Stimulation: Basic, Translational, and Clinical Research in Neuromodulation*, *9*(3), 425–437. https://doi.org/10.1016/j.brs.2016.02.004

Poewe, W., Seppi, K., Tanner, C. M., Halliday, G. M., Brundin, P., Volkmann, J., Schrag, A.-E., & Lang, A. E. (2017). Parkinson disease. *Nature Reviews Disease Primers*, *3*(1), 17013. https://doi.org/10.1038/nrdp.2017.13

Poldrack, R. A., & Gorgolewski, K. J. (2014). Making big data open: Data sharing in neuroimaging. *Nature Neuroscience*, *17*(11), 1510–1517. https://doi.org/10.1038/nn.3818

Postuma, R. B., Berg, D., Stern, M., Poewe, W., Olanow, C. W., Oertel, W., Obeso, J., Marek, K., Litvan, I., Lang, A. E., Halliday, G., Goetz, C. G., Gasser, T., Dubois, B., Chan, P., Bloem, B. R., Adler, C. H., & Deuschl, G. (2015). MDS clinical diagnostic criteria for Parkinson's disease. *Movement Disorders*, *30*(12), 1591–1601. https://doi.org/10.1002/mds.26424

Purves, D., Augustine, G. J., Fitzpatrick, D., Katz, L. C., LaMantia, A.-S., McNamara, J. O., & Williams, S. M. (2001). Circuits within the Basal Ganglia System. In *Neuroscience. 2nd edition*. Sinauer Associates. https://www.ncbi.nlm.nih.gov/books/NBK10847/

Quian Quiroga, R., & Panzeri, S. (2009). Extracting information from neuronal populations: Information theory and decoding approaches. *Nature Reviews. Neuroscience*, *10*(3), 173–185. https://doi.org/10.1038/nrn2578

Rajkomar, A., Dean, J., & Kohane, I. (2019). Machine Learning in Medicine. *The New England Journal of Medicine*, *380*(14), 1347–1358. https://doi.org/10.1056/NEJMra1814259

Rascol, O., Brooks, D. J., Korczyn, A. D., Deyn, P. P. D., Clarke, C. E., & Lang, A. E. (2000). A Five-Year Study of the Incidence of Dyskinesia in Patients with Early Parkinson's Disease Who Were Treated with Ropinirole or Levodopa. *New England Journal of Medicine*, *342*(20), 1484–1491. https://doi.org/10.1056/NEJM200005183422004

Rassoulou, F., Sharma, A., Steina, A., Butz, M., Hartmann, C. J., Bahners, B. H., Vesper, J., Schnitzler, A., & Hirschmann, J. (2025). Electrophysiological signatures predict the therapeutic window of deep brain stimulation electrode contacts. *Npj Digital Medicine*, *8*(1), 635. https://doi.org/10.1038/s41746-025-02089-w

Rassoulou, F., Steina, A., Hartmann, C. J., Vesper, J., Butz, M., Schnitzler, A., & Hirschmann, J. (2024). Exploring the electrophysiology of Parkinson's disease with magnetoencephalography and deep brain recordings. *Scientific Data*, *11*(1), 889. https://doi.org/10.1038/s41597-024-03768-1

Ray, N. J., Jenkinson, N., Wang, S., Holland, P., Brittain, J. S., Joint, C., Stein, J. F., & Aziz, T. (2008). Local field potential beta activity in the subthalamic nucleus of patients with Parkinson's disease is associated with improvements in bradykinesia after dopamine and deep brain stimulation. *Experimental Neurology*, *213*(1), 108–113. https://doi.org/10.1016/j.expneurol.2008.05.008

Rocha, T. F. da, Costa, V., Camargo, L., Fernandes, E. B., Gianlorenço, A. C., Rocha, T. F. da, Costa, V., Camargo, L., Fernandes, E. B., & Gianlorenço, A. C. (2025). Resting-State EEG Alpha Asymmetry as a Potential Marker of Clinical Features in Parkinson's Disease. *Journal of Personalized Medicine*, *15*(7). https://doi.org/10.3390/jpm15070291

Rocha, G. S., Freire, M. A. M., Britto, A. M., Paiva, K. M., Oliveira, R. F., Fonseca, I. A. T., Araújo, D. P., Oliveira, L. C., Guzen, F. P., Morais, P. L. A. G., & Cavalcanti, J. R. L. P. (2023). Basal ganglia for beginners: The basic concepts you need to know and their role in movement control. *Frontiers in Systems Neuroscience*, *17*, 1242929. https://doi.org/10.3389/fnsys.2023.1242929

Russell, S. J., & Norvig, P. (with Davis, E., & Edwards, D.). (2016). *Artificial intelligence: A modern approach* (Third edition, Global edition). Pearson.

Sarvas, J. (1987). Basic mathematical and electromagnetic concepts of the biomagnetic inverse problem. *Physics in Medicine & Biology*, *32*(1), 11. https://doi.org/10.1088/0031-9155/32/1/004

Schmidt, H., Avitabile, D., Montbrió, E., & Roxin, A. (2018). Network mechanisms underlying the role of oscillations in cognitive tasks. *PLOS Computational Biology*, *14*(9), e1006430. https://doi.org/10.1371/journal.pcbi.1006430

Schoffelen, J.-M., & Gross, J. (2009). Source connectivity analysis with MEG and EEG. *Human Brain Mapping*, *30*(6), 1857–1865. https://doi.org/10.1002/hbm.20745

Schreglmann, S. R., Wang, D., Peach, R. L., Li, J., Zhang, X., Latorre, A., Rhodes, E., Panella, E., Cassara, A. M., Boyden, E. S., Barahona, M., Santaniello, S., Rothwell, J., Bhatia, K. P., & Grossman, N. (2021). Non-invasive suppression of essential tremor via phase-locked disruption of its temporal coherence. *Nature Communications*, *12*(1), 363. https://doi.org/10.1038/s41467-020-20581-7

Schuepbach, W. M. M., Rau, J., Knudsen, K., Volkmann, J., Krack, P., Timmermann, L., Hälbig, T. D., Hesekamp, H., Navarro, S. M., Meier, N., Falk, D., Mehdorn, M., Paschen, S., Maarouf, M., Barbe, M. T., Fink, G. R., Kupsch, A., Gruber, D., Schneider, G.-H., … Deuschl, G. (2013). Neurostimulation for Parkinson's Disease with Early Motor Complications. *New England Journal of Medicine*, *368*(7), 610–622. https://doi.org/10.1056/NEJMoa1205158

Schultz, W. (2007). Multiple dopamine functions at different time courses. *Annual Review of Neuroscience*, *30*, 259–288. https://doi.org/10.1146/annurev.neuro.28.061604.135722

Shah, A., Nguyen, T.-A. K., Peterman, K., Khawaldeh, S., Debove, I., Shah, S. A., Torrecillos, F., Tan, H., Pogosyan, A., Lachenmayer, M. L., Michelis, J., Brown, P., Pollo, C., Krack, P., Nowacki, A., & Tinkhauser, G. (2023). Combining Multimodal Biomarkers to Guide Deep Brain Stimulation Programming in Parkinson Disease. *Neuromodulation: Journal of the International Neuromodulation Society*, *26*(2), 320–332. https://doi.org/10.1016/j.neurom.2022.01.017

Siegel, M., Donner, T. H., & Engel, A. K. (2012). Spectral fingerprints of large-scale neuronal interactions. *Nature Reviews Neuroscience*, *13*(2), 121–134. https://doi.org/10.1038/nrn3137

Singh, S. P. (2014). Magnetoencephalography: Basic principles. *Annals of Indian Academy of Neurology*, *17*(Suppl 1), S107. https://doi.org/10.4103/0972-2327.128676

Smith, Y., Bevan, M. D., Shink, E., & Bolam, J. P. (1998). Microcircuitry of the direct and indirect pathways of the basal ganglia. *Neuroscience*, *86*(2), 353–387. https://doi.org/10.1016/s0306-4522(98)00004-9

Spillantini, M. G., Schmidt, M. L., Lee, V. M.-Y., Trojanowski, J. Q., Jakes, R., & Goedert, M. (1997). α-Synuclein in Lewy bodies. *Nature*, *388*(6645), 839–840. https://doi.org/10.1038/42166

Steina, A., Sure, S., Butz, M., Vesper, J., Schnitzler, A., & Hirschmann, J. (2025). Oscillatory Coupling Between Thalamus, Cerebellum, and Motor Cortex in Essential Tremor. *Movement Disorders: Official Journal of the Movement Disorder Society*. https://doi.org/10.1002/mds.30165

Stone, M. (1974). Cross-Validatory Choice and Assessment of Statistical Predictions. *Journal of the Royal Statistical Society Series B: Statistical Methodology*, *36*(2), 111–133. https://doi.org/10.1111/j.2517-6161.1974.tb00994.x

Strelow, J. N., Dembek, T. A., Baldermann, J. C., Andrade, P., Jergas, H., Visser-Vandewalle, V., & Barbe, M. T. (2022). Local Field Potential-Guided Contact Selection Using Chronically Implanted Sensing Devices for Deep Brain Stimulation in Parkinson's Disease. *Brain Sciences*, *12*(12), 1726. https://doi.org/10.3390/brainsci12121726

Sutton, R. S., & Barto, A. (2018). *Reinforcement learning: An introduction* (Second edition). The MIT Press.

Swann, N. C., de Hemptinne, C., Miocinovic, S., Qasim, S., Wang, S. S., Ziman, N., Ostrem, J. L., San Luciano, M., Galifianakis, N. B., & Starr, P. A. (2016). Gamma Oscillations in the Hyperkinetic State Detected with Chronic Human Brain Recordings in Parkinson's Disease. *The Journal of Neuroscience*, *36*(24), 6445–6458. https://doi.org/10.1523/JNEUROSCI.1128-16.2016

Telkes, I., Jimenez-Shahed, J., Viswanathan, A., Abosch, A., & Ince, N. F. (2016). Prediction of STN-DBS Electrode Implantation Track in Parkinson's Disease by Using Local Field Potentials. *Frontiers in Neuroscience*, *10*. https://doi.org/10.3389/fnins.2016.00198

Telkes, I., Viswanathan, A., Jimenez-Shahed, J., Abosch, A., Ozturk, M., Gupte, A., Jankovic, J., & Ince, N. F. (2018). Local field potentials of subthalamic nucleus contain electrophysiological footprints of motor subtypes of Parkinson's disease. *Proceedings of the National Academy of Sciences*, *115*(36). https://doi.org/10.1073/pnas.1810589115

Tinkhauser, G., Pogosyan, A., Little, S., Beudel, M., Herz, D. M., Tan, H., & Brown, P. (2017). The modulatory effect of adaptive deep brain stimulation on beta bursts in Parkinson's disease. *Brain: A Journal of Neurology*, *140*(4), 1053–1067. https://doi.org/10.1093/brain/awx010

Todorov, D., Schnitzler, A., & Hirschmann, J. (2024). Parkinsonian rest tremor can be distinguished from voluntary hand movements based on subthalamic and cortical activity. *Clinical Neurophysiology*, *157*, 146–155. https://doi.org/10.1016/j.clinph.2023.10.018

Torrecillos, F., Tinkhauser, G., Fischer, P., Green, A. L., Aziz, T. Z., Foltynie, T., Limousin, P., Zrinzo, L., Ashkan, K., Brown, P., & Tan, H. (2018). Modulation of Beta Bursts in the Subthalamic Nucleus Predicts Motor Performance. *The Journal of Neuroscience*, *38*(41), 8905–8917. https://doi.org/10.1523/JNEUROSCI.1314-18.2018

Van Veen, B. D., Van Drongelen, W., Yuchtman, M., & Suzuki, A. (1997). Localization of brain electrical activity via linearly constrained minimum variance spatial filtering. *IEEE*

Transactions on Biomedical Engineering, *44*(9), 867–880. https://doi.org/10.1109/10.623056

van Wijk, B. C. M., Beudel, M., Jha, A., Oswal, A., Foltynie, T., Hariz, M. I., Limousin, P., Zrinzo, L., Aziz, T. Z., Green, A. L., Brown, P., & Litvak, V. (2016). Subthalamic nucleus phase–amplitude coupling correlates with motor impairment in Parkinson's disease. *Clinical Neurophysiology*, *127*(4), 2010–2019. https://doi.org/10.1016/j.clinph.2016.01.015

van Wijk, B. C. M., Neumann, W.-J., Kroneberg, D., Horn, A., Irmen, F., Sander, T. H., Wang, Q., Litvak, V., & Kühn, A. A. (2022). Functional connectivity maps of theta/alpha and beta coherence within the subthalamic nucleus region. *NeuroImage*, *257*, 119320. https://doi.org/10.1016/j.neuroimage.2022.119320

Van Wijk, B. C. M., Neumann, W.-J., Schneider, G.-H., Sander, T. H., Litvak, V., & Kühn, A. A. (2017). Low-beta cortico-pallidal coherence decreases during movement and correlates with overall reaction time. *NeuroImage*, *159*, 1–8. https://doi.org/10.1016/j.neuroimage.2017.07.024

Vanegas-Arroyave, N., Lauro, P. M., Huang, L., Hallett, M., Horovitz, S. G., Zaghloul, K. A., & Lungu, C. (2016). Tractography patterns of subthalamic nucleus deep brain stimulation. *Brain*, *139*(4), 1200–1210. https://doi.org/10.1093/brain/aww020

Vieira, S., Pinaya, W. H. L., & Mechelli, A. (2017). Using deep learning to investigate the neuroimaging correlates of psychiatric and neurological disorders: Methods and applications. *Neuroscience and Biobehavioral Reviews*, *74*(Pt A), 58–75. https://doi.org/10.1016/j.neubiorev.2017.01.002

Volkmann, J., Herzog, J., Kopper, F., & Deuschl, G. (2002). Introduction to the programming of deep brain stimulators. *Movement Disorders: Official Journal of the Movement Disorder Society*, *17 Suppl 3*, S181-187. https://doi.org/10.1002/mds.10162

Wang, J., Hirschmann, J., Elben, S., Hartmann, C. J., Vesper, J., Wojtecki, L., & Schnitzler, A. (2014). High-frequency oscillations in Parkinson's disease: Spatial distribution and clinical relevance. *Movement Disorders*, *29*(10), 1265–1272. https://doi.org/10.1002/mds.25962

Wang, X.-J. (2010). Neurophysiological and Computational Principles of Cortical Rhythms in Cognition. *Physiological Reviews*, *90*(3), 1195–1268. https://doi.org/10.1152/physrev.00035.2008

Ward, L. M. (2003). Synchronous neural oscillations and cognitive processes. *Trends in Cognitive Sciences*, *7*(12), 553–559. https://doi.org/10.1016/j.tics.2003.10.012

Weinberger, M., Mahant, N., Hutchison, W. D., Lozano, A. M., Moro, E., Hodaie, M., Lang, A. E., & Dostrovsky, J. O. (2006). Beta Oscillatory Activity in the Subthalamic Nucleus and Its Relation to Dopaminergic Response in Parkinson's Disease. *Journal of Neurophysiology*, *96*(6), 3248–3256. https://doi.org/10.1152/jn.00697.2006

Welch, P. (1967). The use of fast Fourier transform for the estimation of power spectra: A method based on time averaging over short, modified periodograms. *IEEE Transactions on Audio and Electroacoustics*, *15*(2), 70–73. IEEE Transactions on Audio and Electroacoustics. https://doi.org/10.1109/TAU.1967.1161901

Wichmann, T., & DeLong, M. R. (1996). Functional and pathophysiological models of the basal ganglia. *Current Opinion in Neurobiology*, *6*(6), 751–758. https://doi.org/10.1016/S0959-4388(96)80024-9

Wiest, C., Tinkhauser, G., Pogosyan, A., He, S., Baig, F., Morgante, F., Mostofi, A., Pereira, E. A., Tan, H., Brown, P., & Torrecillos, F. (2021). Subthalamic deep brain stimulation induces finely-tuned gamma oscillations in the absence of levodopa. *Neurobiology of Disease*, *152*, 105287. https://doi.org/10.1016/j.nbd.2021.105287

Wilkinson, M. D., Dumontier, M., Aalbersberg, Ij. J., Appleton, G., Axton, M., Baak, A., Blomberg, N., Boiten, J.-W., Da Silva Santos, L. B., Bourne, P. E., Bouwman, J., Brookes, A. J., Clark, T., Crosas, M., Dillo, I., Dumon, O., Edmunds, S., Evelo, C. T., Finkers, R., … Mons, B. (2016). The FAIR Guiding Principles for scientific data management and stewardship. *Scientific Data*, *3*(1), 160018. https://doi.org/10.1038/sdata.2016.18

Willmott, C. J., & Matsuura, K. (2005). Advantages of the mean absolute error (MAE) over the root mean square error (RMSE) in assessing average model performance. *Climate Research*, *30*, 79–82. https://doi.org/10.3354/cr030079

Winkler, L., Werner, L. M., Butz, M., Hartmann, C. J., Schnitzler, A., & Hirschmann, J. (2026). Deep brain stimulation-responsive subthalamo-cortical coupling in obsessive-compulsive disorder. *Brain Stimulation*, *19*(1), 103008. https://doi.org/10.1016/j.brs.2025.103008

Wipf, D., & Nagarajan, S. (2009). A Unified Bayesian Framework for MEG/EEG Source Imaging. *NeuroImage*, *44*(3), 947–966. https://doi.org/10.1016/j.neuroimage.2008.02.059

Xia, R., & Mao, Z.-H. (2012). Progression of motor symptoms in Parkinson's disease. *Neuroscience Bulletin*, *28*(1), 39–48. https://doi.org/10.1007/s12264-012-1050-z

Ye, Z., Heldmann, M., Herrmann, L., Brüggemann, N., & Münte, T. F. (2022). Altered alpha and theta oscillations correlate with sequential working memory in Parkinson's disease. *Brain Communications*, *4*(3), fcac096. https://doi.org/10.1093/braincomms/fcac096

Zaidel, A., Spivak, A., Grieb, B., Bergman, H., & Israel, Z. (2010). Subthalamic span of oscillations predicts deep brain stimulation efficacy for patients with Parkinson's disease. *Brain*, *133*(7), 2007–2021. https://doi.org/10.1093/brain/awq144

Zhao, Y., Cai, J., Song, J., Shi, H., Kong, W., Li, X., Wei, W., & Xue, X. (2025). Peak alpha frequency and alpha power spectral density as vulnerability markers of cognitive impairment in Parkinson's disease: An exploratory EEG study. *Frontiers in Neuroscience*, *19*. https://doi.org/10.3389/fnins.2025.1575815

Acknowledgements

I would like to thank all the people who contributed directly or indirectly to the success of this dissertation.

First and foremost, I wish to express my deep gratitude to PD Dr. Jan Hirschmann, without whom this thesis would not have been possible. My time here was an enriching and truly enjoyable experience thanks to his patience, availability, and unwavering support from the very beginning.

I would also like to thank Prof. Dr. Markus Butz, Prof. Dr. Eckart Zimmermann and Prof. Dr. Alfons Schnitzler for their great feedback and guidance.

My sincere thanks go to the Brunhilde Moll Stiftung for generously funding my research.

I am grateful to the entire AG Hirschmann research group, within which I had the chance to meet wonderful people. In particular, I thank Marius and Abhinav for their invaluable advice, which helped shape my thinking throughout my doctoral work.

Many thanks to Alex, Lucy, Lucie, and Elisabeth for their contributions and for always being there whenever I needed help.

Thank you to Thomas, Fabrice, and Agnes for making me feel at home.

I would especially like to thank Vai, who has been there by my side since the very beginning of this long journey and who, I am certain, will continue to play an important role in my life. My time here in Düsseldorf would not have been the same without our countless enjoyable outings together.

My heartfelt thanks also go to my childhood friends, who managed to bring a smile to my face even from hundreds of kilometers away. I would also like to thank the friends I made along the way, in particular Guillaume Pech, who has been a great source of inspiration. I learned so much from all of them; they have changed me profoundly, and thanks to them I have been able to see the path toward the person I aspire to become.

I am immensely grateful to my brothers and sisters, who encouraged me to pursue my studies, took care of me, never doubted my success, and constantly pushed me to surpass myself. A special thank-you to Lydia for the beautiful figures she created for me.

And finally, I am infinitely grateful to my parents, who raised and educated me with love. I will continue striving to make them proud.

To all those involved, I offer my sincere thanks, respect, and gratitude.

Eidesstattliche Erklärung

An Eides statt erkläre ich, dass ich die vorgelegte Dissertation selbstständig und ohne unzulässige fremde Hilfe unter der Beachtung der "Grundsätze zur Sicherheit guter wissenschaftlicher Praxis an der Heinrich-Heine-Universität Düsseldorf" angefertigt habe und dass ich diese in der jetzigen oder einer ähnlichen Form noch keiner anderen Fakultät eingereicht habe.

Düsseldorf, den

RASSOULOU FAYED